RIGA TECHNICAL UNIVERSITY

Miķelis Kirpļuks

DEVELOPMENT OF RENEWABLE FEEDSTOCK BASED RIGID POLYURETHANE FOAM AND NANOCLAY COMPOSITES

Summary of the Doctoral Thesis

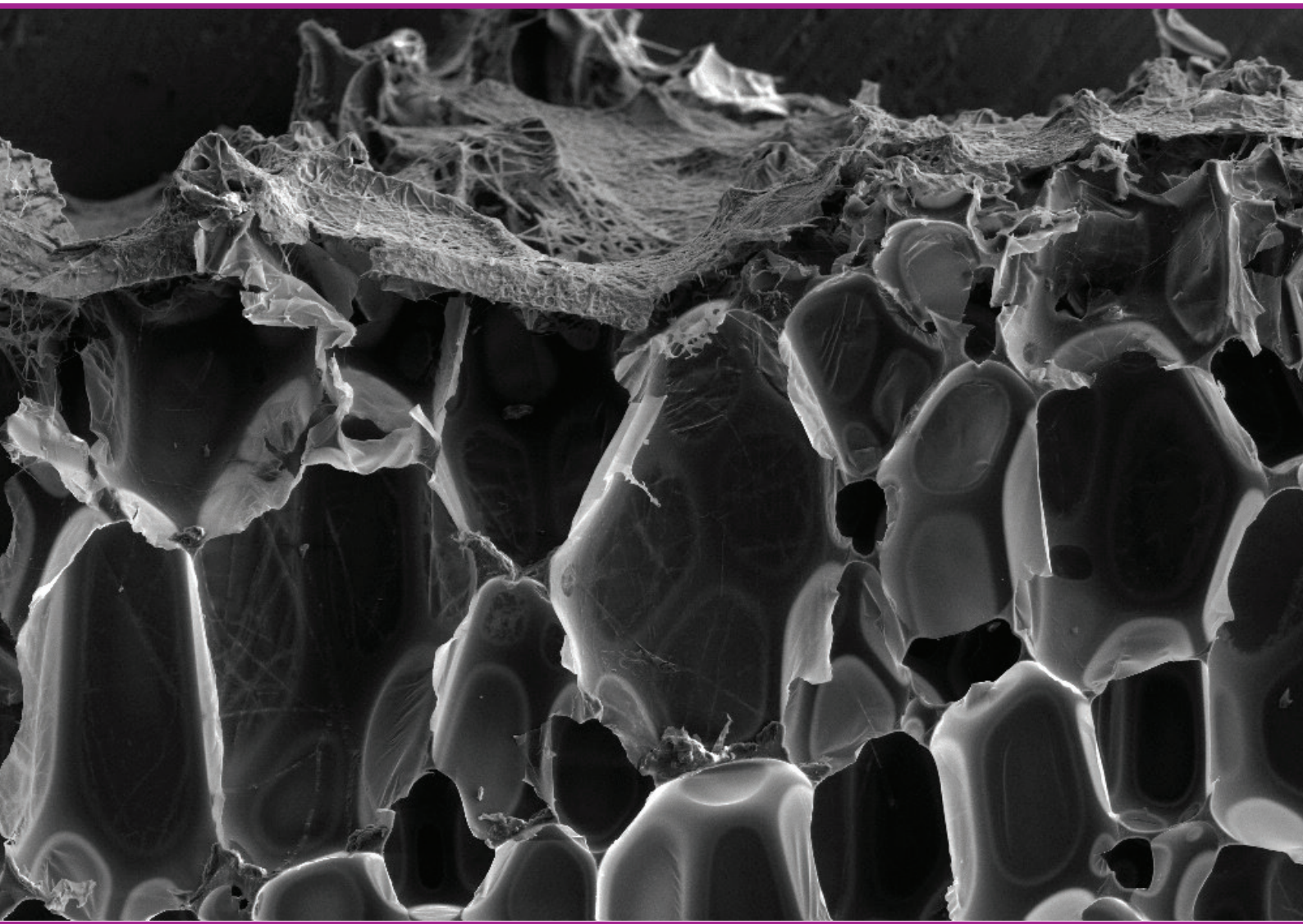

RTU Press
Riga 2020

RIGA TECHNICAL UNIVERSITY
Faculty of Materials Science and Applied Chemistry
Institute of Polymer Chemistry and Technology

Miķelis Kirpļuks
Doctoral Student of the Study Programme "Chemical Engineering"

DEVELOPMENT OF RENEWABLE FEEDSTOCK BASED RIGID POLYURETHANE FOAM AND NANOCLAY COMPOSITES

Summary of the Doctoral Thesis

Scientific supervisors:

Dr. sc. ing.
UĢIS CĀBULIS

Dr. sc. ing. Associate Professor
SERGEJS GAIDUKOVS

RTU Press
Riga 2020

Kirpļuk , M. Dev lopment of Renewable Feedstock Based Rigid Polyurethane Foam and Nanoclay Composites. Summary of the Doctoral Thesis. Riga: RTU Press, 2064 p.

Published in accordance with the decision of Promotion Council "RTU P-" of May 5–6, 2020, Minutes No. 04 9 1/ 3.

The Ph. D. Thesis has been carried out in the frame of the following research projects funded by European Community:

- FP 7 project EVOLUTION, 11/2012 – 11/2016; The Electric Vehicle revOLUTION enabled by adv nced materials highly hybridized into lightweight components for easy integration and dismantling prov ding a reduced life-cycle cost logic;

- IMATECH – Latvian National Research program project: Innov tiv and multifunctional composite materials for sustainable buildings;

- COST action MP 1105 Flaretex, FLARETEX, 05/2012- / 206; Sustainable flame retardancy for textiles and related materials based on nanoparticles substituting conv ntional chemicals;

- Project "Rigid polyurethane/polyisocyanurate foam thermal insulation material reinforced with nano/micro size cellulose" funded by ERDF, contract No. 1.1.1.1/16/A/ 1, / 207 02/209

MINISTRY OF FINANCE REPUBLIC OF LATVIA | NATIONAL DEVELOPMENT PLAN 2020 | EUROPEAN UNION European Regional Development Fund

INVESTING IN YOUR FUTURE

ISBN 9 9 2 6 0 (print)
ISBN 9 9 2 4 6 (pdf)

DOCTORAL THESIS PROPOSED TO RIGA TECHNICAL UNIVERSITY FOR THE PROMOTION TO THE SCIENTIFIC DEGREE OF DOCTOR OF SCIENCE

To be granted the scientific degree of Doctor of Science (Ph. D.), the present Doctoral Thesis has been submitted for the defence at the open meeting of RTU Promotion Council on September 3, 2020 at the Faculty of Materials Science and Applied Chemistry of Riga Technical University, 3/7 Paula Valdena Street, Room 272.

OFFICIAL REVIEWERS

Professor Dr. sc. ing. Jurijs Ozoliņš
Riga Technical University, Latvia

Professor Dr. habil. chem. Andris Actiņš
University of Latvia, Latvia

Professor Dr. Arantxa Eceiza
Universidad del Pais Vasco, Leioa, Spain

DECLARATION OF ACADEMIC INTEGRITY

I hereby declare that the Doctoral Thesis submitted for the review to Riga Technical University for the promotion to the scientific degree of Doctor of Science (Ph. D.) is my own. I confirm that this Doctoral Thesis had not been submitted to any other university for the promotion to a scientific degree.

Miķelis Kirpļuks ……. (signature)

Date: ……

The Doctoral Thesis has been written in English. It consists of an Introduction; 3 Chapters; Conclusions; 123 figures; 27 tables; the total number of pages is 161. The Bibliography contains 12 titles.

TABLE OF CONTENTS

ABBREVIATIONS

[AA]	Acetic acid content, mol per 100 g oil
[AAs]	Adsorbed acetic acid content, mol per 100 g oil
[EU]	Ethylenic unsaturation content, mol per 100 g oil
[H_2O]	Water content, mol per 100 g oil
[H_2O_2]	Hydrogen peroxide content, mol per 100 g oil
[OO]	Oxirane oxygen content, mol/L
[PA]	Peracetic acid content, mol per 100 g oil
[PAs]	Adsorbed peracetic acid content, mol per 100 g oil
APP	Aromatic polyester polyol
DEG	Diethylene glycol
DEOA	Diethanolamine
DMA	Dynamic mechanical analysis
DMPP	Dimethyl-propyl-phosphate
DSC	Differential Scanning Calorimetry
EG	Expandable graphite
EU	Ethylenic unsaturation
FEM	Finite element modelling
FR	Flame retardant
HRR	Heat release rate, kW/m^2
IF	Intumescent unwoven fabric
LS IWC	Latvian State Institute of Wood Chemistry
MARHE	Maximum average rate of heat emission, kW/m^2
M_c	Molecular weight between cross-links, g/mol
pbw	Parts by weight
PET	Polyethylene terephthalate
pHRR	Peak of heat release rate, kW/m^2
PIR	Polyisocyanurate
Project EVolution	The Electric Vehicle revOLUTION enabled by advanced materials highly Hybridized into lightweight components for easy integration and dismantling providing a reduced life cycle cost logic
PU	Polyurethane
RCO	Relative conversion to oxirane, %
REU	Relative ethylenic unsaturation, %
RO	Rapeseed oil
RO_DEOA	Rapeseed oil polyol from transamidation reaction with diethanolamine
RO_TEOA	Rapeseed oil polyol from transesterification reaction with triethanolamine
SEM	Scanning electron microscope
TCPP	Tris(1-chloro-2-propyl)phosphate
TEOA	Triethanolamine
TGA	Thermogravimetric analysis

TO	Tall oil
TO_DEOA	Tall oil polyol from amidation reaction with diethanolamine
TO_TEOA	Tall oil polyol from esterification reaction with triethanolamine
TOFA	Tall oil fatty acids
TSR	Total smoke released, m^2/m^2
XRD	X-ray diffraction
λ	Thermal conductivity, mW/(m·K)

INTRODUCTION

The world is facing a rising variety of challenges due to increasing public concern about global sustainability, therefore, the development of advanced new materials and technologies for sustainable bio-based products is critical. Widespread R&D activities have been conducted to develop polymeric materials from sustainable feedstock and replace their petrochemical counterparts. Rigid polyurethane (PU) foams are an inseparable part of the global polymer market as they are utilized in a wide range of applications, such as thermal insulation in civil engineering and appliance industry, structural material and impact absorption material in the automotive industry, structural and buoyancy material in the marine industry, etc. In this work polymer material sustainability challenge is answered by the development of high-quality rigid PU from various bio-based and recycled feedstocks. The properties of the developed materials are up to industry quality standards and ready for the next stage of technology upscale.

Presented Doctoral Thesis demonstrates the development of rigid PU foam materials from sustainable feedstock with several large scale applications. PU materials are obtained in the reaction between a polyisocyanate moiety containing isocyanate groups (−NCO) and a polyol component containing hydroxyl groups (−OH). Sustainable origin polyols are the most promising way of introducing “green” chemistry into PU materials. Previously studied bio-based polyols from tall oil (TO) and rapeseed oil (RO) have been utilized to develop high-density structural strength rigid PU foams applicable in the automotive industry. Furthermore, sustainable polyols derived from recycled polyethylene terephthalate (PET) side-stream were also investigated for the same application. The mechanical properties of the developed high-density rigid PU foam were further increased by the addition of montmorillonite nanoclay reinforcement filler. Materials with the most optimal properties were chosen for real scale automotive part development and testing.

In the frame of this Doctoral Thesis rigid PU foam, thermal insulation material from TO based polyol with the goal to reduce material’s flammability was also developed. It was concluded that it is possible to replace conventional potentially harmful halogenated flame retardants with intumescent expandable graphite flame retardant.

Lastly, during high-density rigid PU foam development it was discovered that bio-based polyols lack the functionality to obtain mechanically strong material, thus a new approach of high functionality bio-based polyol synthesis was investigated. The roadmap of presented Doctoral Thesis is depicted in Fig. 1 in which the work is split into three parts where the first part describes studies related to the automotive industry, the second part is related to the development of low flammability thermal insulation material, and the third part depicts improvement of rapeseed oil and tall oil polyol synthesis methods.

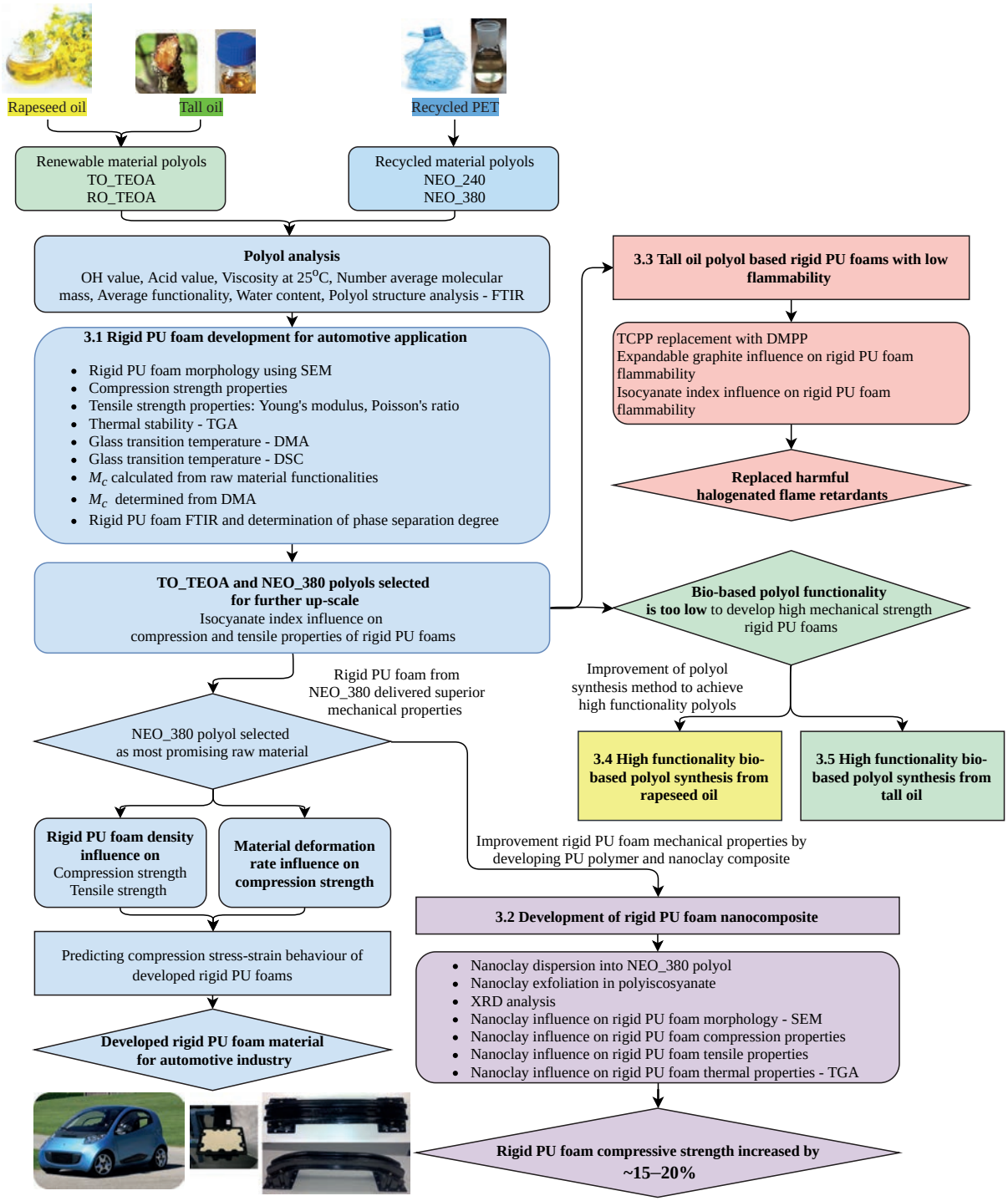

Fig 1. The roadmap of Doctoral Thesis.

Aim of the Doctoral Thesis

To develop rigid PU foam material from sustainable raw materials with increased mechanical properties and to develop novel polyol synthesis method from renewable materials available in Northern Europe.

Tasks of the Doctoral Thesis

1. To develop high-density rigid PU foam material from bio-based polyols.
2. To develop high-density rigid PU foam material from APP polyols obtained from recycled PET.
3. To test mechanical and thermal properties of the developed high-density rigid PU foams and access their viability as impact absorption material for automotive industry applications.
4. To reinforce developed high-density rigid PU foams with montmorillonite nanoclay particles to increase the mechanical properties of the composite.
5. To develop low-density rigid PU foam as a thermal insulation material from renewable feedstock with low flammability characteristics by replacing harmful halogenated flame retardants with intumescent flame retardant alternative.
6. To develop a synthesis method for high functional bio-based polyols from RO and TOFA.

Thesis Statements to be Defended

1. APP polyols are more suited for structural high-density rigid PU production when compared to polyols obtained form TO and RO.
2. Montmorillonite nanoclay filler increases compression properties of rigid PU foams.
3. Halogenated flame retardants are not required to develop highly flame retardant rigid PU foam thermal insulation.
4. RO and TOFA are well suited for high functional bio-based polyol synthesis.

Scientific Novelty

1. Demonstration of sustainable material viability for the development of structural engineering materials with high-performance requirements.
2. Replacement of halogenated flame retardants with more sustainable alternatives.
3. RO based high functionality polyol synthesis method has been developed by combining oxirane ring opening reaction with transesterification/transamidation reactions with polyfunctional alcohols, and synthesised polyols have been used for rigid PU foam thermal insulation material development
4. Development of TOFA epoxidation method using innovative heterogeneous phase catalysts such as ion exchange resin and immobilised Lipase enzyme.
5. TOFA epoxidation has been modelled using heterogeneous phase reaction model that can be used for synthesis parameter optimization.

Practical Significance

1. Developed high-density rigid PU foam materials that can be applied as a structural material in various engineering solutions especially in the automotive industry.
2. Developed high-efficiency thermal insulation material from renewable raw materials with increased fire resistance performance, which is suitable for civil engineering applications.
3. Developed high functionality bio-based polyols can be applied as a crosslink reagent in various PU materials.

Approbation of PhD thesis in Scopus indexed articles

- **M. Kirpluks**, U. Cabulis, M. Kurańska, A. Prociak, Three Different Approaches for Polyol Synthesis from Rapeseed Oil, Key Eng. Mater. 559 (2013) 69–74. doi:10.4028/www.scientific.net/KEM.559.69.
- **M. Kirpluks**, U. Cabulis, A. Ivdre, M. Kuranska, M. Zieleniewska, M. Auguscik, Mechanical and Thermal Properties of High-Density Rigid Polyurethane Foams from Renewable Resources, J. Renew. Mater. 4 (2016) 86–100. doi:10.7569/JRM.2015.634132.
- **M. Kirpluks**, U. Cabulis, J. Andersons, G. Japins, K. Kalnins, Modeling the Effect of Foam Density and Strain Rate on the Compressive Response of Polyurethane Foams, SAE Int. J. Mater. Manuf. 11 (2018). doi:10.4271/05-11-02-0014.
- E. Cischino, Z. Vuluga, C.E. Ezeiza, I.L. Benito, E. Mangino, J. De Claville Christiansen, C.-G. Sanporean, F. Di Paolo, **M. Kirpluks**, P. Cabulis, A Concrete and Viable Example of Multimaterial Body: The Evolution Project Main Outcomes, in: Procedia CIRP, (2017) 300–305. doi:10.1016/j.procir.2017.03.292.
- **M. Kirpluks**, E. Cischino, U. Cabulis, J. Andersons, Rigid PUR foam impact absorption material obtained from sustainable resources, AIP Conf. Proc. (2019) *2139*. doi.org/10.1063/1.5121686
- **M. Kirpluks**, L. Stiebra, A. Trubaca-Boginska, U. Cabulis, J. Andersons, Rigid closed-cell PUR foams containing polyols derived from renewable resources: The effect of polymer composition, foam density, and organoclay filler on their mechanical properties, in: K. Thakur, Vijay, M.K. Thakur, M.R. Kessler (Eds.), Handb. Compos. from Renew. Mater., Scrivener Publishing LLC, 2017: pp. 313–339. doi:10.1002/9781119441632.ch31.
- U. Cabulis, **M. Kirpļuks**, J. Andersons, The Effect of Montmorillonite Type Nanoparticles on Stiffness and Flammability of Rapeseed Oil Based Polyisocyanurate Foams, Key Eng. Mater. 559 (2013) 19–24. doi:10.4028/www.scientific.net/KEM.559.19.
- **M. Kirpluks**, U. Cabulis, V. Zeltins, L. Stiebra, A. Avots, Rigid Polyurethane Foam Thermal Insulation Protected with Mineral Intumescent Mat, Autex Res. J. 14 (2014) 259–269. doi:10.2478/aut-2014-0026.

- **M. Kirpluks**, U. Cabulis, A. Avots, Flammability of Bio-Based Rigid Polyurethane Foam as Sustainable Thermal Insulation Material, in: Insul. Mater. Context Sustain., InTech, 2016: p. 148. doi:DOI: 10.5772/61361.
- **M. Kirpluks**, D. Kalnbunde, Z. Walterova, U. Cabulis, Rapeseed Oil as Feedstock for High Functionality Polyol Synthesis, J. Renew. Mater. 5 (2017) 1–23. doi:10.7569/JRM.2017.634116.
- **M. Kirpluks**, D. Kalnbunde, H. Benes, U. Cabulis, Natural oil based highly functional polyols as feedstock for rigid polyurethane foam thermal insulation, Ind. Crops Prod. 122 (2018) 627–636. doi:10.1016/j.indcrop.2018.06.040.
- **M. Kirpluks**, E. Vanags, A. Abolins, A. Fridrihsone, U. Cabulis, Chemo-enzymatic oxidation of tall oil fatty acids as a precursor for further polyol production, J. Clean. Prod. 215 (2019) 390–398. doi:10.1016/j.jclepro.2018.12.323.

1. LITERATURE REVIEW

1.1. Polyurethane Foams in Brief

Polyurethane Material Chemistry

The main difference between polyurethane (PU) materials and other common polymers is that there is no urethane monomer. Typically, the PU polymer is created in a chemical polycondensation reaction between −NCO groups and −OH groups. This main chemical reaction is the foundation of the majority of the PU materials. However, the term "polyurethane" can be deceiving as it refers to the broad variety of different materials with different properties and applications. Polyurethanes can be soft or hard, flexible or rigid, thermoplastic or thermoset. Properties of the PU polymer matrix are derived from the chemical composition of raw materials used in the polymerization reaction. The length and the chemical nature of the moieties R_1 and R_2 depicted in Fig. 1.1 play the most significant role on the properties of the final material [1].

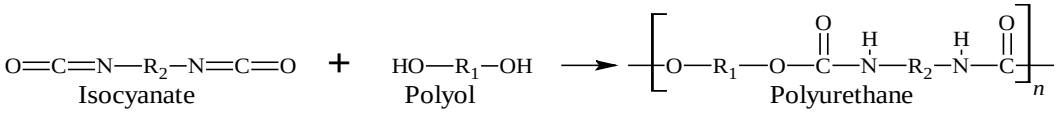

Fig. 1.1.Generic urethane linkage reaction [1].

Polyols

In general, polyols can be separated into two distinct groups: polyether and polyester based polyols from which the vast majority produced are polyether type polyols [2]. Polyether-type polyols are obtained in an oxiethylation or oxipropylation reactions by developing and extending glycol chains of starter alcohol. For rigid PU foam production, higher functionality polyols are necessary, thus the starter alcohol also needs to have a high OH group functionality. Commonly glycerol with $f_n = 3$ and sorbitol $f_n = 6$ among other glycols are used as a starter. Ethylene oxide and propylene oxide are obtained from ethylene and propylene oxidation, which are a direct product of naphtha cracking process. From now on polyols obtained by oxyethylation and oxypropylation reactions will be referred as petrochemical origin polyols. Polyol functionality and its molecular mass have a significant influence on the properties of the final material. The common characteristics of polyols that are used in PU material industry are as follows: OH value (mg_{KOH}/g), acid value (mg_{KOH}/g), viscosity (mPa·s), number of average functionality – f_n, number of average molecular mass – M_n (Da or g/mol), and moisture content (wt. %).

The global polyol market size is expected to reach 45.17 billion USD by 2025 at an 8.5 % annual growth rate during the forecast period [3]. Besides typical production technologies, there have been new developments in sustainable polyol production on an industrial scale from different bio-based feedstock as well as CO_2 based polyols [4], [5]. Development of sustainable raw material origin and bio-based polyols is especially promising as their market share is expected to increase faster than common petrochemical polyol growth rate. The

global *green* and bio-based polyol market was valued at 2.63 billion USD in 2015 and is projected to reach 4.71 billion USD by 2021 at a 9.5 % annual growth rate.

Polyisocyanate

PU material production would not be possible without other main polycondensation reaction component – polyisocyanate. Polyisocyanates are compounds that have at least two NCO groups in their chemical structure. The NCO group reacts with any active hydrogen, thus polyisocyanates are used in various polymer production, such as polyurethanes, polyureas and polyamides. The chemical reaction of the isocyanate group with an "active hydrogen" is depicted in Fig. 1.2. Isocyanate group can react with alcohols, water, carboxylic acids, amine, ureas, urethanes and amides. Furthermore, the NCO group can react with other NCO groups forming dimerization products or trimerization product – isocyanurate ring, if the conditions are right. During the PU material production, several of mentioned reactions occur at the same time, thus the final polymer matrix is a copolymer with a varied chemical functionality, which reflects on the material properties.

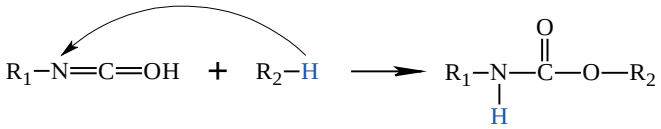

Fig. 1.2. Isocyanate reaction with active hydrogen compounds [1].

1.2. Sustainable Polyol Development

The 21st century is the bioeconomy century where a great deal of effort, research and investment will be devoted on moving towards post-petroleum society. The development of advanced new materials and technologies of bio-based products is critical [6], [7]. Widespread R&D activities have been conducted to develop bio-based polymeric materials and replace their petrochemical counterparts [8].

Plant oils have been considered as an alternative resource for the production of polymeric materials and have been extensively studied [9]–[11]. Although there has already been major progress, the potential of the available bio-resources in value-added sectors still needs to be maximised, and new approaches through the more complete deployment of the twelve Principles of Green Chemistry have to be delivered [12].

The main feedstock for bio-based polyol production are different natural oils, like soybean oil, palm oil, sunflower oil, corn, oil, linseed oil, olive oil, castor oil, etc., as well as animal origin oils, like fish oil [2], [11]. All natural oils, with the exception of castor oil, have to be chemically modified before they can be used for PU material production as they do not contain hydroxyl groups. A generic triglyceride structure of the natural oils is depicted in Fig. 1.3. [13]–[15]. Two approaches for polyol synthesis from vegetable oils can be distinguished, modification of double bonds of the unsaturated fatty acids and transesterification of triglyceride backbone [16].

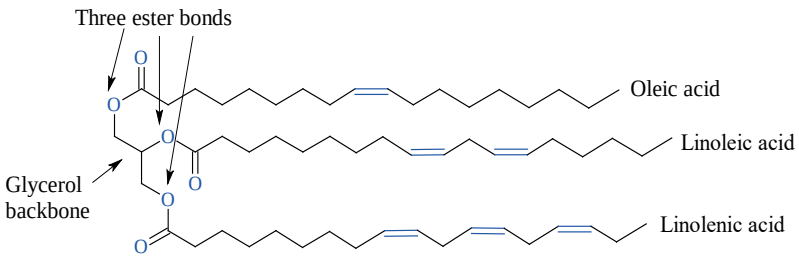

Fig. 1.3. The generic structure of vegetable oil containing oleic, linoleic and linolenic acid chains.

Epoxidation and Epoxy Ring Opening of Natural Oils

Plant oil double bond epoxidation has attracted a lot of attention as chemical reaction yields epoxides that are easily convertible intermediates and have a wide commercial use because of their varied chemical activity. Epoxides have been used as raw materials for products such as alcohols, glycols, plasticizers, high-temperature lubricants, polyols and polymers, e.g. polyurethane, polyesters and epoxy resins [17], [18]. The polyol production from epoxidized vegetable oils is already a well-studied topic. Various epoxidation methods of different kind of plant oils such as soybean [19], palm, canola [20]–[22], castor [23], jatropha [24], [25], wild safflower [26], and others [27]–[30] have been reported. The most widely used method in above-mentioned studies is triglyceride or fatty acid methyl ester epoxidation with *in-situ* formed peroxycarboxylic acid, such as performic or peracetic acids, in the presence of a strongly acidic catalyst. The main disadvantage of the chemical epoxidation method is the acid-catalyzed side-reaction occurrence with oxirane rings, which leads to the formation of by-products [31]. Furthermore, the use of additional acid as an oxygen carrier means that it has to be separated from the reaction media after oil epoxidation, which, along with the use of hazardous chemicals, is not desired from the viewpoint of green chemistry. The use of performic or peracetic acids in the epoxidation process could lead to the thermal runaway of the reaction, which is highly undesired for an industrial upscale and due to safety concerns [32]–[34].

Most frequently epoxidation with in-situ generated peroxy acid and subsequent epoxy ring opening reaction with haloacids or alcohols is used to functionalize unsaturated fatty acids into polyols [2], [11], [16]. The reagent used in the epoxy ring opening has the largest influence on the properties of the polyol and final PU material. Polyols with secondary OH groups and lower average functionality (f_n = 2–3) are more suitable for elastomer and flexible PU foam production [1], [35], [36]. Polyols obtained from epoxy group opening with diethylenglycol (DEG) are more suitable for rigid PU foam production as they deliver higher functionality, f_n = 3–5 [1], [37], [38]. Such polyols have primary and secondary hydroxyl groups in their structure. Primary hydroxyl groups are more reactive with isocyanate, which makes them more useful for spray applied rigid PU foam formulations [39], [40].

A combination of epoxy ring opening and transesterification of fatty acid triglycerides could lead to higher polyol functionality, which would ensure high crosslink density of PU matrix resulting in a rigid PU foam with increased mechanical properties, good dimensional stability and high ageing stability. This is investigated in Part 3 of the presented Thesis. A similar idea was explored to obtain water-soluble soybean oil-based polyols. Although polyol molecular weight was 3800–5900 Da and reported structure had plenty of primary OH groups, no PU materials were obtained [41].

2. MATERIALS AND METHODS

High-Density Rigid PU Foam Development From Sustainable Raw Materials

The most significant properties of the polyols used in the development of high-density rigid PU foams are presented in Table 2.1. For the development of high-density rigid PU foams, two different polyols from renewable raw materials were used TO_TEAO and RO_TEOA, which were synthesized at LS IWC [15], [42], [43]. APPs used in this study were produced by Neo Group, Lithuania, from PET industrial waste [44]. Described polyols were used to formulate high-density rigid PU foam systems.

Table 2.1

Technical Characteristics of Polyols Obtained From Sustainable Resources

Polyol type		OH value, mg_{KOH}/g	Viscosity at 25 °C, mPa·s	Acid value, mg_{KOH}/g	M_n, g/mol	f_n	Water content, %
Bio-based polyols	TO_TEOA	342	280 ± 25	<5	391	2.4	0.24
	RO_TEOA	301	190 ± 25	<5	474	2.6	0.05
Recycled APP polyols	Neopolyol 240 (NEO 240)	258	5000 ± 500	<5	683	3.1	0.04
	Neopolyol 380 (NEO 380)	366	3500 ± 500	<5	505	3.3	0.12

Rigid PU Foam Nanocomposite Development

In the frame of the Doctoral Thesis, rigid PU foams were reinforced with two different modified nanoclay particles. The goal was to increase the mechanical properties of developed materials. For this purpose, two commercially available montmorillonite nanoparticles were used: Cloisite 15A and Cloisite 30B, and their characteristics are depicted in Table 2.2. Nanoparticles were dispersed into NEO 380 polyol. Furthermore, Cloisite 30B nanoparticles were exfoliated into polyisocyanate component. Methods used to disperse nanoclay particles and experimental workflow are depicted in Fig. 2.1.

Table 2.2

Characteristics of Two Different Nanoclay Particles – Cloisite 15A and Cloisite 30B

Nanoparticle	Organic modifier	Modifier concentration	Moisture	Weight loss on ignition	Density	Interplanar distance
Cloisite 15A	2M2HT*	125 meq per 100 g clay	<2 %	43 %	1.66 g/cm^3	31.5 Å
Cloisite 30B	MT2EtOH*	90 meq per 100 g clay	<2 %	30 %	1.98 g/cm^3	18.5 Å

2M2HT: dimethyl, dehydrogenated tallow, quaternary ammonium
HT – hydrogenated tallow
MT2EtOH: methyl, tallow, bis-2-hydroxyethyl, quaternary ammonium
T – Tallow

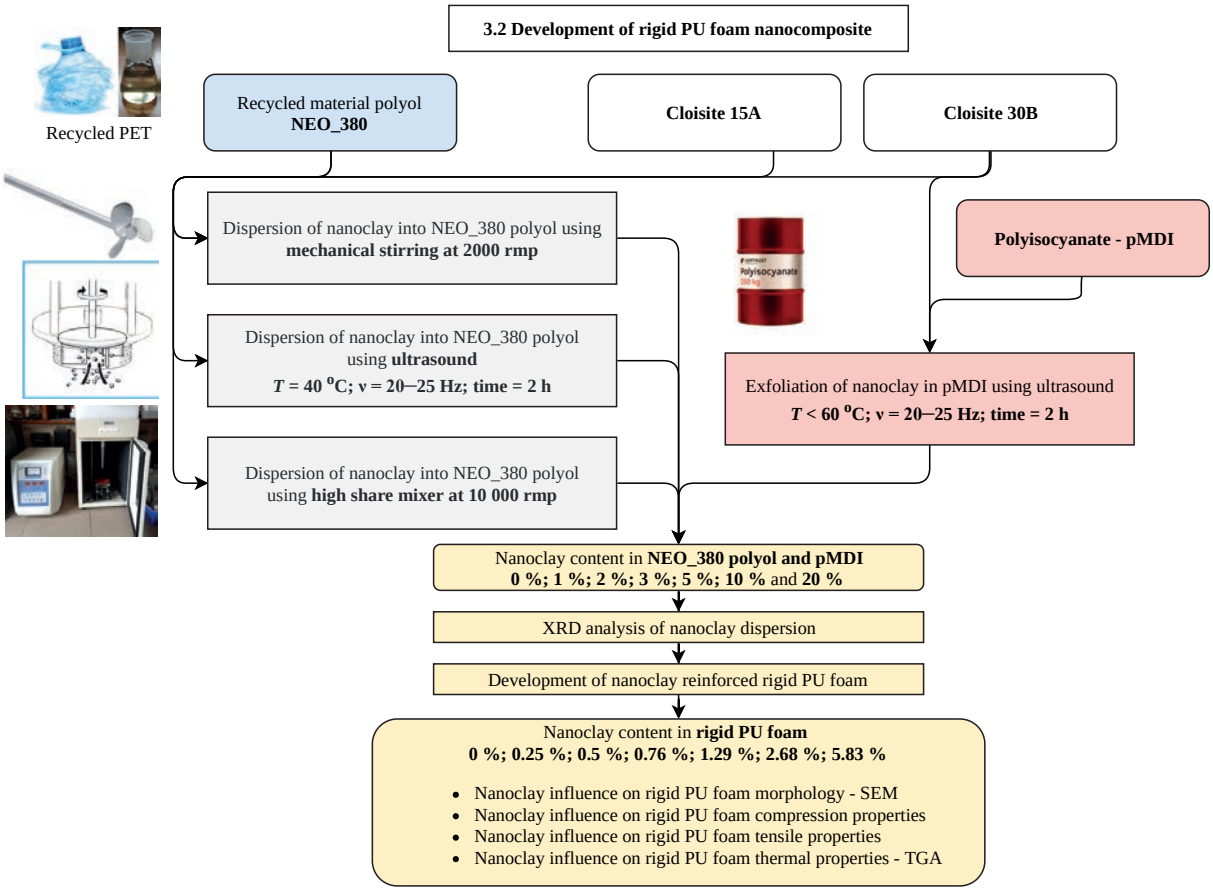

Fig. 2.1. Work flow of nanoclay introduction into rigid PU foam structure and its influence on the foam characteristics.

Development of Low Flammability Rigid PU Foam Thermal Insulation Composite

The flammability of rigid PU foams was decreased by adding non-halogenated flame retardants (FR), dimethyl-propyl-phosphate (DMPP), as well as expandable graphite (EG). Furthermore, a composite rigid PU foam was developed where one side of the material was protected with glass fibre non-woven intumescent fabric (IF). The non-halogenated FRs were compared to conventional additive FR tris(chloropropyl)phosphate (TCPP). The work flow of low flammability rigid PU foam thermal insulation development is depicted in Fig. 2.2 where the different samples with respective FR loadings are listed as well as the different tests and flammability analysis used to evaluate FR performance.

TCPP flame retardant was replaced in the neat formulation of TOFA_DEOA polyol based rigid PU foam. Conventional, liquid flame retardants TCPP and DMPP were compared at 7 wt. % of rigid PU foam mass. The EG flakes were also added into the polyol component. A possible synergistic effect between PIR groups and non-halogenated flame retardants was studied by changing the isocyanate index of the rigid PU foams (indices of 110; 150; 200 and 250 were tested). A sandwich like composite where rigid PU foam is protected by non-woven IF was obtained by producing samples in a stainless steel mould. The bottom of the mould was lined with the intumescent non-woven fabric and reacting rigid PU foam mass was poured on top of it. No additional adhesive was necessary, which shows the potential of this technology in the state of art rigid PU/PIR continuous panel production.

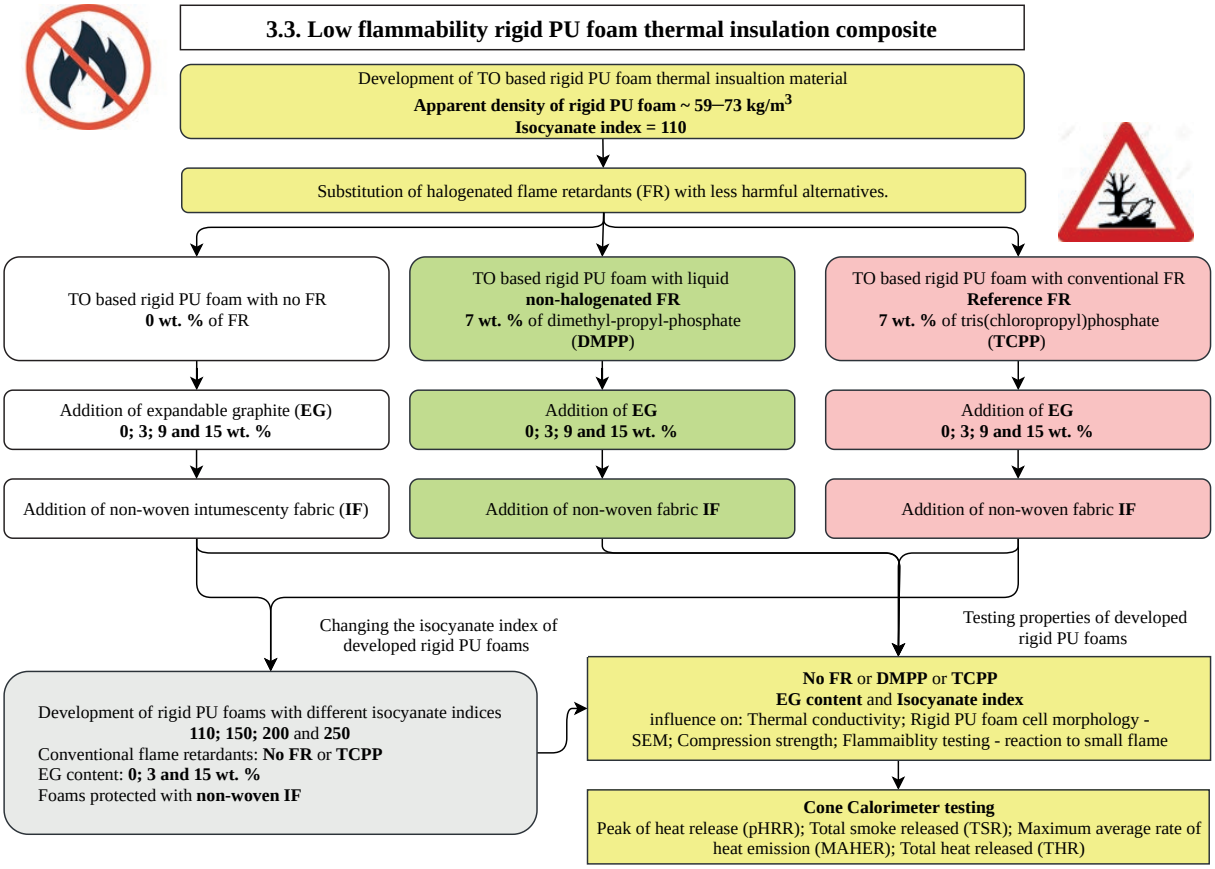

Fig. 2.2. Work flow of low flammability rigid PU foam thermal insulation development.

High Functionality Bio-Based Polyol Synthesis From RO

To increase feasibility of the bio-based polyols, high functional polyols from epoxidized rapeseed oil (ROEP) were obtained using oxirane ring opening reaction with polyfunctional alcohols, such as DEOA and TEOA. Epoxy ring opening with DEG was used to obtain a comparison material because this type of polyol is most commonly reported in the literature [38], [45]–[48]. The molar ratios between oxirane rings and polyfunctional alcohols were set as 1.0/1.1 and the following polyols were obtained: RODEA_0; ROTEA_0 and RODEG_0. In case of RODEA and ROTEA polyols, after the epoxy ring opening reaction, more DEOA and TEOA were added to carry out transamidation/transesterification of the glycerol backbone. Additional 1.5 M; 2.0 M and 2.5 M of DEOA and TEOA were added to carry out the transamidation/transesterification. The experiment scheme, the molar ratios between reagents and abbreviations of nine green polyols are depicted in Fig. 2.3. The epoxy ring opening with DEOA and subsequent transamidation is depicted in Fig. 2.4, and epoxy ring opening with TEOA and subsequent transesterification is depicted in Fig. 2.5.

3.4. High functionality bio-based polyol synthesis from RO

RO epoxidation using in-situ generated peroxycarboxylic acid in presence of ion-exchange resin catalyst

- Molar ratios between acetic acid (**AA**), hydrogen peroxide (H_2O_2) and double bonds (**EU**): **0.5/1.5/1.0**
- Amberlite IR-120 H catalyst content = **20 wt. %** of **RO mass**
- Mixing speed = **900 rpm**
- Synthesis temperature = **55; 60** and **65 ± 1 °C**
- RO epoxidation kinetics studied for **7 h** with **1 h** intervals

High functionality bio-based polyol synthesis from epoxidized rapeseed oil (**ROEP**) combining oxirane ring opening reaction and transesterification/transamidation reactions

ROEP oxirane ring opening with **DEOA**

- **ROEP+DEOA** molar ratios **1.0/1.1 M**
- Synthesis temperature = **110–115 °C**
- **LiOH** catalyst = **0.3 wt. %**
- Synthesis time = **3 h**
- Mixing speed = **700 rpm**

Polyol **RODEA_0**

ROEP oxirane ring opening with **DEG**

- **ROEP+DEG** molar ratios **1.0/1.1 M**
- Synthesis temperature = **110–115 °C**
- H_2SO_4 catalyst = **0.3 wt. %**
- Synthesis time = **3 h**
- Mixing speed = **700 rpm**

Polyol **RODEG_0**

ROEP oxirane ring opening with **TEOA**

- **ROEP+TEOA** molar ratios **1.0/1.1 M**
- Synthesis temperature = **140–145 °C**
- **LiOH** catalyst = **0.3 wt. %**
- Synthesis time = **3 h**
- Mixing speed = **700 rpm**

Polyol **ROTEA_0**

Continuation of RO based high functionality polyol synthesis by **transamidation**

ROEP oxirane ring opening and transamidation with **DEOA**

- **ROEP+DEOA** molar ratios **1.0/1.1 + 1.5; 2.0; 2.5 M**
- Synthesis temperature = **110–115 °C** for **3h** after **140–145 °C** for **2 h**
- Oxirane ring opening catalyst **LiOH** = **0.3 wt. %**
- Transamidation catalyst **zinc acetate = 0.15 wt. %**
- Synthesis time = **3 h + 2 h**
- Mixing speed = **700 rpm**

Polyol **RODEA_1.5** | Polyol **RODEA_2.0** | Polyol **RODEA_2.5**

Continuation of RO based high functionality polyol synthesis by **transesterification**

ROEP oxirane ring opening and transesterification with **TEOA**

- **ROEP+TEOA** molar ratios **1.0/1.1 + 1.5; 2.0; 2.5 M**
- Synthesis temperature = **140–145 °C** for **3h** after **170–175 °C** for **2 h**
- Oxirane ring opening catalyst **LiOH** = **0.3 wt. %**
- Transesterification catalyst **zinc acetate = 0.15 wt. %**
- Synthesis time = **3 h + 2 h**
- Mixing speed = **700 rpm**

Polyol **RODEA_1.5** | Polyol **RODEA_2.0** | Polyol **RODEA_2.5**

Characterization of developed RO based high functionality polyols

OH value; Acid value; Viscosity at 25 °C; Number average molecular mass; Average functionality; Water content, Density at 25 °C; Polyol structure analysis using **FTIR;** Polyol structutre analysis using **MALDI TOF** spectroscopy

Development of rigid PU foam thermal insulation from nine RO based high functionality polyols

Determination of technological parameters: start time; string time; tack free time and rise time; Apparent density of rigid PU foam ~ 40 kg/m^3; Closed cell content > 90 %; Determination of thermal conductivity of rigid PU foams; Determination of compression strength properties

Fig. 2.3. Work flow of high functionality polyol development from RO.

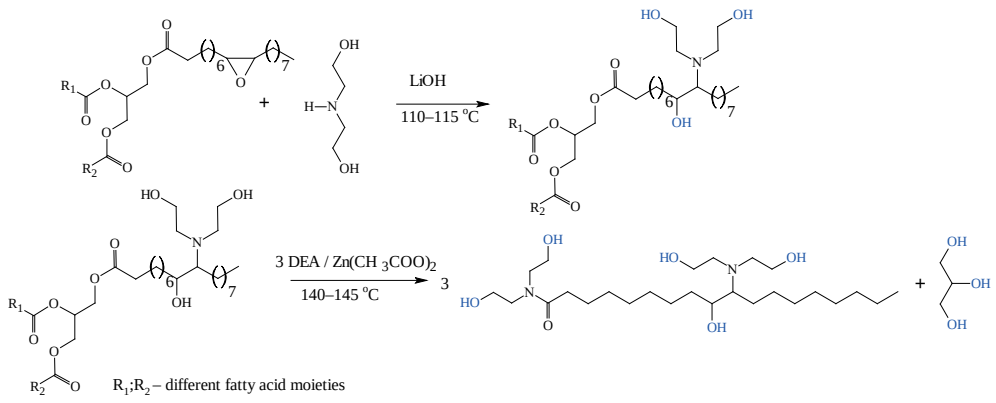

Fig. 2.4. Idealized ROEP epoxy ring opening and transamidation with DEOA.

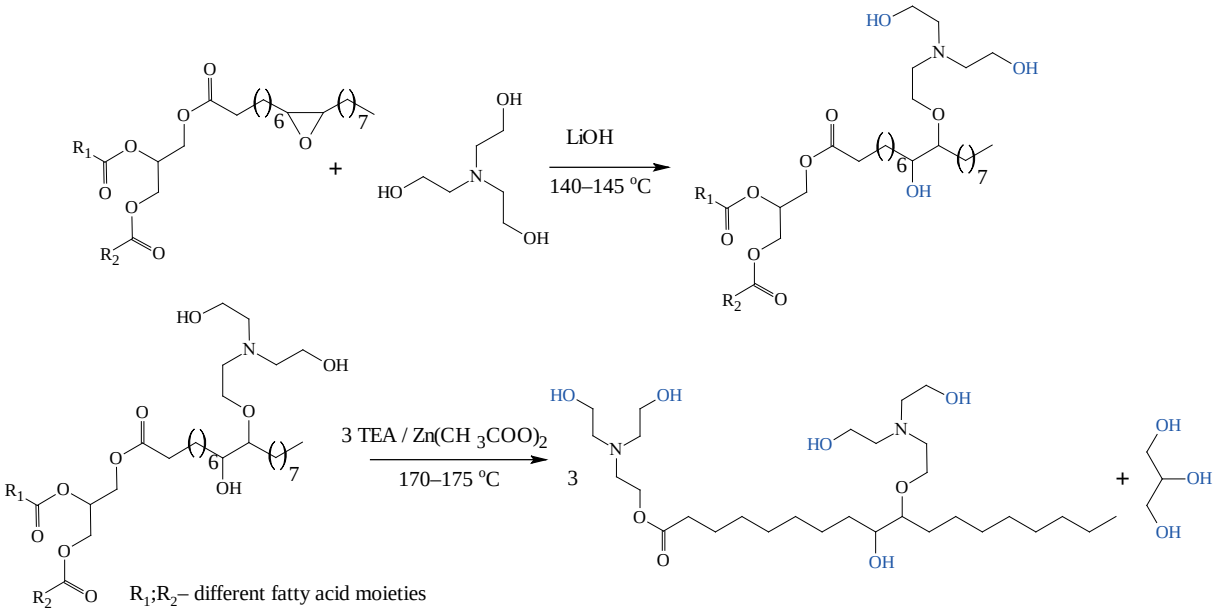

Fig. 2.5. Idealized ROEP epoxy ring opening and transesterification with TEOA.

High Functionality Bio-Based Polyol Synthesis From TOFA

Similar to RO based polyols the properties of the polyols could be improved by increasing average functionality of the polyols by epoxidation and subsequent epoxy ring opening reactions. Different parameter influence on the TOFA epoxidation process was studied in the frame of this Doctoral Thesis. Three different catalysts were used, such as H_2SO_4, ion exchange resin *Amberlite IR 120* as well as enzymatic catalyst *Novozym 435*. Furthermore, other synthesis parameters, such as Acetic acid content, H_2O_2 content and molar ratio as well as temperature influence on the TOFA epoxidation was investigated. Different catalysts were compared to select TOFA epoxidation method with highest relative conversion to oxirane, also the regeneration of the *Amberlite IR 120* catalyst was studied to confirm its commercial viability. The TOFA epoxidation kinetics were evaluated using mathematical model based on surface reaction mechanism. The overall work flow of TOFA epoxidation is depicted in Fig. 2.6.

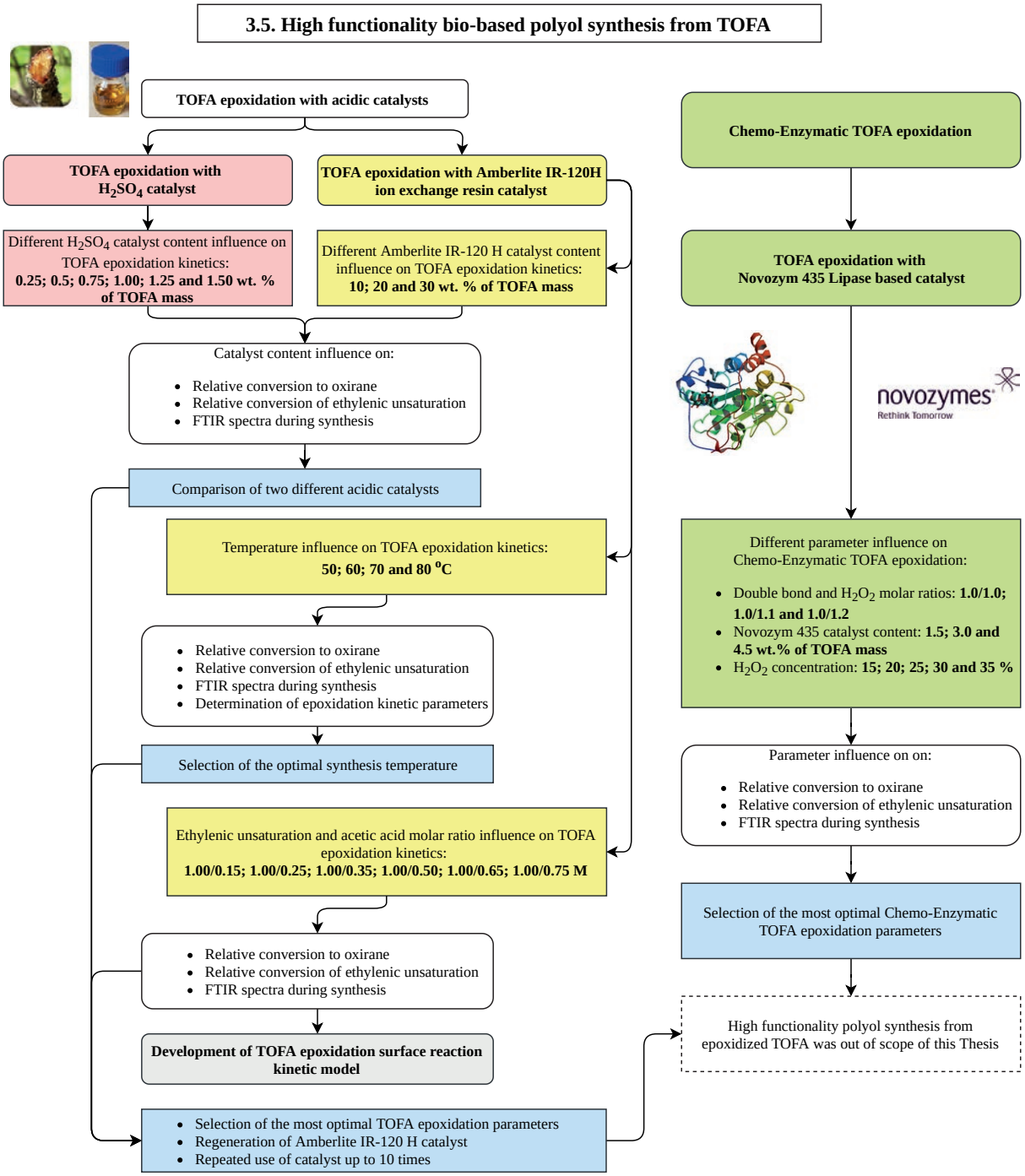

Fig.2.6. Work flow of TOFA epoxidation as a precursor for high functionality polyol synthesis.

Analysis Methods

The different methods and equipment used to characterise polyols are listed in Table 2.3, whereas the different methods and equipment used to characterise rigid PU foams are listed in Table 2.4.

Table 2.3

Analysis Methods of Polyols, Polyol Synthesis Products and Intermediates

Analysis method	Determined characteristic	Equipment	Relevant standard
Titrimetric	OH value	Laboratory burette, volume 25 mL, accuracy ±0.03 mL	DIN 53240-2
	Acid value		DIN 53402
	Iodine value		ISO 3961:2013
	Epoxy group content (OO_{ex}); the content of oxirane oxygen		ASTM D1652-11
	Polyol moisture	Denver Instrument Model 275KF automatic titration equipment	Alternative method to DIN 51777
Viscosity	Viscosity	Thermo Scientific HAAKE (Medium-High Range Rotational Viscometer).	
Gel permeation chromatography (GPC)	Number-average molecular weight (M_n) and number-average functionality (f_n) of the synthesized polyols	GPC from Knauer equipped with refractive index detector (Detector RI) and polystyrene/divinylbenzene matrix gel column with a measurement range up to 30 000 Da at eluent tetrahydrofuran eluent flow of 0.8 ml/min was used to analyse synthesized polyols.	
Fourier transform infrared (FTIR) spectroscopy	Polyol chemical structure	Thermo Fisher Nicolet iS50 spectrometer at a resolution of 4 cm^{-1}, 32 scans. The FTIR data was collected using an attenuated total reflectance technique with a ZnSe and Diamond crystals.	
Mass spectroscopy	Polyol chemical structure	The MALDI-TOF mass spectra were acquired with an Ultraflex, Bruker Daltonics, Bremen, Germany. The spectra were taken as the sum of 30000 shots with a DPSS Nd: YAG laser (355 nm, 1000 Hz). The specimens were prepared by the dried droplet method. The sample solution (10 mg/mL), DHB (2,5-Dihydroxybenzoic acid; 20 mg/mL) used as the matrix and sodium trifluoroacetate ($NaCF_3COO$; 10 mg/mL) as a cationization agent in THF were mixed at a volume ratio of 4:20:1.1 μL, and the mixture was deposited on the ground-steel target plate. The drop was dried in the ambient atmosphere.	

Table 2.4

Equipment Used for Rigid PU Foam Characterization and Relevant Testing Standards

Determined characteristic	Equipment
Rigid PU foam apparent density	Digital callipers, resolution 0.01 mm; laboratory balance, resolution 0.001 g; testing according to ISO 845
Rigid PU foam foaming technological parameters	Rigid PU foam formulation was optimized using FOAMAT equipment. This equipment measures foaming parameters (cream time, gel time, end time and track free time). Furthermore, the kinetics of the foaming process is represented as a change of the foam height, the temperature in the foam core, the pressure fluctuations at the base of the mould and change of dielectric polarization of the foamed material.
Compression strength	Zwick/Roel l1000 N testing machine, testing according to ISO 844
Tensile strength	Zwick/Roel l1000 N testing machine, testing according to ISO 1926
Closed cell content	Equipment developed at LS IWC, testing according to ISO 4590
Thermal conductivity	Linseis HMF 200, measurement range 0 °C to +20 °C, testing according to ISO 8301.

Continuation of Table 2.4

Determined characteristic	Equipment
Scanning electron microscope (SEM) imaging	Tescan TS 5136 MM SEM with a secondary electron (SE) detector. Before the SEM investigation, samples with a size of 1 cm × 1 cm × 0.2 cm were cut and sputtered with a gold layer using an Emitech K550X sputter coater (current 25 mA, coating time 2 min). Obtained data and images were processed with Vega TC software.
Rigid PU foam chemical structure analysis using FTIR spectroscopy	Thermo Fisher Nicolet iS50 spectrometer at a resolution of 4 cm^{-1}, 32 scans. The FTIR data was collected using an attenuated total reflectance technique with a ZnSe and Diamond crystals.
Glass transition temperature determination using dynamic mechanical analysis (DMA)	Mettler Toledo DMA/SDTA 861e equipment in the compression regime. DMA was performed using a constant frequency of 1 Hz and an amplitude of 20 µm. A heating rate of 3 °C/min and a temperature range between –50 °C and 200 °C were also used. The glass transition temperature (T_g) from DMA analysis was considered as a peak point of tanδ.
Thermal degradation of PU foams was analysed by thermogravimetric analysis (TGA).	Discovery TGA equipment from TA instruments. Foam samples of 10 mg ± 1 mg were placed on platinum scale pans and heated in an air or nitrogen atmosphere at 10 °C/min in a temperature range between 25–1000 °C. Data processing was performed using the OriginPro 8.5.1. and TA Instruments Universal Analysis 2000 v4.5A software.
Flammability analysis – Cone Calorimeter	The reaction to the 35 kW/m^2 heat flux was tested using FTT Dual Cone Calorimeter from Fire Testing Technology Ltd. The peak heat release rate (pHRR, kW/m^2); time to pHRR (TTP, s); ignition time (IT, s); time to flame out (FOT, s); total smoke release (TSR, m^2/m^2) and maximum average rate of heat emission (MARHE, kW/m^2) were determined according to the ISO 5660 standard.
Flammability analysis – reaction to flame source	Single-Flame Source Test (Ignitability Apparatus) from Fire Testing Technologies, UK. Developed rigid PU/PIR foams were tested according to ISO 11925-2 standard. The foam sample was exposed to a small propane flame which was applied at a 45 ° degree angle at the bottom of the sample. The propane flame was applied for 15 s after which the flame source was removed from the sample surface and the material was allowed to burn autonomously for additional 15 s.

3. RESULTS AND DISCUSSION

3.1. High-Density Rigid PU Foam Development From Sustainable Raw Materials

High-Density Rigid PU Foam Formulations

To compare the different polyols, isocyanate index was chosen 160 for all PU foam formulations. Isocyanate index is the ratio of the equivalent amount of isocyanate used relative to the theoretical equivalent amount of times 100. Developed rigid PU foam formulations are depicted in Table 3.1. Sustainable material content was calculated based on the mass of renewable/recycled materials used in PU foam formulation. Stoichiometric ratios of tall oil and rapeseed oil in polyols were taken into account as well as approximate sorbitol content in Lupranol 3422. The technological parameters of the developed formulations were determined from the cup tests from which the free rise density and closed cell content samples were cut (Table 3.1; PU Foam Properties). Furthermore, the molecular weight between two crosslinking points (M_c) was calculated based on proposed formulation and average molecular mass of the polyols and their average functionality using the method proposed by U. Stirna et al. [2], [39].

Table 3.1

Polyol Formulation, Renewable Material Content in PU Foams, FreeRise Density, ClosedCell Content and a Molecular Weight Between Two Crosslinking Points of PU Foams

Polyol formulation	TO_TEOA polyol	RO_TEOA polyol	NEO 240	NEO 380
Green Polyol, pbw	80.0			
Cross-linkage reagent, Lupranol 3422, pbw	20.0			
Flame retardant, TCPP, pbw	20.0			
Blowing reagent, water, pbw	1.0			
Reactive catalyst, PC CAT NP 10, pbw	0.3	0.3	1.6	1.6
Surfactant, NIAX Silicone L6915, pbw	2.0			
Polyisocyanate, pbw	184	189	150	193
Isocyanate index	160	160	160	160
Formulation characteristics				
Renewable/recycled materials in PU foam, %	**26**	**26**	**29**	**25**
PU foam properties				
Free rise, apparent density, kg/m^3	140	155	161	145
Closed cell count, %	96	99	91	99
Apparent density of moulded PU foams, kg/m^3	203	203	208	210
M_c, g/mol	552	536	499	453

High-density rigid PU foam samples were obtained in the stainless steel mould. This was done to ensure the uniformity of the different formulations. The targeted density of the rigid PU foams was 200 kg/m^3, which was achieved with acceptable deviations. It can be seen that despite the equal amount of blowing agent (water) the free rise density of the foams is not

equivalent due to the differences in polyol viscosities and reactivity. It was not possible to change the blowing agent amount, because that would change the chemical composition of the PU polymer matrix as water reacts with the isocyanate. Furthermore, the different apparent free rise densities would not allow comparing the mechanical properties of the foams.

Different Sustainable Polyol Influence on High-Density Rigid PU Foam Cell Morphology

SEM was used to obtain images of the developed high-density rigid PU foams from which average cell length, width and anisotropy index were determined (Table 3.2). It can be seen that the polyol type did not influence the isotropic properties of the PU foams. The average anisotropy coefficient across all types of polyols used to develop rigid PU foams was 0.98 ± 0.03. The stainless steel mould constrained the PU foam rise, thus the foam cells could not elongate parallel to the foaming direction. Nevertheless, there was a noticeable difference in cell density of PU foams, which were based on the NEO 380 APP polyol. The SEM images of the developed rigid PU foams from renewable and recycled resources and their cell size distribution histograms are shown in Fig. 3.1 and Fig. 3.2, respectively.

Table 3.2

Cell Dimensions and Coefficient of Anisotropy for Obtained PU Foams

Polyol type	Cell length, μm	Cell width, μm	Anisotropy coefficient	Cell density, cells per $cm^3 \cdot 10^{12}$
TO_TEOA	158 ± 33	165 ± 34	0.96 ± 0.02	1.360
RO_TEOA	252 ± 42	268 ± 45	0.94 ± 0.02	0.323
NEO 240	155 ± 23	153 ± 21	1.01 ± 0.02	1.550
NEO 380	123 ± 21	123 ± 21	1.00 ± 0.02	5.180

It can be seen that foams from RO/TEOA polyol have largest cells as well as most broad/uneven cell size distribution. Further results will indicate that the large cell size of rigid PU foams based on RO_TEOA polyol directly influence the mechanical properties. The idealised chemical structure of TO_TEOA and RO_TEOA should be similar. The slight difference in the viscosity of the polyols (280 mPa·s and 190 mPa·s), as well as glycerine that is formed during the transesterification reaction, could be the main contributors for the cell size difference.

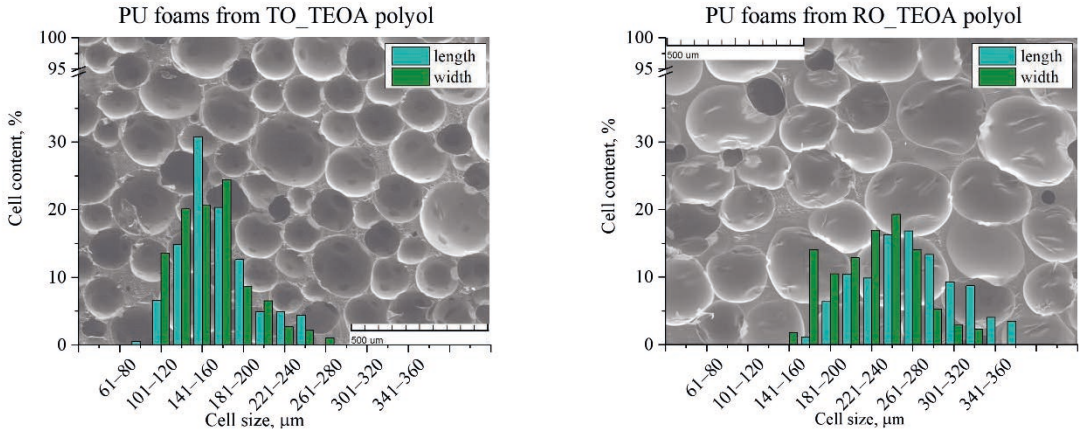

Fig. 3.1. SEM images of high-density rigid PU foams from bio-based polyols.

When compared to PU foams from bio-based polyols, PU foams from recycled PET-based polyols showed smaller cell size and more uniform cell size distribution as seen in Fig. 3.2. The high repeatability and even structure of rigid PU foam from recycled PET polyol was one of the reasons that this material was selected for further investigations.

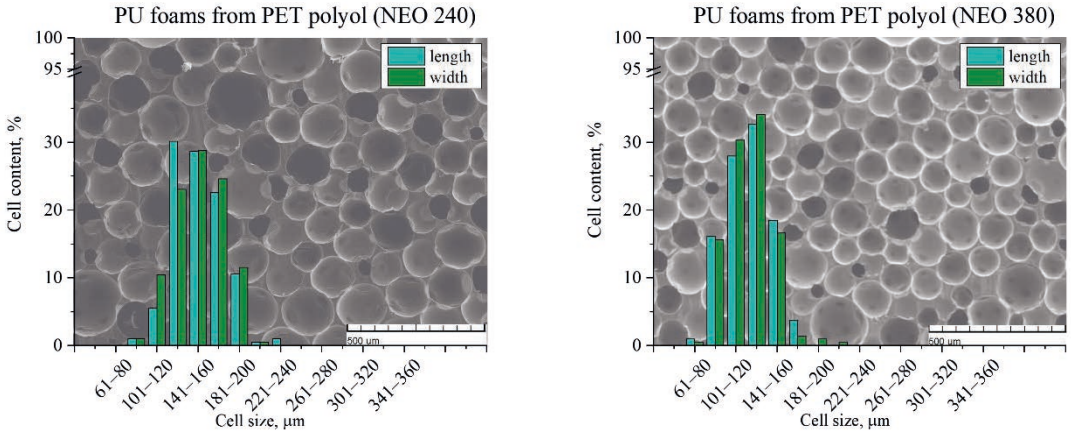

Fig 3.2. SEM images of high-density rigid PU foams from recycled PET-based polyols.

The Compression Strength of PU Foams From Sustainable Polyols

Compression strength was measured parallel and perpendicular to the foaming direction to confirm the isotropic properties of developed materials. It must be noted that isotropic properties of the foamed material are more dependent on foam production method and mould design than on material formulation. Compression strength and Young's modulus of developed PU foams are shown in Fig. 3.3. The apparent density of tested foams was 200 kg/m^3 ± 3 kg/m^3 and 200 kg/m^3 ± 5 kg/m^3 parallel and perpendicular to the foaming direction. The developed rigid PU foam showed almost isotropic mechanical properties, which correlate with the measured cell size distribution of the foams (Figs. 3.1 and 3.2). The slight deviation from ideal isotropic material is explained by the difference in apparent densities of the samples. Rigid PU foam does not have perfect apparent density distribution through the whole material. Foam near the mould walls tends to increase its density, this results in the relatively high standard deviation of the mechanical characteristics [49].

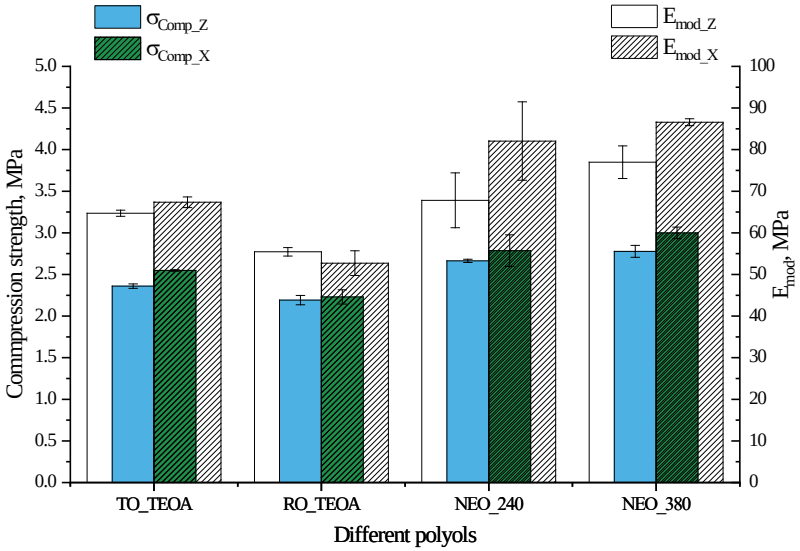

Fig. 3.3. Compression strength and Young's modulus of rigid PU foams from sustainable polyols measured parallel (*z*) and perpendicular (*x*) to foaming direction.

There is a slight difference in compression strength (~15−21 %) and Young's modulus (~22−39 %) between rigid PU foams obtained from bio-based polyols and APP polyols. APP polyol based rigid PU foams exhibit higher mechanical stiffness and load-bearing capability. The main reason for the different mechanical properties is different chemical structure of base polyols as other factors influencing rigid PU foam mechanical properties were the same for the set of experiments (apparent density; isocyanate index; blowing agent content; foaming and curing conditions). Aromatic ring structure delivers higher stiffness of the polymer matrix as aromatic chains are less flexible than aliphatic structures. Furthermore, the difference in the mechanical properties of the developed foams can be explained by the different molecular weight of links between two crosslinking points M_c. Rigid PU foams obtained from TO_TEOA and RO_TEOA polyols had lower compression strength and Young's modulus than APP based PU foams, which correlates with the M_c of different PU polymer matrices. Higher compression performance of NEO_380 polyol based foams is explained by higher aromaticity of polymer matrix due to APP polyol structure. The bio-based polyols showed the lowest mechanical strength value also when neat monolithic (solid) PU polymer was obtained [50].

Thermal Properties of PU Foams From Sustainable Polyols

For polymers, one of the most important characteristics is the glass transition temperature (T_g), which is a temperature region where polymer an amorphous substance transfers from hard, glassy material to a soft, rubbery material. Contrary to crystalline materials T_g is not a distinct thermodynamic transition like melting/crystallisation temperature but a temperature region, sometimes up to 50 K wide. Different factors can influence the T_g of PU materials, like hard segment content, the crosslink density of polymer matrix, different plasticisers as well as the chemical structure of raw materials (polyols, isocyanate – aliphatic/aromatic) [51].

For this work, the T_g of developed rigid PU foams was determined using DMA and DSC analysis methods. The summary of obtained T_g results is depicted in Table 3.3. Interpretation of obtained results is problematic, as they do not correlate with calculated M_c values in the case of rigid PU foam obtained from bio-based polyols. Furthermore, there is a noticeable discrepancy between T_g obtained using the DMA method and T_g obtained from DSC curves. Usually, the difference between these two different methods is about 10−20 K [51]. The drop of E' and tanδ can differ up to 25 K, which is accurate for rigid PU foams developed from APP polyols but not for rigid PU foams from bio-based polyols [51]. It should be mentioned that another method for T_g determination − Thermo Mechanical Analysis (TMA) − was used, but it was observed that it is not sensitive enough to evaluate T_g of the developed rigid PU foams. To sum up, the T_g of the developed rigid PU foams is higher than intended work temperature, thus material will be in glassy state during its exploitation. Further increase of T_g should not be needed as at temperatures above 150−200 °C a thermal degradation of the PU matrix can occur.

Table 3.3

T_g of Developed Rigid PU Foams from Sustainable Raw Materials

Polyol type	DMA T_g, °C	tanδ, °C	DSC T_g, °C
TO_TEOA	51.2	142.3	104.8
RO_TEOA	76.6	145.7	108.8
NEO 240	71.0	112.7	102.5
NEO 380	90.5	136.3	108.0

Density Influence on Mechanical Properties of Rigid PU Foams

Rigid PU foams are employed as an impact absorption material in the automotive industry due to their high energy absorption capacity while maintaining low apparent density. High mechanical properties at low apparent densities allow reducing the weight of the car part while fulfilling safety requirements of the vehicle. For impact absorption application rigid PU foams with apparent density ranging from 30 kg/m^3 to 400 kg/m^3 have been employed [52], [53]. For precise development of impact absorption material as well as modelling of rigid PU foam filled car part it is necessary to measure the stress-strain response of developed PU foams.

In the frame of this project, rigid PU foams in vast apparent density range between 50−600 kg/m^3 have been developed. The density of the rigid PU foams based on NEO 380 polyol was varied by modifying rigid PU foam formulation depicted in Table 3.1. To reach lower densities than the free rise density of described formulation of 145 kg/m^3, a physical blowing agent was added (Solkane 87/13) 4−10 pbw in the polyol component. Higher densities were achieved by a high degree of overfilling the stainless steel mould, more reacting mass was poured into the mould. The physical blowing agent was used to keep the same polymer matrix as the chemical blowing agent – water will change the composition of polymer structure. Obtained experimental data for compression yield strength and compression elastic modulus (Fig. 3.4) closely correlates to a power-law function $\sigma_{comp} \sim \rho^{1.75}$ and $E_{comp} \sim \rho^{1.68}$. Obtained relations are similar to previously reported by M. C. Hawkins et al. [54] and S. H. Goods [55].

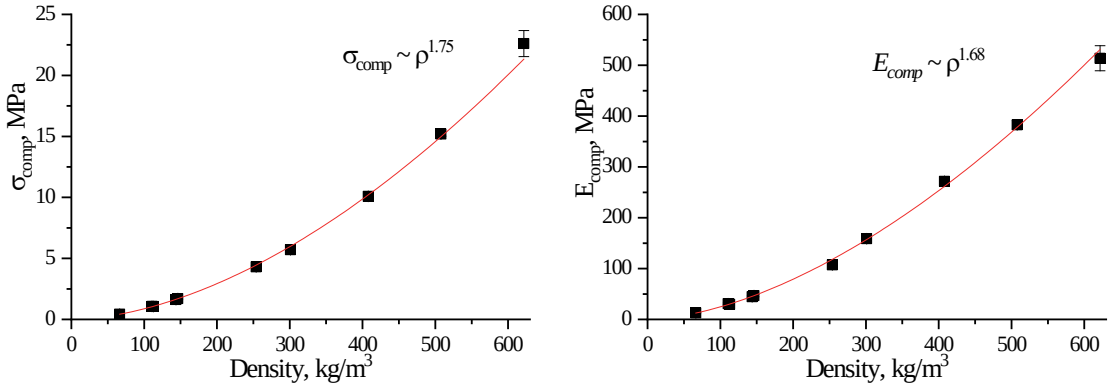

Fig. 3.4. Density influence on compression yield strength and elastic modulus of rigid PU foam from NEO 380 polyol.

Rigid PU foam apparent density influence on the tensile stiffness and strength is depicted in Fig. 3.5. Similar to compression strength results the experimental data can be closely approximated by a power-law relation $\sigma_{max} \sim \rho^{1.30}$ and $E_{mod} \sim \rho^{1.75}$. Obtained mechanical characteristics are comparable to the commercial materials obtained from petrochemical raw materials with similar apparent densities. Furthermore, developed formulations showed slightly superior tensile strength and Young's modulus than commercial rigid PU foams produced by NECUMER GmbH, Germany [56] and PUR 240 for Utah Foam Products, Inc. [57].

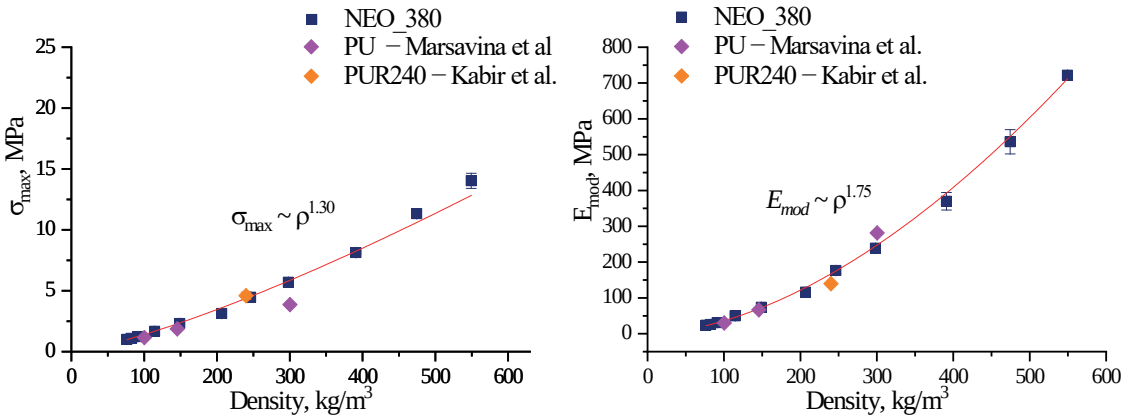

Fig. 3.5. Apparent density influence on tensile strength and Young's modulus of rigid PU foam from NEO 380 polyol.

Predicting Compression Stress-Strain Behaviour of Developed Rigid PU Foams

The mechanical characteristics of foams are strongly affected by their apparent density as well as strain rate during mechanical deformation. The design of structural parts with an impact mitigation functionality is generally performed using numerical simulation codes by employing the finite element modelling (FEM) for crash simulation. As input data for such simulations, compressive stress-strain diagrams of foams are utilized. A model of strain-rate and density-dependent stress-strain response that could be calibrated against a limited set of test data would allow reducing the number of actual foam tests needed to optimise material properties for car impact absorption part development

An analytical model of compression stress-strain response of rigid PU foams could be calibrated against a limited set of test data. This would allow reducing the number of tested samples of actual rigid PU foams needed for design of the automotive part. Several models of compressive stress σ as a function of strain ε have been proposed (Eq. 3.1). Furthermore, a multiplicative factor *g* allows to correct the model for different strain rates $\dot{\varepsilon}$.

$$\sigma(\varepsilon) = f(\varepsilon)g(\dot{\varepsilon}). \tag{3.1}$$

Explicit analytical relations for the parameters of $f(\varepsilon) = f(\dot{\varepsilon}, \rho)$ as functions of foam density ρ have been considered by Avalle, M. et al. and Liu Q. et al. [58], [59]. Such an approach makes it possible to predict the compressive response of foams at densities different from those against which the model has been calibrated.

In order to apply the Eq. 3.1 for predicting rigid PU foam compression strength properties the functions $f(\varepsilon)$ and $g(\dot{\varepsilon})$ need to be specified. Furthermore, function parameter dependency on rigid PU foam density must be accounted for. The analytical form of $f(\varepsilon)$ is expressed in Eq. 3.2 [53].

$$f(\varepsilon) = A\left(1 - \mathrm{e}^{-\frac{E}{A}\cdot\varepsilon(1-\varepsilon)^m}\right) + B\left(\frac{\varepsilon}{1-\varepsilon}\right)^n. \tag{3.2}$$

The parameters E, A and B can be interpreted as Young's modulus, the plateau of plastic deformation and modulus of densification respectively. Whereas the exponents *m* and *n* are density independent material characteristics. The parameters *E*, *A* and *B* dependency from rigid PU foam density is described by a power-law function.

$$E(\rho) = C_E\left(\frac{\rho}{\rho_S}\right)^{k_E};\ A(\rho) = C_A\left(\frac{\rho}{\rho_S}\right)^{k_A};\ B(\rho) = C_B\left(\frac{\rho}{\rho_S}\right)^{k_B}. \tag{3.3), (3.4), (3.5}$$

The C_E, C_A and C_B are pre-factors with the dimension of stress, k_E, k_A and k_B designate the respective exponents, and ρ_S is the density of monolithic (solid) PU polymer matrix.

The strain rate effect on compression properties of rigid PU foams was described by Nagy et al. [60] as depicted in Eq. 3.2.

$$g(\dot{\varepsilon}) = \left(\frac{\dot{\varepsilon}}{\dot{\varepsilon}_0}\right)^{a+b\varepsilon}. \tag{3.6}$$

Results presented by D. A. Apostol et al. suggest that exponent parameters *a* and *b* have relatively modest variation with PU foam density [61]. For simplification it was assumed them to be linear functions of density:

$$a(\rho) = C_a + k_a\frac{\rho}{\rho_S};\ b(\rho) = C_b + k_b\frac{\rho}{\rho_S}. \tag{3.7), (3.8}$$

Inserting Eqs. 3.2 and 3.6 into Eq. 3.1 an expression for engineering stress as a function of strain, strain rate and foam density was obtained:

$$\sigma(\varepsilon) = \left[A\left(1 - \mathrm{e}^{-\frac{E}{A}\cdot\varepsilon(1-\varepsilon)^m}\right) + B\left(\frac{\varepsilon}{1-\varepsilon}\right)^n\right]\left(\frac{\dot{\varepsilon}}{\dot{\varepsilon}_0}\right)^{a+b\varepsilon}. \tag{3.9}$$

Eq. 3.9 has seven different parameters, five describing the response at a reference strain rate $\dot{\varepsilon}_0$ (Eq. 3.2) and two for the strain rate effect (Eq. 3.6). All of the parameters except *m* and

n exponents are density-dependent parameters described by power-law or linear function containing two material constants C_i and k_i. A minimal set of experiments must be performed to calibrate Eq. 3.9. A compression test of foams of two different densities at two different strain rates (i.e. reference strain rate and another one).

Rigid PU foams with two different densities of 113 kg/m^3 ± 1 kg/m^3 and 311 kg/m^3 ± 3 kg/m^3 were tested at quasi-static strain rates of $\dot{\varepsilon}_0$ = 0.00167 s^{-1} (10 %/min; 2 mm/min) according to standard procedure ISO 844. The stress-strain response of tested rigid PU foams was used to determine the value parameters of Eq. 3.2 by minimizing the relative squared errors between the model and experimental data.

The approximation of the experimental data using Eq. 3.2 was successful as depicted in Fig. 3.6. The model reasonably well agrees with the experimental curves in broad rigid PU foam density range 113−513 kg/m^3. Using this model it will be possible to fine-tune the apparent density of rigid PU foams required for the development of impact absorption vehicle part.

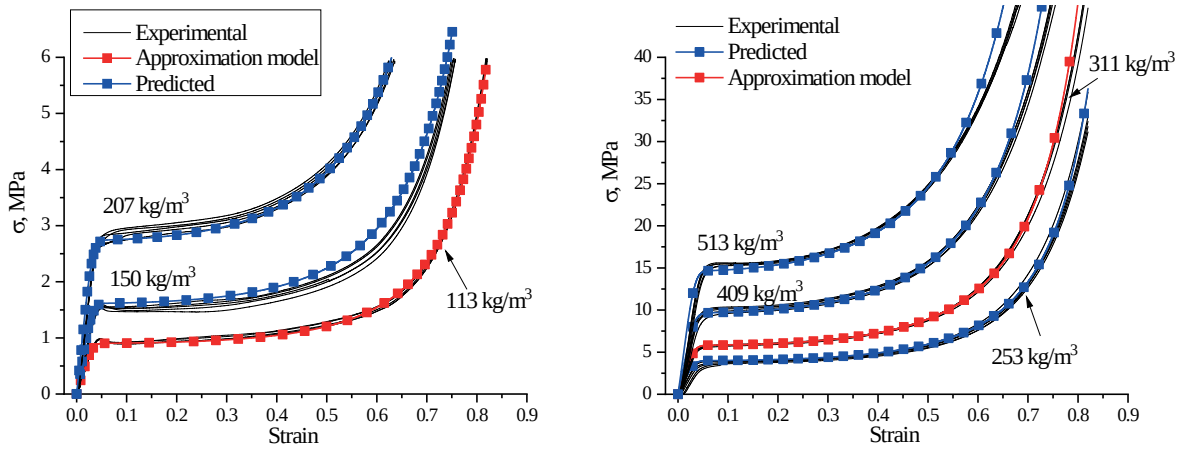

Fig. 3.6. Experimental stress-strain curves of rigid PU foams with different densities for strain rate $\dot{\varepsilon}$ = 0.00167 s^{-1} (10 %/min), an approximation of data and predicted stress strain curves using Eq. 3.2.

The strain rate effect on PU foam compression strength was evaluated after parameters of Eq. 3.2 were established for reference strain rate tests. Experimental data from tests at $\dot{\varepsilon}$ = 0.167 s^{-1} (1000 %/min; 200 mm/min) were used for the rigid PU foams with the same apparent density as before.

The approximation of rigid PU foam stress-strain curves at a strain rate of $\dot{\varepsilon}$ = 0.167 s^{-1} (1000 %/min) also agrees with the experimental data as depicted in Fig. 3.7. Furthermore, it was possible to predict the stress strain curves at different densities (150 kg/m^3; 207 kg/m^3; 253 kg/m^3; 409 kg/m^3 and 513 kg/m^3). The obtained coefficients of Eq. 3.4 allow to predict stress strain response of rigid PU foam at different densities as well as at different strain rates.

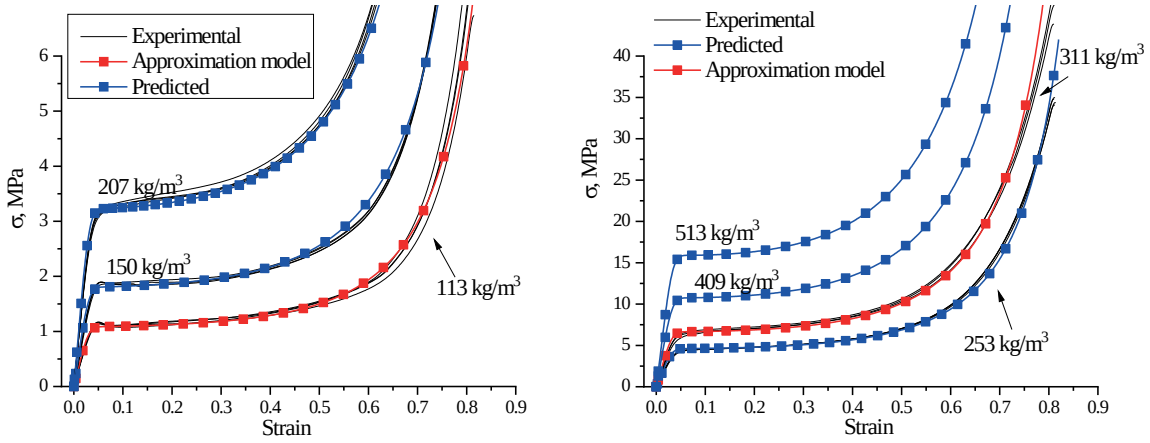

Fig. 3.7. Experimental stress-strain curves of rigid PU foams with different densities for strain rate $\varepsilon = 0.167\ s^{-1}$ (1000 %/min), an approximation of data and predicted stress-strain curves using Eq. 3.9.

The data obtained from dynamic compression of rigid PU foam using CEAST 9340 Drop Tower (Instron) equipment relatively well agreed with the proposed model as depicted in Fig. 3.8. It was difficult to optimise the speed of the striker and to choose the force gauge because the collected data contained a lot of noise signals. Nevertheless, the developed technique allowed to obtain stress-strain curves of rigid PU foams at relatively high strain rates (up to $180\ s^{-1}$; 3.6 m/s) which is not possible using standard mechanical analysis testing equipment. The results of dynamic compression of rigid PU foams validated the proposed model at high strain rates so it can be a useful tool to be used in FEM analysis [53]. To compare the different density and strain rate influence on material impact absorption ability, it is advantageous to evaluate values of absorbed energy at the same strain, which is represented as the area under the stress-strain curve [62]. For this study rigid PU foams were evaluated till strain of 0.6, which corresponds with the end of plastic deformation of material. Absorbed energy of rigid PU foams depicted in Fig. 3.8b shows that the density of the material has most significant influence on the impact absorption properties of the material and that the rigid PU foam are only lightly strain rate sensitive.

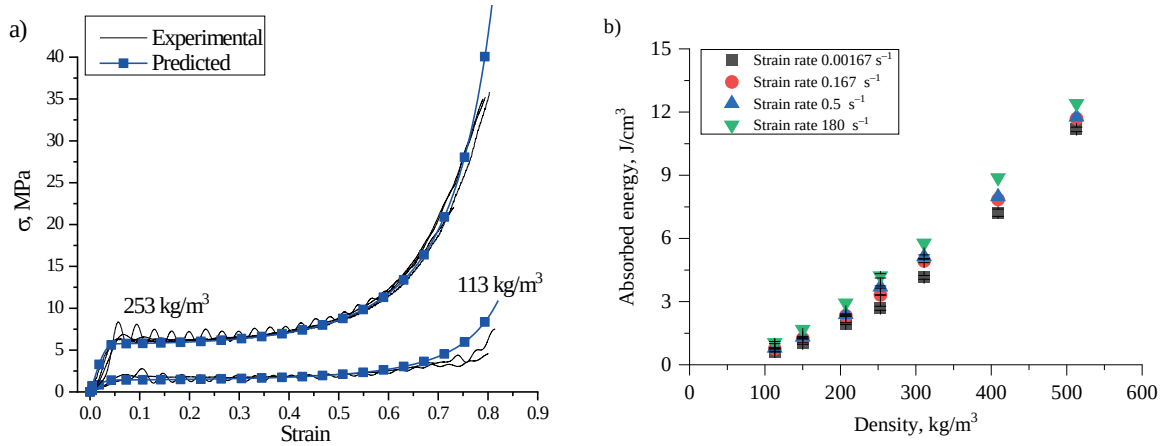

Fig. 3.8. a) Experimental stress-strain curves of rigid PU foams with different densities for strain rate $\varepsilon = 180\ s^{-1}$ (3.6 m/s) and predicted stress-strain curves using Eq. 3.9; b) absorbed energy of developed rigid PU foams till 0.6 strain of material at different densities and strain rates.

Development of Impact Absorption Demonstrator for the Automotive Industry

Global trends toward CO_2 reduction and resource efficiency have significantly increased the importance of lightweight materials over the last years. The European Commission (EC) has set severe targets for average new car CO_2 emissions of 95 g/km by 2020, and by 2030 it aims to reduce CO_2 emissions down to 75 g/km [63].Weight reduction of the vehicle directly decreases the energy consumption and subsequently reduces the CO_2 emissions. Additional reduction of the CO_2 emissions could be achieved by the use of materials that are obtained from the renewable or recycled feedstock, like polyurethane (PU) foams [64].

The weight reduction is particularly important for electric vehicles whose broader implementation is crucial to reduce the CO_2 emissions. Currently, the battery costs and the expected range of the vehicle are the most limiting factors for the slow rate of fully electric vehicles (FEVs) adoption for a larger consumer base. As a rough estimation, considering the battery costs for the year 2015, each slot of vehicle weight reduction of 50 kg implies a battery cost decreasing of about 500 EUR per car. This cost reduction can compensate for the additional cost due to light weighting, contributing to market penetration of EVs [65].

The body in white (BiW) is the heaviest vehicle element, representing about 40 % of total vehicle weight, hence the implementation of lightweight measures here appears effective. The project EVolution stands for “The Electric Vehicle revOLUTION enabled by advanced materials highly hybridized into lightweight components for easy integration and dismantling providing a reduced life-cycle cost logic”. Project EVolution finished in November 2016 and was a result of collaboration of 24 partners from 11 different European Union countries, with the goal to demonstrate the sustainable production of a fully electric 600 kg vehicle. EVolution project was principally based on Pininfarina Nido concept, which is fully electric and is an A-segment car conceived as a multifunctional rolling chassis plus a non-structural upper frame [66], [67]. The Nido FEV and the Nido BiW concept is shown in Fig. 3.9.

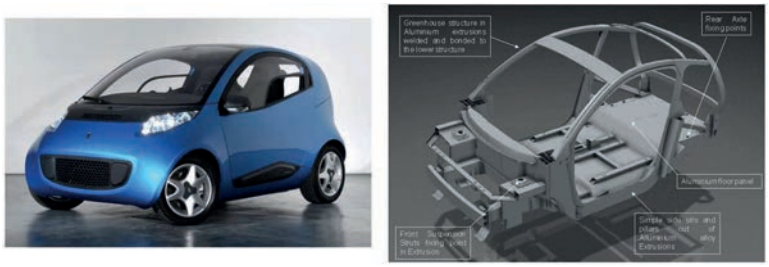

Fig. 3.9. Nido concept (left) and Nido BiW (right).

Latvian State Institute of Wood Chemistry (LS IWC) was one of the partners collaborating in EVolution project to design novel rigid PU foam material for impact absorption used in the front crossbeam of the vehicle. Rigid PU foams were developed from sustainable resources, polyols obtained from vegetable oils and recycled PET. Rigid PU foams were developed in a broad range of the apparent densities (50−600 kg/m^3) and their mechanical properties were investigated to select the material that is best suited for the core of the impact absorption element. The performance of the designed concept in vehicle crash was evaluated using FEM and subsequent crash test of the developed front crossbeam. The author was the main contributor from LS IWC

in frame of the project EVolution and rigid PU foam impact absorption element filled by the author is depicted in Fig. 3.10. Developed from cross-beam concept is about 50 % lighter than the steel equivalent while achieving good structural behaviour, considering EU standards of crash homologation and global static and dynamic performances.

Fig. 3.10. EVolution front bumper crossmember demonstrator prototype and the technological mock-up with integrated demonstrators.

The project demonstrated that it is possible to implement sustainable materials where high-performance requirements are demanded. Rigid PU foam formulations obtained from recycled PET showed high stability and good mechanical properties. Recycled PET polyols could be used to replace aromatic polyester polyols obtained from petrochemical materials.

3.2. Rigid PU Foam Nanocomposite Development

Addition of nanoparticles into the polymer matrix can significantly change the properties of the end composite. Reinforcement of polymer matrix usually is done to increase the mechanical properties of the material or to obtain other beneficial properties. Filling a rigid PU foam polymer matrix with nanoclay affects both the morphology and mechanical properties of the material. Well-dispersed nanoclay particles serve as nucleation sites promoting the bubble formation, which leads to a reduction of cell size of foams [68] , [69]. Furthermore, the nanoclay particles inside the cell walls work as a gas barrier, reducing the gas diffusivity through the foam. T. Widya & C. Macosko demonstrated that addition of nanoclays into rigid PU foam structure can decrease the gas permeability up to 82 %. The strong reduction in permeability is caused by the reduction of cell size as well as gas barrier effect of nanoclay particles [70] –[72]. Such an effect is important for the longevity of the thermal insulation as it allows to reduce the ageing of the thermal insulation material [73] .

Part 1B of the presented Doctoral Thesis describes the increase of the mechanical properties of previously developed high-density rigid PU foam by reinforcing their structure with nanoclay particles. With the aim of enhancing the physical and mechanical properties of rigid PU foams without detrimentally affecting their morphology, filling with nanoparticles was carried out by dispersing them either in the polyol or isocyanate component. Different dispersion methods were compared and their effect on intercalation/exfoliation of the layered structure of nanoclays were investigated.

Nanoclay dispersion trials showed that the dispersion method does not influence the change of the distance between lattice planes. In both nanoclay samples, the distance between

lattice plates increased. In the case of Cloisite 15A from 31.5 Å to 37.9 Å and in the case of Cloisite 30B from 18.5 Å to 37.6 Å. This indicates that the type of organic modifier of the montmorillonite has little influence on the intercalation/exfoliation of the nanoclay in the polyol. It was observed, that dispersions with Cloisite 30B are much more stable and nanoclay sediments at a much slower rate. The increased stability of the Cloisite 30B dispersions could be explained by the formation of hydrogen bonds of the nanoclays organic modifier and the carboxyl groups of the NEO_380 polyol. The XRD spectra of both Cloisite 15A and Cloisite 30B nanoclay dispersions in the NEO_380 polyol obtained by all three dispersion methods are depicted in Fig. 3.11a. The image clearly depicts that the X-ray diffraction spectra of the different dispersions are similar, thus it can be concluded that the mixing method does not influence the intercalation of the nanoclay. Furthermore, the exfoliation of the nanoclay lattice structure has not been achieved.

Exfoliation of the nanoclay lattice layers could be achieved by introducing major elastic forces in-between the nanoclay layers that overcome opposing electrostatic and Van der Waals forces. This was reported by J. H. Park and S. C. Jana where exfoliation of different nanoclays was achieved by curing reaction of epoxy resins [74]. A similar approach could be used for polyurethane materials where raw materials like pMDI, polyol, and/or catalysts are diffused inside the interlayer spacing of nanoplatelets of clay in presence/absence of a suitable solvent. A successful exfoliation of Cloisite 30B nanoclay in the isocyanate component of rigid PU foams was reported by P. Mondal and D. Khakhar [69]. During subsequent polymerization, the polymer chains grow leading to the expansion of inter-layer spacing and exfoliation of nanoplatelets in the polymer matrix [75].

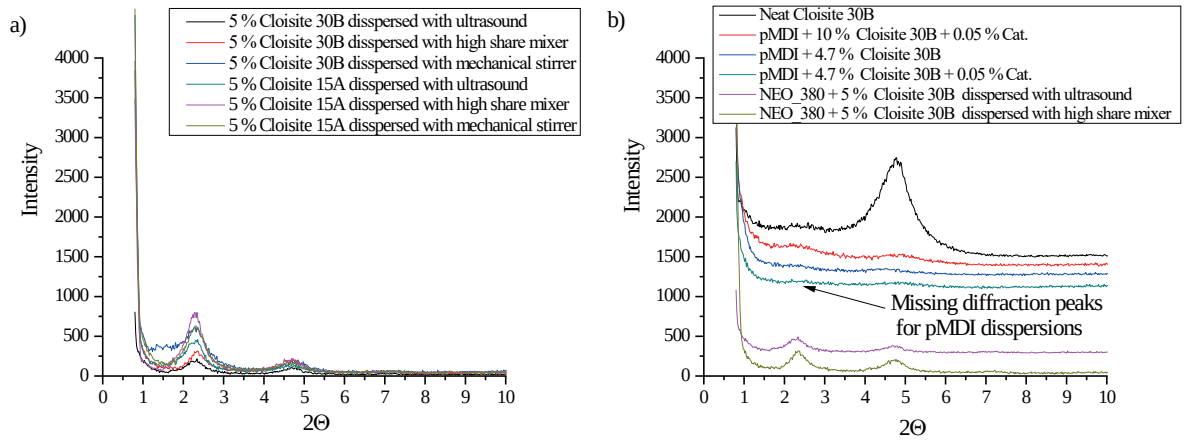

Fig. 3.11. X-ray diffraction spectra a) for 5 wt. % of Cloisite 30B and Cloisite 15A dispersions in NEO_380 polyol; b) for Cloisite 30B dispersion in polyisocyanate.

The organic modifier of Cloisite 30B contains OH groups that are reactive with isocyanate. The exfoliation of Cloisite 30B was done by adding the nanoclay particles into a pMDI component of rigid PU foam formulation. Two different Cloisite 30B contents of 4.7 wt. % and 10 wt. % were evaluated. The reaction between OH and NCO groups was catalysed by adding 0.05 wt. % of dibutyltin dilaurate urethane formation catalyst. The X-ray diffraction spectra of exfoliated Cloisite 30B nanoclay are depicted in Fig. 3.11b. It is clear

that Cloisite 30B dispersion in the pMDI component is much different than nanoclay dispersion in NEO_380 polyol. Even at high Cloisite 30B nanoclay load of 10 wt. % the diffraction peaks disappeared, which indicated the exfoliation of the layered structure of the Cloisite 30B.

Morphological Properties of PU Foams Modified With Nanoclay

Cloisite 15A nanoclay influence on the morphological properties of rigid PU foams were investigated at several different filler contents, 0.0 wt. %; 0.5 wt. %; 1.29 wt. %; 2.68 wt. % and 5.83 wt. % in rigid PU foam by mass. Furthermore, Cloisite 30B was also investigated at 0.6 wt. % and 0.7 wt. %. Nanoclay was dispersed using ultrasound sonification method. The average cell size distribution histograms for the Cloisite 15A filled rigid PU foams, as well as the measured average cell size, are depicted in Fig. 3.12.

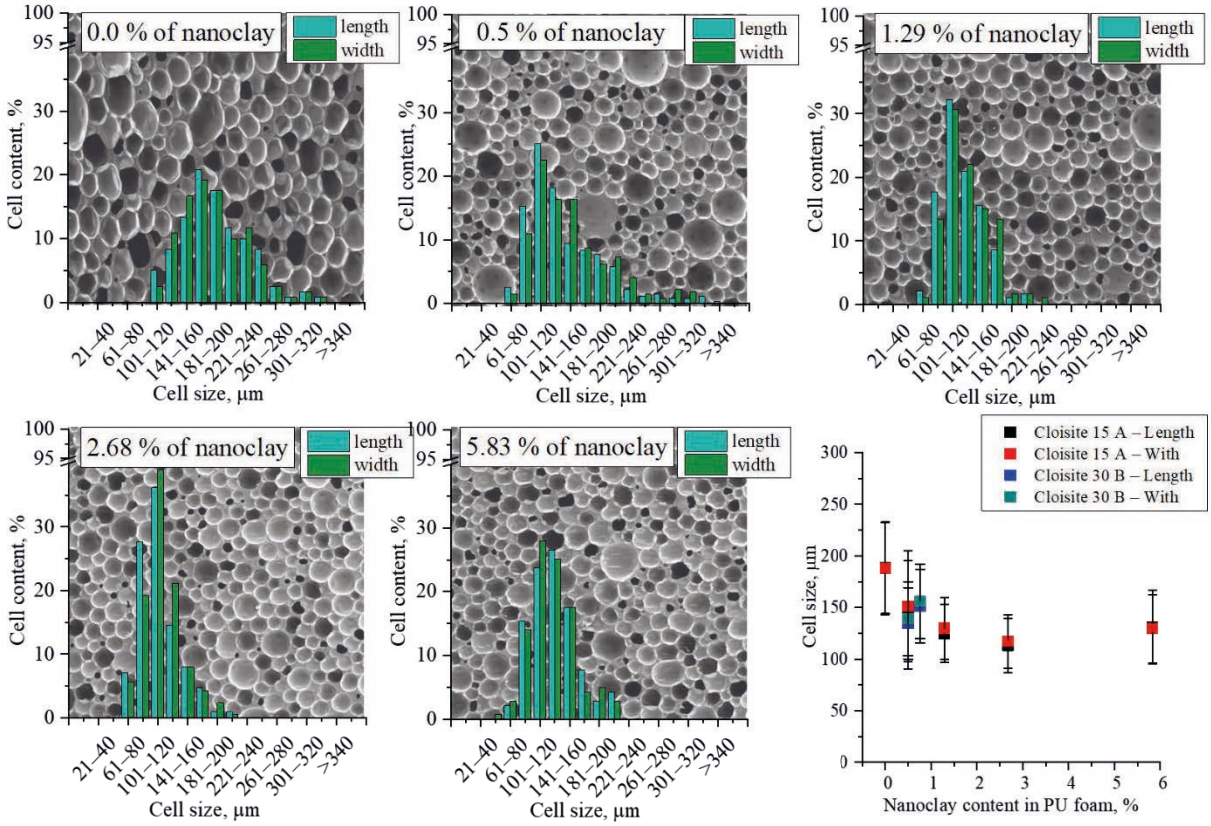

Fig. 3.12. The cell size distribution of rigid PU foams filled with Cloisite 15 A nanoclay.

The addition of nanoclay into rigid PU foam structure did not disturb the isotropic cell structure. The anisotropy coefficient was in-between 0.9 – 1.0 for all of the measured samples. Nanoclay addition into rigid PU foam matrix decreased the average cell size from 118 to 113 µm for the neat rigid PU foam and 2.68 wt. % nanoclay content, respectively. The decrease of cell size can be explained by the nucleation effect of gas micro-bubbles on the surface of the nanoparticles thus increasing cell count and decreasing overall cell size. The decrease of average cell size was similar for Cloisite 15A and Cloisite 30B nanoclay fillers. Which indicates that the organic modifier of the nanoclays does not influence cell formation

of rigid PU foams. At higher nanoclay loads above 2.68 wt. % the decrease of the cell size reached a plateau. A similar trend of rigid PU foam cell size decrease was observed by M. Thirumal et al. where Cloisite 30B was used as a filler [76]. Addition of nanoclay filler into rigid PU foam formulation significantly increased component viscosity. This introduces several technological issues for material production. At higher viscosities, it was difficult to sufficiently mix the polyol and isocyanate components. Furthermore, higher viscosity of the reacting mass hinders foam growth and formation of uniform material [77].

Mechanical Properties of Rigid PU Foams Modified With Nanoclay

Nanoclay dispersion method, as well as the two different nanoclay filler influence on the mechanical properties, were determined by compression and tensile tests at quasi-static strain rates. The X-ray diffraction analysis showed that Cloisite 30B nanoclay is exfoliated in dispersion in isocyanate (Fig. 3.10). Thus, compression properties of the developed rigid PU foams with Cloisite 30B dispersion in the isocyanate component were also tested. The targeted apparent density of tested rigid PU foams was 200 kg/m^3. The apparent density of the produced samples deviated by 200 ± 15 kg/m^3, thus compression strength test results were normalized to the average density of 200 kg/m^3 according to power law function described previously.

All nanoclay dispersion methods showed a similar increase of compression strength and Young's modulus of developed rigid PU foam samples. Cloisite 30 B showed slightly better performance as rigid PU foam reinforcement filler than Cloisite 15 A due to the presence of OH groups in the organic modifier of the nanoclay. At 1.29−2.68 wt. % of Cloisite 30B compression strength was increased by 15−24 % and Young's modulus by 13−29 %. An exfoliated nanoclay filler should yield a higher increase of the mechanical properties at lower nanoclay loading [75], [78]. Exfoliated Cloisite 30 B nanoclay allowed to achieve similar increase of mechanical properties at lower filler loadings of ~0.25−0.76 wt. % (Fig. 3.13). Achieved increase of the compression properties corresponds to literature data. Nevertheless, the achieved increase of the compression properties is not significant enough to counterweight the technological difficulties what the preparation of the nanocomposite implies.

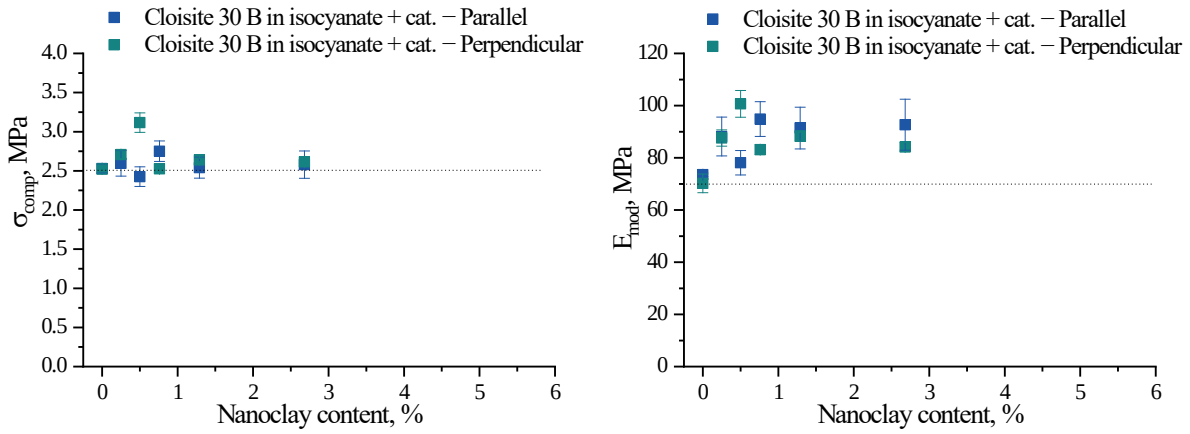

Fig. 3.13. Compression strength and Young's modulus of rigid PU foams filled with Cloisite 30B dispersed in isocyanate with added catalyst.

3.3. Low Flammability Rigid PU Foam Thermal Insulation Composite

Part 2 of this Thesis was performed in the frame of COST Action MP1105, FLARETEX: "Sustainable flame retardancy for textiles and related materials based on nanoparticles substituting conventional chemicals". In the frame of this project, alternative flame retardants were explored to replace halogenated flame retardants in bio-based rigid PU foam thermal insulation material. Several different options were investigated to replace commercially commonly used tris(chloropropyl)phosphate (TCPP). An additive dimethyl-propyl-phosphate (DMPP) was used as a direct replacement in typical rigid PU foam formulations. Furthermore, a composite material containing expandable graphite (EG) filler was developed by introducing EG particles in rigid PU foam matrix and by developing the layered sandwich structure of rigid PU foam and intumescent flame retardant non-woven fabric (IF). The effect on the flammability of developed rigid PU foams with more sustainable flame retardants was studied using Cone Calorimeter (ISO 5660) equipment and single-flame source test according to ISO 11925 -2 standard. Rigid PU foam formulation developed during M. Kirpluks' Master's Thesis was used as a base material to test the novel flame retardants. The main polyol in this rigid PU foam formulation was obtained from TOFA using amidation process with DEOA. The obtained results will show that non-halogenated flame retardants can yield significant reduction of rigid PU foam flammability.

The neat formulation of TOFA_DEOA polyol based rigid PU foam was modified by adding different flame retardants into the polyol component. Conventional, liquid flame retardants TCPP and DMPP were compared at 7 wt. % of rigid PU foam mass. The EG flakes were also added into the polyol component. A possible synergistic effect between PIR groups and non-halogenated flame retardants was studied by changing the isocyanate index of the rigid PU foams (indices of 110, 150, 200 and 250 were tested). A sandwich like composite where rigid PU foam is protected by non-woven IF was obtained by producing samples in a stainless steel mould. The bottom of the mould was lined with the intumescent non-woven fabric, and reacting rigid PU foam mass was poured on top of it. The long start time of the foam formulation (τ_{cream} ~ 35 s) insured good adhesion between the intumescent non-woven fabric and rigid PU foam. No additional adhesive was necessary, which shows the potential of this technology in the state of art rigid PU/PIR continuous panel production. Different types of developed rigid PU foam samples are depicted in Fig. 3.14.

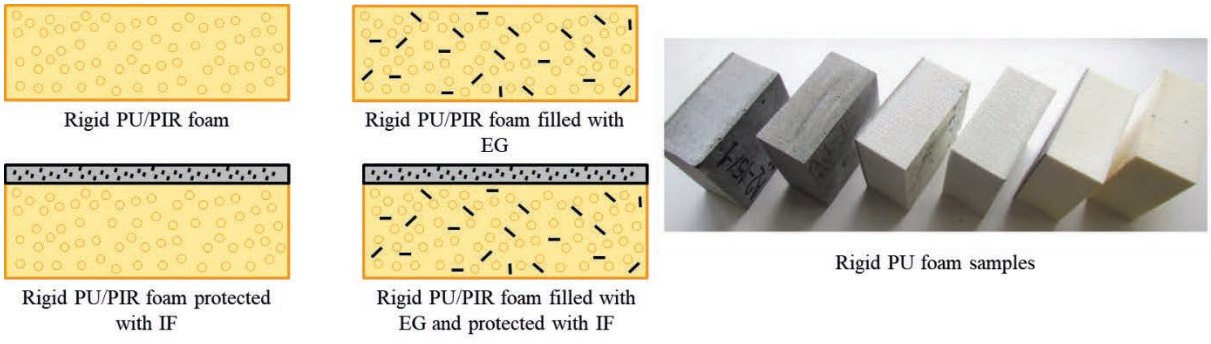

Fig. 3.14. Rigid PU foam sample types used for flammability analysis.

Thermal Conductivity of the Developed Rigid PU/PIR Foams

The main characteristics of any thermal insulation material are thermal conductivity (λ) and thermal resistance. Fig. 3.15 shows the measured λ for the rigid PU foam obtained from the TOFA_DEOA polyol and filled with different amounts of EG particles. The λ of rigid PU foams containing EG loadings of 0 wt. %; 3 wt. %; 9 wt. %; and 15 wt. % are compared for rigid PU foams without liquid flame retardant (Fig. 3.15a) and with 7 wt. % of DMPP (Fig. 3.17b). Furthermore, the λ of rigid PU foam composites containing non-woven IF layer was also measured. It can be seen that non-woven IF layer has no effect on the λ value of the rigid PU foams but there is a clear increase of λ with the addition of EG. Graphite is a good heat conductor, thus it is no surprise that λ value increased. Furthermore, the EG particles disrupt the cell morphology of rigid PU foams further decreasing the efficiency of the insulation material. The λ value of the neat rigid PU foams with no DMPP FR was 24.44 mW/(m·K), which is considered acceptable for the material that could be used in civil engineering. Unfortunately, the addition of DMPP increased λ value up to 28.74 mW/(m·K). The increase of λ value with the addition of DMPP is explained by plasticization and decrease of the overall crosslink density of the rigid PU foam polymer matrix. Most of the conventional additive liquid flame retardants decrease the glass transition temperature of the PU polymer matrix [79]. The rapid jump of λ value can be explained by CO_2 emission from closed cells of rigid PU foam and its substitution with air (O_2 and N_2). Such effect is highly undesirable because, at λ value of 28.74 mW/(m·K), the thermal insulation properties of the developed rigid PU foams are comparable to XPS/EPS. Rigid PU foams cannot compete with XPS/EPS in terms of price, and bio-based feedstock will not counterweigh the price/performance of increased λ value. It must be mentioned that the closed cell content of all developed rigid PU foams was above 90 %. The substitution of CO_2 or another gas (blowing agent) with air in conventional PU foams is a slow process and takes years [80]. However, even with a λ value of 28.74 mW/(m·K), the developed rigid PU foams are an efficient thermal insulation material that can be applied in civil engineering. A similar increase of λ value (from 26 mW/(m·K) to 28 mW/(m·K)) was observed by L. Gao et al. for EG and diethyl ethyl phosphonate filled rigid PU/PIR foams [81].

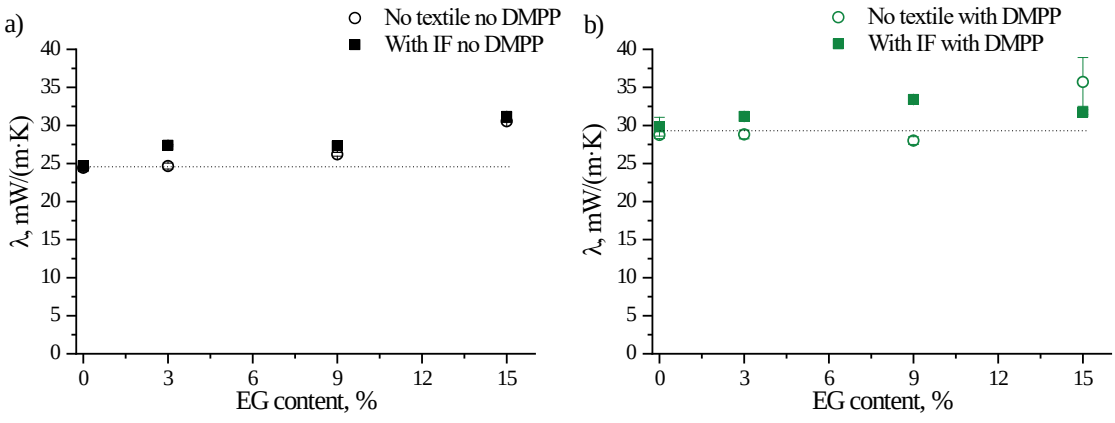

Fig. 3.15. Thermal conductivity of rigid PU foams (II-110) protected with IF: a) with no liquid FR and with EG; b) with DMPP as FR and EG.

Developed composites had good surface adhesion between EG particles and rigid PU/PIR foam polymer matrix (Fig. 3.16). The SEM images clearly depict the disruption of the even cell structure of rigid PU/PIR foams by EG particles. The main objective of this study was to obtain rigid PU/PIR foams with decreased flammability without losing superior thermal insulation properties. This was done by protecting one side of the PU foam material with non-woven IF, as shown in Fig. 3.14. Reacting foam mass was poured on top of the non-woven IF, which insured good adhesion of the foam material to the glass fibres. The adhesion layer of the composite is depicted in Fig. 3.16. It can be seen that the rigid PU/PIR polymer matrix is incorporated into the glass fibre structure of the non-woven fabric. Some rigid PU/PIR foam cells are undoubtedly formed in-between glass fibres. No additional adhesive was necessary for the developed composite.

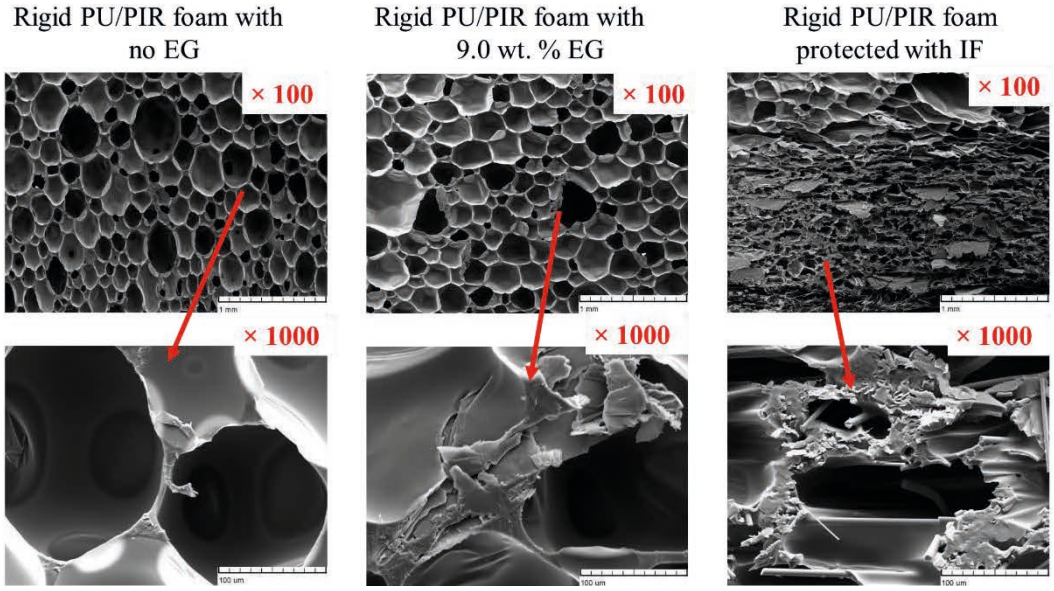

Fig. 3.16. SEM images of neat rigid PU/PIR foams, PU/PIR foams filled with 9 % EG and intumescent non-woven fabric and rigid PU/PIR foam composite.

Flammability of Developed Rigid PU/PIR Foams

The cone calorimeter test gives a significant amount of information about the flammability of the tested materials and their reaction to the heat flux. This test is a useful technique to compare different materials and gain an initial idea of how a material will react in a fire disaster scenario. In the cone calorimeter test, the material is subjected to the constant radiant heat flux $q_{ext} = 00$ kW/m^2, where the flux of 35 kW/m^2 or 0 kW/m^2 is most commonly used [8] [– 83]. The small sample size of 10 mm × 10 mm × 0 mm makes this technique particularly useful to compare and optimize materials, as for the Single Burning Item (EN 13823) test much bigger samples are required [8] . The cone calorimeter test gives an initial idea of how a material will behave in an open fire scenario. Common material characteristics that are obtained during this test are kinetic curves of the heat release rate (HRR), time to ignition (TTI), total heat released (THR), peak of heat release rate (pHRR), total smoke release (TSR), and maximum average rate of heat emission (MARHE). pHRR can be used to compare materials provided that the test setup conditions are kept constant for

all tested samples (sample thickness, sample holder, distance from the heater, heat flux, air flow, etc.). Furthermore, the kinetic curves of the HRR give an excellent idea about material flammability as the data monitors sample behaviour through the whole burning process.

The addition of trimerization products of isocyanate groups into the PU/PIR polymer matrix increases its thermal stability and decreases flammability, which is depicted as a smaller area under the HRR curve in Fig. 3.17a. The increase of the isocyanate index from 110 to 250 decreased pHRR from 355 kW/m^2 to 300 kW/m^2. The increase of the isocyanate index prolonged the burning of PU/PIR foam but the material burned with less intensity. Fig. 3.17b depicts HRR curves of PU/PIR foams protected with IF. There was no heat release detected because the material did not ignite during the test time when subjugated to a heat flux of 35 kW/m^2. The unwoven intumescent fabric did what it was designed to do and formed a protective char layer on top of the rigid PU/PIR foam. The images of rigid PU/PIR foam during cone calorimeter test are depicted in Fig. 3.17. The IF formed a thick char layer on top of the PU/PIR foam that stopped the thermal degradation of the PU/PIR polymer matrix. The unwoven intumescent fabric gives excellent flame protection while keeping low thermal conductivity values as seen in Fig. 3.15.

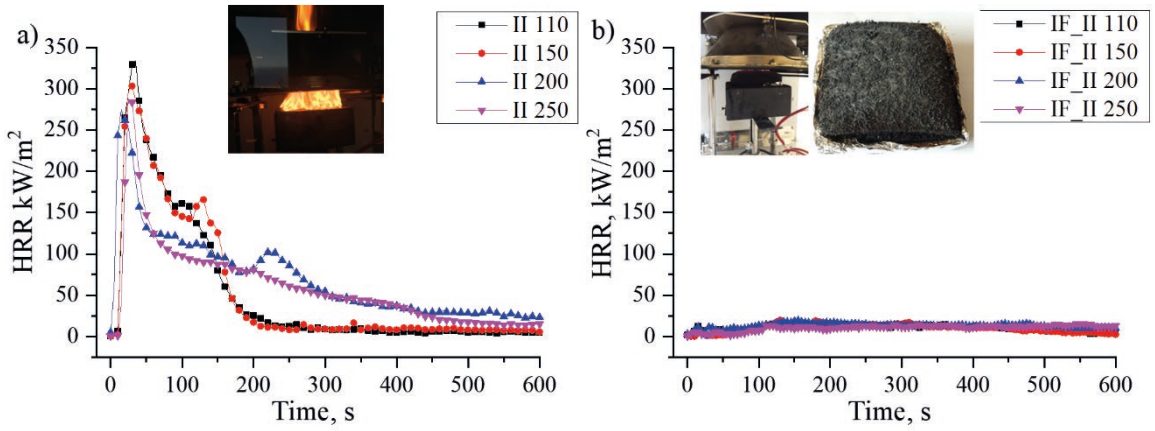

Fig. 3.17. Rigid PU/PIR foam HRR curves: a) foams with different isocyanate index; b) PU/PIR foams with IF protection.

Reaction of Developed Rigid PU/PIR Foam to Fire

One of the simplest flammability tests is material analysis according to EN 11925-2 standard. The test takes place inside a test chamber where the test specimen is mounted vertically. The test specimen is subjected to edge and/or surface exposure from a propane gas flame. During the test, time of ignition, burning droplets, and whether the flames reach the top marking of the test specimen within a prescribed time period, is registered. The top marking is positioned 150 mm from the flame application spot. This is the most basic test, which is required for materials used in civil engineering. Reaction to fire test is required to classify building materials according to European fire classification of construction products (EN 13501-1) Euro-class E. Such products are capable of resisting for a short period a small flame attack without substantial flame spread. Furthermore, the test gives information on

flaming droplet formation. To satisfy Euro-class E, the material has to be subjugated to the small flame for 15 s [8] , [8] .

Visually most distinguishing influence of EG flame retardant is depicted in Fig. 3.18. At isocyanate index 110 the rigid PU foam does not pass the reaction to a flame test, but the addition of EG flame retardant allows to do it. Furthermore, the fourth sample in the picture is rigid PU foam cov red with unwov n intumescent fabric. The picture depicts excellent flame retardant properties of the composite.

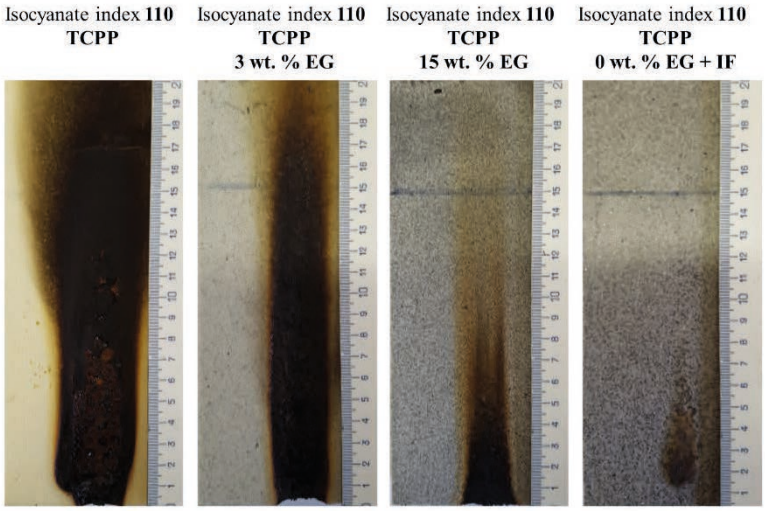

Fig. 3.18. Comparison of rigid PU/PIR foam samples after reaction to the small fire test.

3.4. High Functionality Bio-Based Polyol Synthesis from RO

Rapeseed oil (RO) as well as tall oil (TO) can be used as renewable and abundant feedstock for bio-based polyol synthesis. The simplest way how to introduce OH groups into natural oil structure is by employing the one-step method of transamidation/transesterification or amidation/esterification with TEOA and DEOA respectively. Bio-based polyol synthesis by this method was prev ously studied in the frame of M. Kirpluks' graduate and Master's Thesis [86]. The results discussed in Section 3.1 indicated that polyols obtained in one-step methods do not deliv r rigid PU foams with comparable mechanical properties to foams obtained from APP polyol. Furthermore, polyol synthesis from RO epoxidation and subsequent oxirane ring opening with DEG resulted in rigid PU foams that had much higher compression strength and higher thermal stability [87] . Double bond epoxidation and epoxy ring opening is an excellent way to introduce additional functional OH groups into the chemical structure of fatty acid moieties [24]. One of the goals of this Doctoral Thesis was to improv on the one step bio-based polyol synthesis to obtain polyols with higher functionality, which would deliv r better mechanical and thermal properties of rigid PU foams. A general approach improv ng the one step bio-based polyol synthesis method from RO would be to combine the epoxidation of the double bonds and epoxy ring opening with transesterification/transamidation process. This would result in bio-based polyols with increased functionality and additional beneficial properties deriv d from the chemical

structure of the oxirane ring opening reagent. The TEOA and DEOA epoxy ring opening reagents would introduce tertiary amine moieties into the chemical structure of the bio-polyol delivering auto-catalytical properties increasing the reactivity of the rigid PU foam formulation, which was demonstrated by A. Fridrihsone et al [88].

Characteristics of High Functionality Polyols From Epoxidized RO

The nine green polyols presented in experiment plan (depicted in Fig. 2.3) were characterised by the OH value, apparent viscosity, acid value, moisture content, density, f_n, M_n, M_w, and RO content in polyol (Table 3.4). The OH value of RODEG reference polyol was 242 mg_{KOH}/g, which is similar to what is reported in the literature [37]. The high acid value of 8.6 mg_{KOH}/g is due to a sulphuric acid catalyst, which was not separated or neutralized. The calculated f_n of RODEG was 3.0, i.e. high enough for rigid PU foam production. The novelty of the work is the next two sets of RO based polyols RODEA 0; 1.5; 2.0 and 2.5 and ROTEA 0; 1.5; 2.0 and 2.5 where the epoxy ring was opened with DEOA and TEOA, respectively, and transamidation and transesterification of the glycerol backbone were carried out. The obtained polyols have a much higher OH value ranging between 471−635 mg_{KOH}/g and 430−557 mg_{KOH}/g in the case of RODEA and ROTEA sets, respectively. The calculated f_n of synthesised polyols was much higher for RODEA polyol between 4.4−5.8 than for RODEG polyol where it was $f_n = 3.0$. The f_n increased with the increase of the ratio between DEOA (or TEOA) and the triglyceride. In the case of RODEA, polyol set the viscosity was quite high 22 000–23 600 mPa·s, but the polyols were still suitable for rigid PU foam formulation development. The high viscosity of the RODEA polyol set is explained by the hydrogen bonding of the polar amide groups present in the polyol chemical structure. Polyols with such high f_n are almost never used as the only component in rigid PU foam formulation. Their main application is as crosslinking reagents and their parts by weight (pbw) ratio in polyol component formulation usually is between 10−30 pbw [1]. Tertiary amine groups of synthesised polyols have autocatalytic properties that could be useful for the development of fast curing systems used for spray applied rigid PU foams.

Table 3.4

Hydroxyl Value, Viscosity, Acid Value, Moisture Content, Density, Number Average Functionality, Number and Mass Average Molar Mass, Polydispersity Index and Rapeseed Oil Content in the Polyol

Polyol	OH val., mg_{KOH}/g	Viscosity (20 °C), mPa·s	Acid val., mg KOH/g	W_{H2O}, wt. %	Density at 20 °C, g/cm^3	f_n	M_n	p_d	RO content in polyol, %
RODEG	242	6 500	8.6	0.322	1.025	3.0	695	1.36	70.8
RODEA 0	471	22 000	<2.0	0.046	1.022	4.4	520	1.15	71.0
RODEA 1.5	603	23 400	<2.0	0.041	1.029	5.5	508	1.11	63.5
RODEA 2.0	614	23 600	<2.0	0.044	1.035	5.7	518	1.09	61.3
RODEA 2.5	635	23 400	<2.0	0.055	1.041	5.8	511	1.06	59.3
ROTEA 0	430	1 800	<2.0	0.026	1.031	3.6	467	1.22	63.4
ROTEA 1.5	528	2 400	<2.0	0.028	1.037	4.9	524	1.33	55.1
ROTEA 2.0	550	2 400	<2.0	0.039	1.045	5.5	560	1.33	52.8
ROTEA 2.5	557	2 400	<2.0	0.044	1.053	5.2	528	1.25	50.7

FTIR Analysis of High Functionality Polyols From Epoxidized RO

The chemical structure of synthesised polyols was studied by FTIR spectroscopy. FTIR spectra of unmodified RO, RO after epoxidation and RODEG polyol are presented in Fig. 3.19. Peaks at 3416–3370 cm^{-1} indicated the presence of OH groups in the RODEG polyol. Also, as expected, the double bond =C–H stretching at 3008 cm^{-1} of unmodified RO disappeared after epoxidation process. The C–O–C oxirane ring stretching vibrations were identified at 823 cm^{-1} for ROEP, and this peak disappeared after oxirane ring was opened with DEG. Also, after the epoxy group opening an ether bond C–O stretching at 1103 cm^{-1} was observed. C=O bond stretching peak at 1742−1736 cm^{-1} was indicative of fatty acid triglyceride structure. Peaks at ~2930 cm^{-1} and ~2860 cm^{-1} were identified as of $–C–H_2–$ symmetric and asymmetric stretching.

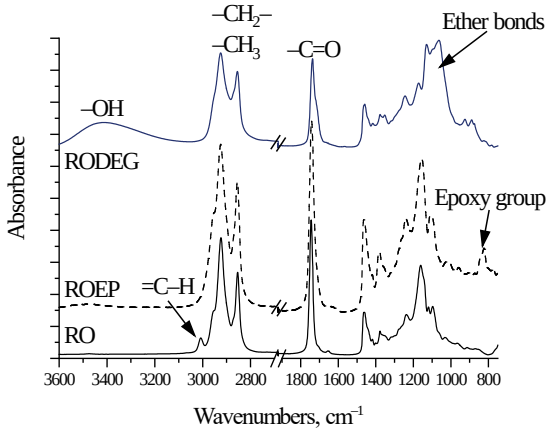

Fig. 3.19. FTIR spectra of RO, ROEP and RODEG polyol.

FTIR spectra of ROEP and RODEA 0–2.5 polyols are presented in Fig 3.20a. The broad peak between 3500−3100 cm^{-1} was identified as stretching vibrations of the O-H and N-H groups. The intensity of this peak increased with the increase of DEOA ratio in polyol synthesis and correlates with the increase of OH value of tested polyols. No quantitative calibration of this FTIR analysis was done for this study. Same as for RODEG the epoxy group stretching vibration peak at 823 cm^{-1} disappeared for the analysed polyols.

FTIR spectra of ROTEA polyol are presented in Fig. 3.20b. The intensity of the OH group broad peak at 3369 cm^{-1} increased with the increase of TEOA ratio in the reaction. Also, the peak of C–O stretching of ether groups at 1070 cm^{-1} and the peak of tertiary amine group stretching vibration at 1036 cm^{-1} were more noticeable. The slight shift of C=O stretching peak from 1742 cm^{-1} to 1735 cm^{-1} is explained with a change of RO triglyceride structure into TEOA fatty acid esters [89].

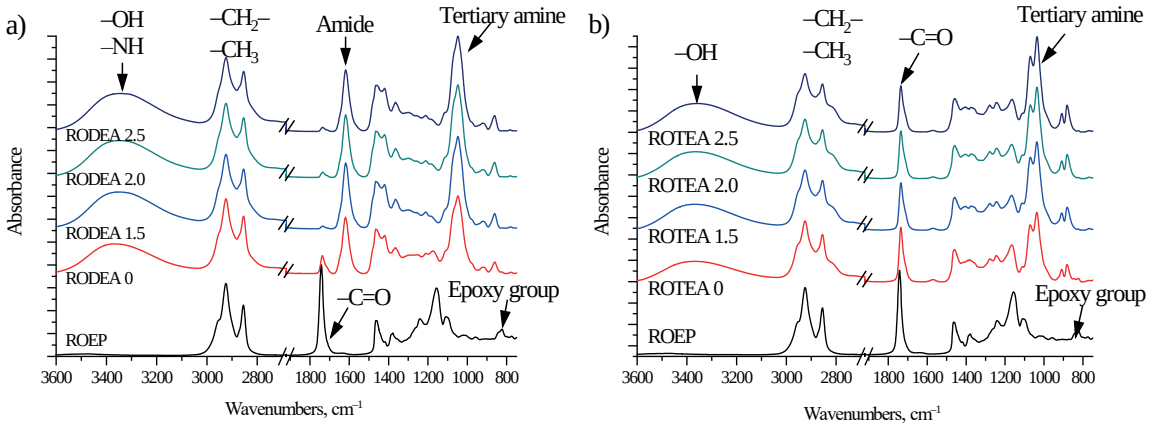

Fig. 3.20. FTIR spectra of ROEP and a) RODEA 0-2.5 and b) ROTEA 0-2.5 polyols.

Rigid PU Foam Development From RO Based High Functionality Polyols

The synthesised polyols were used to prepare rigid PU foams and the common characteristics of rigid PU foams were tested (Table 3.5). The PU foam formulations were developed in order to assess the suitability of prepared RO based polyols for further material optimization. The developed rigid PU foams had an apparent density in the range of 36−41 kg/m^3, which is the common density of the thermal insulation materials. All PU foams had closed cellular structure with the closed cell content above 95 %.

Table 3.5

Technological Characteristics of Rigid PU Foam Formulation (Start Time, String Time, Tack-Free Time, Rise Time), Apparent Density, Closed Cell Content and Thermal Conductivity of Developed Rigid PU Foams.

Polyol formulation	RO DEG	RODEA 0	RODEA 1.5	RODEA 2.0	RODEA 2.5	ROTEA 0	ROTEA 1.5	ROTEA 2.0	ROTEA 2.5
Technological parameters									
Start time, s	17	15	15	17	18	20	17	16	15
String time, s	40	37	35	37	38	43	35	35	35
Tack free time, s	47	47	41	42	43	60	42	41	41
Rise time, s	44	42	45	48	50	55	47	46	45
Temperature of polyol system before foaming, °C	21	21	21	21	21	14	14	14	14
Apparent density of PU foams, kg/m^3	36.3	38.2	37.9	37.2	39.9	35.1	40.9	39.4	39.4
Closed cell content, %	98	95	98	98	96	93	98	98	96
Thermal conductivity, mW/(m·K)	21.58	23.47	21.67	22.27	23.11	23.29	21.46	21.71	21.93

The normalized compression strengths and Young's modulus were calculated in parallel and perpendicular to the foaming direction (Fig. 3.21a,b). All prepared rigid PU foams showed decent mechanical characteristics meeting the industry standard of 0.2 MPa compression strength (in parallel to the foaming direction) for rigid PU foams with a density of 40 kg/m^3. All developed rigid PU foams showed optimal thermal conductivity close to 22.0 mW/(m·K) (Table 3.5), typical for this type of insulation material.

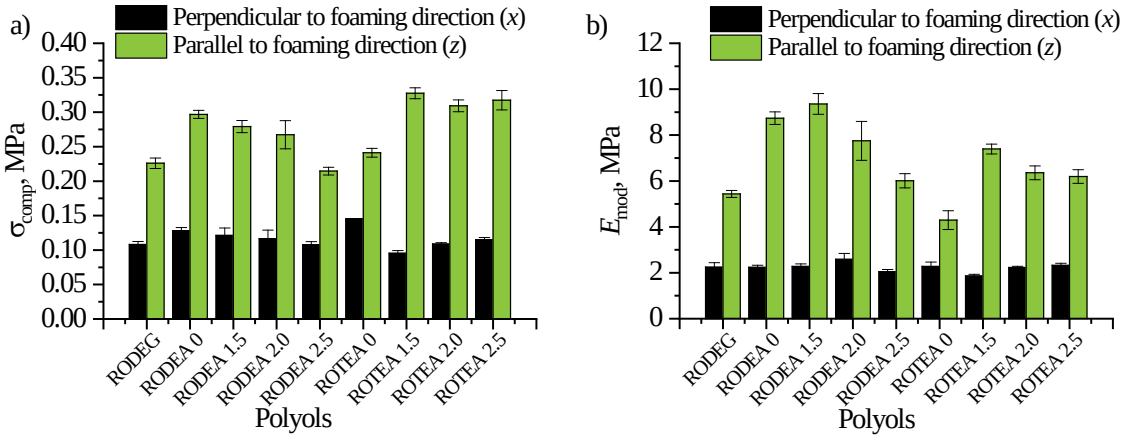

Fig. 3.21. a) Compression strength and b) modulus of elasticity of rigid PU foams obtained from high functional RO polyols.

3.5. High Functionality Bio-Based Polyol Synthesis From TOFA

Previously developed polyols from TOFA in the one-step process by amidation or esterification with DEOA or TEOA delivered unsatisfactory properties of rigid PU foam as discussed in Section 3.1. Similar to RO based polyols the properties of polyols could be improved by increasing average functionality of the polyols by epoxidation and subsequent epoxy ring opening reactions. Although vegetable oil epoxidation is a relatively well-studied topic, the epoxidation of neat fatty acids has not been studied at such detail. Majority of vegetable oils occur in nature as triglyceride esters without carboxylic acid moiety in their chemical structure. TOFA are derived from lignocellulosic biomass after the Kraft pulping process of cellulose pulp extraction [90], [91]. Crude tall oil is most commonly used for heat generation in the pulp mills [92]. Nevertheless, TOFA have been reported as a potential feedstock for numerous value-added products ranging from biodiesel [93], [94], wood-derived olefins for chemical industry [95], non-ionic surfactants [96], drilling and other fluids in mining industry [97], to application in polymer materials in resin production [98], plasticiser production, and in PU material development [42], [99]. The high amount of unsaturated bonds in the TOFA chemical structure makes it an ideal feedstock for epoxidation process where afterwards oxirane rings could be used to introduce desired functional groups on to the TOFA backbone.

This chapter will explore different approaches of TOFA epoxidation. Generally, the epoxidation is done by different peroxycarboxylic acids, which can be *in-situ* generated from different organic acids and hydrogen peroxide (H_2O_2) in the presence of different catalysts. The objective of this chapter was to develop a solvent-free epoxidation method of neat TOFA and achieve as high as possible double bond conversion to oxirane ring. Epoxidized tall oil fatty acids (ETOFA) would be later used for high functionality polyol synthesis. The proposed process allows for bypassing the production of intermediate products, such as TOFA methyl esters. A common epoxidation catalyst – sulphuric acid was compared to novel heterogeneous phase catalysts − ion exchange resin Amberlite IR 120 H and immobilised Lipase catalyst – Novozym® 435.

TOFA Epoxidation With Acidic Catalysts

The epoxidation of TOFA was carried out by *in-situ* generated peracetic acid from the acetic acid reaction with hydrogen peroxide in the presence of an acidic catalyst. The overall epoxidation reaction is depicted in Fig. 3.22 [100], [101]. The main disadvantage of acid catalysed epoxidation method is the side-reaction occurrence with oxirane rings, which leads to the formation of by-products [31]. Unfortunately, the oxirane ring opening is also acid catalysed, which leads to decreased oxirane group yield. In this work, two different acidic catalysts were compared for TOFA epoxidation process. One being homogeneous phase catalyst (H_2SO_4) and other was a heterogeneous phase catalyst (Amberlite IR 120 H). Although the catalyst type is different the general principle is similar as the epoxidation is carried out by the peracetic acid.

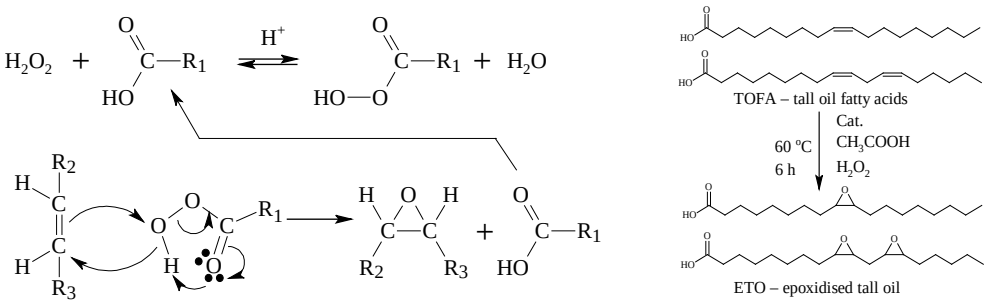

Fig. 3.22. TOFA epoxidation reaction mechanism.

TOFA Epoxidation With Amberlite IR-120 H Ion Exchange Resin Catalyst

Heterogeneous catalysts such as functionalized ion-exchange resins could provide several advantages. Small carboxylic acids, like acetic acid, can easily dissociate into and out of the gel-like structure of the catalyst where the formation of peracetic acid takes place. While the more bulky structure of the TOFA is less likely to penetrate the catalyst. Hence, the ETOFA is more protected from the attack of protons, which are confined inside the gel matrix. Therefore, the ETOFA epoxy ring opening during synthesis is prevented. Furthermore, a heterogeneous phase catalyst can be recovered and reused by simple filtration in a batch-type reactor. Such catalyst is also more suitable in continuous flow reactors, which are more common in industrial processes.

During the epoxidation process with Amberlite IR-120 H ion exchange resin catalyst, RCO gradually increased while the REU decreased as depicted in Fig. 3.23. The rate of decrease of REU was similar to experiments with H_2SO_4 as a catalyst where after 7 hours of synthesis the majority of double bonds have been transformed. In the case of 20 wt. % and 30 wt. % of Amberlite IR 120H catalyst after 7 hours of synthesis, 81.0 % and 86.6 % of double bonds have been transformed, respectively.

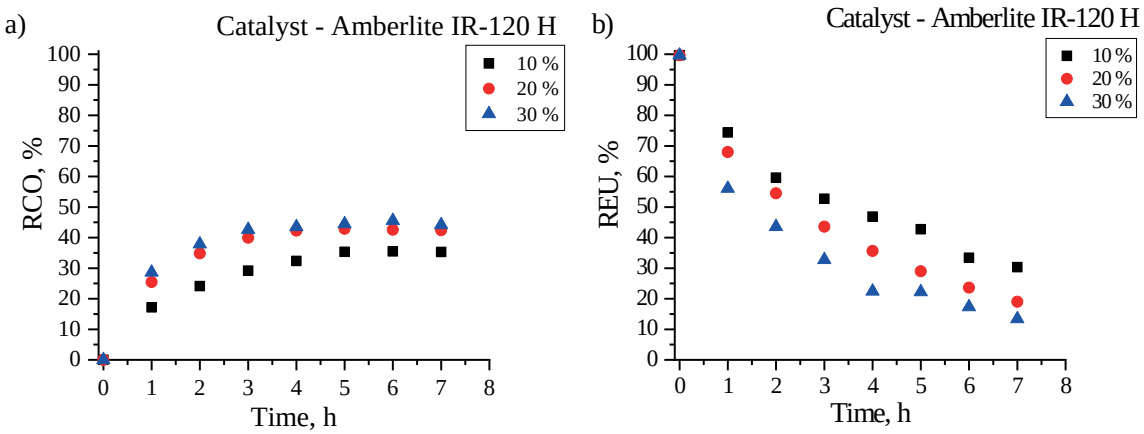

Fig. 3.23. TOFA epoxidation kinetic curves at different Amberlite IR 120 H catalyst contents: a) RCO; and b) REU.

The comparison of the two different acidic catalysts content influence on TOFA epoxidation is depicted in Table 3.6. For H_2SO_4 catalyst, the highest RCO was achieved after 1−2 hours of synthesis. However, the total oxirane yield was two times lower than in the case of Aberlite IR 120 H ion exchange catalyst due to the side reactions. The oxygen content of 3.82 % and 4.05 % (Amberlite IR 120 H = 20 wt. % and 30 wt. %) of synthesised ETOFA is relatively high and comparable to other epoxidized natural oils [23], [98], [102], [103]. Despite the oxirane ring opening side reaction the obtained ETOFA are suitable for further polyol synthesis as well as the development of epoxide based products. Amberlite IR 120 H catalyst content of 20 wt. % was selected for further TOFA optimization as the 30 wt. % of catalyst did not result in a significant increase for RCO.

Table 3.6

Summary of the Highest Achieved Relative Conversion to Oxirane and Relative Conversion of Double Bonds at Respective Synthesis Time

	Synthesis time, h	OO_{ex},%	RCO,%	Iodine value, g_{I2} per 100 g	UBC, %	S, %
Catalyst content	TOFA epoxidation with H_2SO_4 catalyst					
0.25 wt. %	7	1.76	19.7	87.1	43.8	45.1
0.50 wt. %	4	1.50	16.9	88.0	48.9	39.0
0.75 wt. %	2.5	1.65	18.5	108.3	30.1	61.6
1.00 wt. %	2	1.60	18.0	92.8	39.5	45.6
1.25 wt. %	1	1.63	18.4	106.1	31.5	58.2
1.50 wt. %	1	1.54	17.4	98.7	36.3	47.8
Catalyst content	TOFA epoxidation with Amberlite IR-120 H ion exchange resin catalyst					
10 wt. %	6	3.16	35.5	51.8	66.6	53.3
20 wt. %	5	3.82	42.9	45.0	71.0	60.4
30 wt. %	6	4.05	45.5	26.8	82.7	55.1

Tall Oil Fatty Acid Epoxidation Kinetics − Surface Reaction Kinetic Model

An attempt was made to apply the Eley-Rideal surface reaction mechanism to TOFA epoxidation with ion exchange resin catalyst. The Eley-Rideal mechanism was proposed by D. D. Eley and E. K. Rideal in 1938 and it is similar to the Langmuir-Hinshelwood surface

reaction mechanism. The Langmuir-Hinshelwood mechanism is used to explain the interaction of surface charge carriers and excitons with adsorbed molecules that can promote surface chemical processes, whereas the Eley-Rideal mechanism is used to explain the interaction of molecules with surface active centres that can initiate surface chemical processes [104] . In the Langmuir-Hinshelwood mechanism, both molecules adsorb to the catalyst and then undergo a chemical reaction, whereas in the Eley-Rideal mechanism only one molecule is adsorbed and the other reacts without adsorbing.

The overall reaction system of TOFA epoxidation is highly complex with three different phases of reactants. Some assumptions have to be made to simplify the determination of the reaction rate parameters of the studied process. It is assumed that TOFA do not diffuse into the porous structure of the ion exchange resin and do not adsorb to the active sites of the catalyst. Only acetic acid (AA) is adsorbed to the active site of the catalyst where it reacts with hydrogen peroxide (H_2O_2) forming peracetic acid (PA). Afterwards, the PA is desorbed from the catalyst where it is free to react with TOFA ethylenic unsaturation (EU) groups to form epoxy rings. After epoxidation of the double bonds, the AA is released. The rate-limiting step of the TOFA epoxidation is the surface reaction, which happens on the active site of the Amberlite IR120H catalyst. There is a limited amount of oxirane group side reactions, oxirane groups are opened with water (H_2O) and AA forming glycol (G) and acyl-glycol (AG), respectively. It is assumed that mass transfer of AA and H_2O_2 to the catalyst, PA and H_2O from catalyst and PA to TOFA are much faster than the rate-limiting surface reaction step of the process, thus diffusion rates can be neglected. The idealised depiction of TOFA epoxidation process is shown in Fig. 3.24.

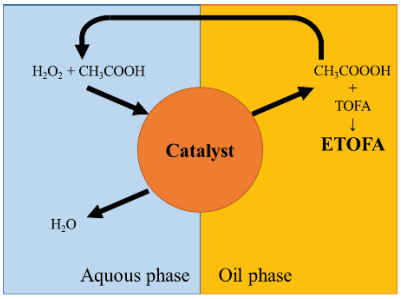

Fig. 3.24. An idealised schematic of different reaction phases of the TOFA epoxidation process with heterogeneous phase Amberlite IR 120H catalyst.

The rate-limiting step of the catalyst surface reaction can be further split into three steps as depicted in Fig. 3.25. In Step 1, AA is adsorbed to the vacant site of the catalyst forming adsorbed acetic acid (AAs). In Step 2, H_2O_2 reacts with AAs forming H_2O and adsorbed peracetic acid (PAs). In the last Step 3, PAs is desorbed and released into the reaction medium.

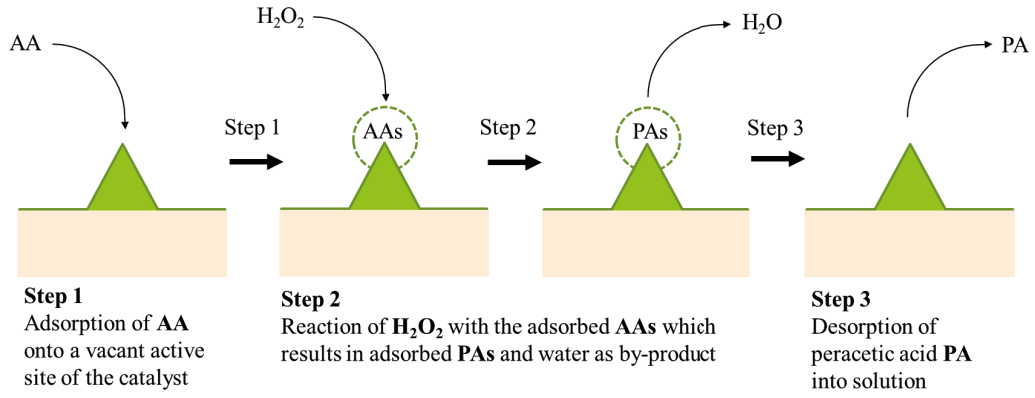

Fig. 3.25. Eley-Rideal mechanism of peracetic acid formation on the surface of ion-exchange resin catalyst.

Summary of TOFA Epoxidation Model

The mechanism for the *in-situ* epoxidation of TOFA in the presence of heterogeneous phase catalyst can be summarized by several reactions that occur simultaneously. The developed model describes the surface reaction of PA formation (I), which is considered as a heterogeneous reaction, and the reaction's order is considered to be 1 [25]. The desired TOFA epoxidation reaction (II) and the two undesired side reactions of oxirane ring opening (III and IV) are considered pseudo homogeneous second order reactions. The reaction equations are depicted in Fig. 3.26. Furthermore, the model assumes that, in the catalytic reaction of PA formation only AA and PA are adsorbed to the catalyst active sides without dissociation, that the PA formation is irreversible and that the catalyst surface reaction is the rate-limiting step of the overall process.

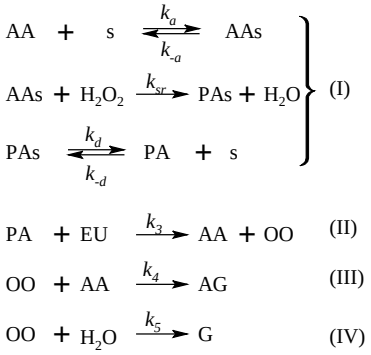

Fig. 3.26. Reactions occurring during TOFA epoxidation with ion exchange resin catalyst.

The change of concentration of the different individual reagents during the TOFA epoxidation process is dependent on more than one of the reactions. Furthermore, the concentration of the different reagents is not constant during the synthesis. Therefore, the rate law for the concentration change of the seven chosen reagents during the TOFA epoxidation is a system of non-linear differential equations, which is depicted in Eq. 3.5 The depicted model describes the complete process of TOFA epoxidation and its solution predicts the concentration change of the reagents over synthesis time. To solve Eq. 3.5, the kinetic rate and equilibrium constants have to be found beforehand.

$$\frac{\mathrm{d}[\mathrm{H_2O_2}]}{\mathrm{d}t} = -\frac{k_{\mathrm{sr}}C_{\mathrm{t}}W_{\mathrm{cat}}K_{\mathrm{AA}}[\mathrm{AA}][\mathrm{H_2O_2}]}{1+K_{\mathrm{AA}}[\mathrm{AA}]+K_{\mathrm{PA}}[\mathrm{PA}]};$$

$$\frac{\mathrm{d}[\mathrm{AA}]}{\mathrm{d}t} = -\frac{k_{\mathrm{sr}}C_{\mathrm{t}}W_{\mathrm{cat}}K_{\mathrm{AA}}[\mathrm{AA}][\mathrm{H_2O_2}]}{1+K_{\mathrm{AA}}[\mathrm{AA}]+K_{\mathrm{PA}}[\mathrm{PA}]} + k_3[\mathrm{PA}][\mathrm{EU}] - k_4[\mathrm{OO}][\mathrm{AA}];$$

$$\frac{\mathrm{d}[\mathrm{PA}]}{\mathrm{d}t} = \frac{k_{\mathrm{sr}}C_{\mathrm{t}}W_{\mathrm{cat}}K_{\mathrm{AA}}[\mathrm{AA}][\mathrm{H_2O_2}]}{1+K_{\mathrm{AA}}[\mathrm{AA}]+K_{\mathrm{PA}}[\mathrm{PA}]} - k_3[\mathrm{PA}][\mathrm{EU}];$$

$$\frac{\mathrm{d}[EU]}{\mathrm{d}t} = -k_3[\mathrm{PA}][\mathrm{EU}]; \qquad (3.10.)$$

$$\frac{\mathrm{d}[\mathrm{OO}]}{\mathrm{d}t} = k_3[\mathrm{PA}][\mathrm{EU}] - k_4[\mathrm{OO}][\mathrm{AA}] - k_5[\mathrm{OO}][\mathrm{H_2O}];$$

$$\frac{\mathrm{d}[\mathrm{H_2O}]}{\mathrm{d}t} = \frac{k_{\mathrm{sr}}C_{\mathrm{t}}W_{\mathrm{cat}}K_{\mathrm{AA}}[\mathrm{AA}][\mathrm{H_2O_2}]}{1+K_{\mathrm{AA}}[\mathrm{AA}]+K_{\mathrm{PA}}[\mathrm{PA}]} - k_5[\mathrm{OO}][\mathrm{H_2O}];$$

$$\frac{\mathrm{d}[\mathrm{AG+G}]}{\mathrm{d}t} = k_4[\mathrm{OO}][\mathrm{AA}] + k_5[\mathrm{OO}][\mathrm{H_2O}].$$

The Eq. 3.10 parameters were estimated using experimental data of the decrease of ethylenic unsaturation ($[EU_{ex}]$, mol per 100 g oil) and the experimentally determined increase of the oxirane oxygen content ($[OO_{ex}]$, mol per 100 g oil) data by using constrained nonlinear multivariable algorithm. Some initial estimates of the selected thermodynamically constants ($k_{sr}C_t$; k_3; k_4; k_5; K_{PA}; K_{AA}) were selected based on previous studies [25], [105], [106]. Then the TOFA epoxidation model was numerically solved using the fourth order Runge-Kutta method. The nonlinear differential equation was solved using "ode45" function of MatLab R2019a software. Afterwards, an objective function of the least squares was targeted to fit numerically calculated reagent concentrations to the experimental data. The "fmincon" function of MatLab R2019a software was used to vary the rate constants according to the Levenberg–Marquardt algorithm. Obtained rate constants of the complete TOFA epoxidation process are depicted in Table 3.7.

Table 3.7

Kinetic Rate Constants of Complete TOFA Epoxidation Process Using Ion Exchange Heterogeneous Phase Resin Catalyst

Rate constants		Unit	Values
$k_{sr}C_t$	surface reaction rate constant multiplied by the catalyst active site content	mol/(s·g(cat))	1.08
k_3	epoxidation reaction rate constant	100 g oil per s·mol	1.50
k_4	the rate constant of the oxirane opening with acetic acid	100 g oil per s·mol	0.99
k_5	the rate constant of the oxirane ring opening with water	100 g oil per s·mol	0.032
K_{PA}	peracetic acid adsorption equilibrium constant	mol/L	49.99
K_{AA}	acetic acid adsorption equilibrium constant	mol/L	0.80

A set of six synthesis experiments were used to fit the TOFA epoxidation model. TOFA were epoxidised in following conditions: synthesis temperature – 60 °C; mixing rate 600 rmp; ethylenic unsaturation and hydrogen peroxide molar ratios were 1.0/1.5, and Amberlite IR 120H content of 20 wt. % of oil mass was tested. The initial content of the acetic acid was varied to obtain different kinetic curves for model fitting. The following ethylenic unsaturation and acetic acid molar ratios were used: 1.00/0.15; 1.00/0.25; 1.00/0.35; 1.00/0.50; 1.00/0.65; 1.00/0.75. The different acetic acid content should not change the rate constants of the model. The obtained kinetic curves of the REU change over synthesis time are depicted in Fig. 3.27 together with the fitted model, which is depicted as straight lines. In a similar way, the RCO kinetic curves of TOFA epoxidation are depicted in Fig. 3.28.

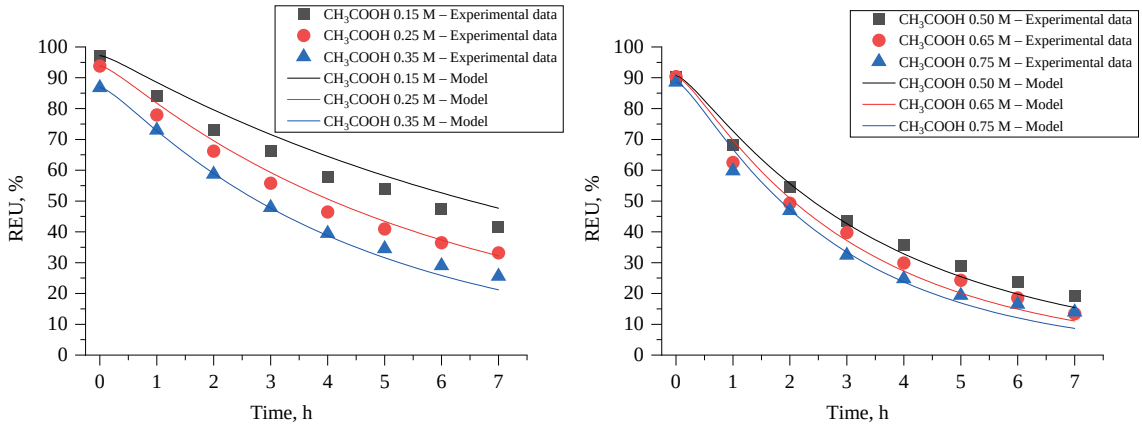

Fig. 3.27. REU kinetic curves of TOFA epoxidation.

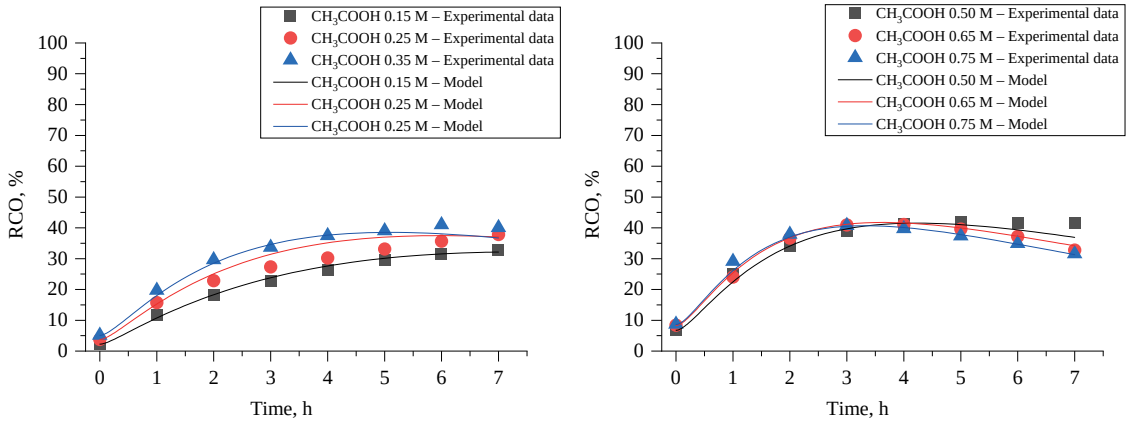

Fig. 3.28. RCO kinetic curves of TOFA epoxidation.

The developed TOFA epoxidation model (Eq. 3.10) fits relatively well to experimental data of RCO and REU. The experimental and calculated values of RCO and REU are depicted in Fig. 3.29. The coefficient of determination was 0.9794 and 0.9879 in case of RCO and REU, respectively. Moreover, the reaction rate parameters depicted in Table 3.7 are similar to previous studies [25], [105], [106]. Thus, it can be concluded that the developed TOFA epoxidation model could be used for synthesis parameter optimization to find the highest RCO values. The biggest drawback of the developed TOFA epoxidation model is that it is not possible to guarantee that this was the only minimum of the least square target function.

Furthermore, other minimums of the optimization function could be found outside boundaries that were set in this work. Not to mention that the TOFA epoxidation model has plenty of assumptions that do not represent the real process. Experimental data depicts that epoxy rings are opened almost at the same rate as they are introduced. Which suggests that TOFA does penetrate into catalyst gel-like structure where epoxy ring opening is catalysed. Previously this type of model was applied to different natural oil epoxidation, like jatropha, soybean and hemp oils [25], [105], [106], which have triglyceride structure and about three times larger average molecular mass than fatty acids of TOFA. Thus, it is reasonable to assume that diffusion of TOFA into the catalyst could be expected. TOFA themselves are carboxylic acids that could potentially be transferred into peroxycarboxylic acids, which could epoxidase themselves. This would further complicate the kinetic process of TOFA epoxidation. Unfortunately, these aspects were not studied in the frame of this Doctoral Thesis.

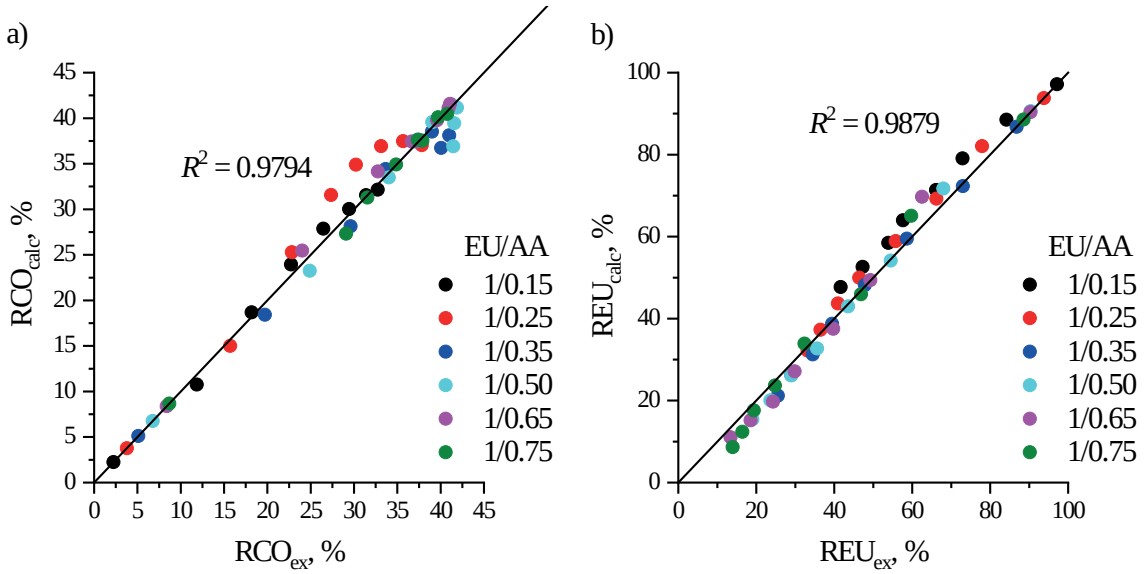

Fig. 3.29. Experimental versus predicted values of RCO and REU.

Chemo-Enzymatic Epoxidation of TOFA

In the frame of this Doctoral Thesis one more novel TOFA epoxidation catalyst was studied. The main disadvantage of the chemical epoxidation method described in previous sections is the acid-catalyzed side-reaction occurrence with oxirane rings, which leads to the formation of by-products [31]. Furthermore, the use of additional acid as an oxygen carrier means that it has to be separated from the reaction media after oil epoxidation, which, along with the use of hazardous chemicals, is not desired from the viewpoint of green chemistry. The use of performic or peracetic acids in the epoxidation process could lead to the thermal runaway of the reaction, which is highly undesired for an industrial upscale and due to safety concerns [32]–[34]. In recent times, various chemo-enzymatic catalysis reactions have been studied as a more sustainable approach to conventional chemical catalysis methods. One of the fields is double-bond epoxidation using a Lipase enzyme to catalyse the peroxycarboxylic acid *in situ* formation. The method is considered to be milder and more selective than traditional acid catalysed *in situ* epoxidation methods [31], [107]. The most effective lipase

for unsaturated bond epoxidation has shown to be Candida Antarctica Lipase B (Novozym® 435 – immobilized Lipase enzyme on acrylic resin beads) [108]. The main advantages of the enzyme catalysed epoxidation are relatively low epoxidation temperatures (30–50 °C) in comparison to chemical epoxidation at 60–100 °C, high selectivity and epoxidation conversion rate (exceeding 90 %), and reusability of the enzyme [109], [110]. Furthermore, it has been reported that Lipase can catalyse a formation of fatty acid peracids, such as perstearic [111], [112] and peroleic [113], which allows avoiding the use of formic and acetic acid in the epoxidation process. Although the possibility to use Lipase as a catalyst for epoxidation has been known for a while, there have been relatively few investigations into the synthesis of polyols for further use in polyurethane production.

The epoxidation of TOFA was carried out by *in situ* generated peroxycarboxylic acids from fatty acids contained in the chemical composition of the distilled tall oil. The idealized reaction mechanism is proposed by Sun et al. [112] (Fig. 3.30 a). The relatively high acidity of the TOFA mixture can lead to undesired side reactions of the fatty acid carboxyl groups with newly introduced oxirane rings resulting in dimerization and oligomerization products. The idealized TOFA epoxidation and side reaction scheme is depicted in Fig. 3.30b.

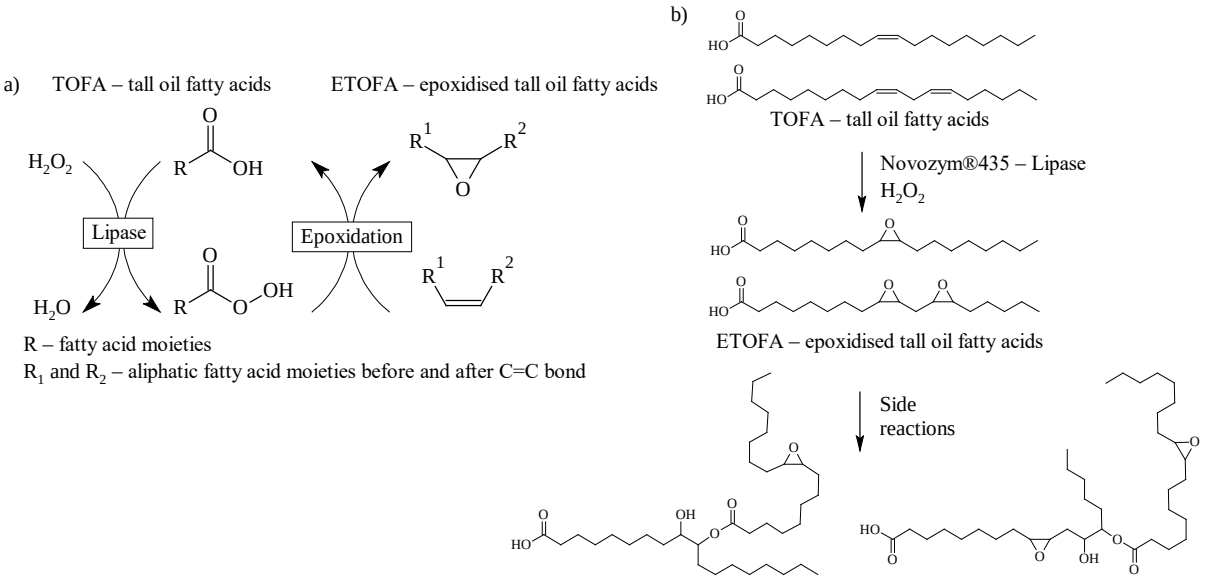

Fig. 3.30. a) The idealized chemo-enzymatic epoxidation mechanism of aliphatic double bonds; b) TOFA epoxidation and the side reaction for oxirane ring opening.

Overview of Chemo-Enzymatic TOFA Epoxidation

The summary of the chemo-enzymatic epoxidation of TOFA by the *in situ* generation of peroxycarboxylic fatty acids is presented in Table 3.8. An excess of H_2O_2 should be used at molar ratios C=C/H_2O_2 of 1.0/1.1 to achieve the higher conversion of the double bonds. Novozym®435 catalyst load of 3.0 wt. % is enough to successfully epoxidase the double bonds of TOFA. Although higher catalyst content led to higher conversion to oxirane, the increase was not significant enough to justify the use of a higher load of Novozym®435 catalyst. It is important to keep the catalyst load as low as possible because it is the most expensive component of the synthesis. An H_2O_2 with a concentration between 20–30 % should be used, as a higher concentration H_2O_2 could lead to catalyst degradation. In the frame of this study, the catalyst regeneration was not studied. The successful regeneration of the Lipase-based catalyst is the main requirement for the development of up scalable technology. The developed process allowed to obtain ETOFA with an epoxide oxygen content of 4.49–6.00 %, which is sufficient to consider this material for polyol synthesis as well as other epoxide-based products. The obtained results are in good agreement with previous studies with a similar concept. Solvent-free chemo-enzymatic epoxidation of oleic acid showed the relative conversion to oxirane above 60 % for epoxidation at 40 °C and H_2O_2 concentration of 30 % [114]. Obtained results are also similar to oleic acid self-epoxidation reported by Yadav and Manjula Devi where the similar oxygen content of 4.0–5.0 % has been achieved. It must be mentioned that this epoxidation was carried out in toluene solution and reported oxirane oxygen contents were achieved for much higher H_2O_2 excess than reported here (1.6–3.7 H_2O_2 per 1.0 mole of oleic acid) [115]. Lastly, the presented results can be compared to the solvent-free epoxidation of linoleic acid reported by Orellana-Coca et al. where about 70 % of relative conversion to oxirane was achieved. When a much higher excess of H_2O_2 was used (3.5–8 mmol H_2O_2 per mmol of linoleic acid) conversion to oxirane was close to 90–100 % after 8 hours [116]. This indicates that our epoxidation method could be improved by using higher excess of H_2O_2, which will be carried out in future studies.

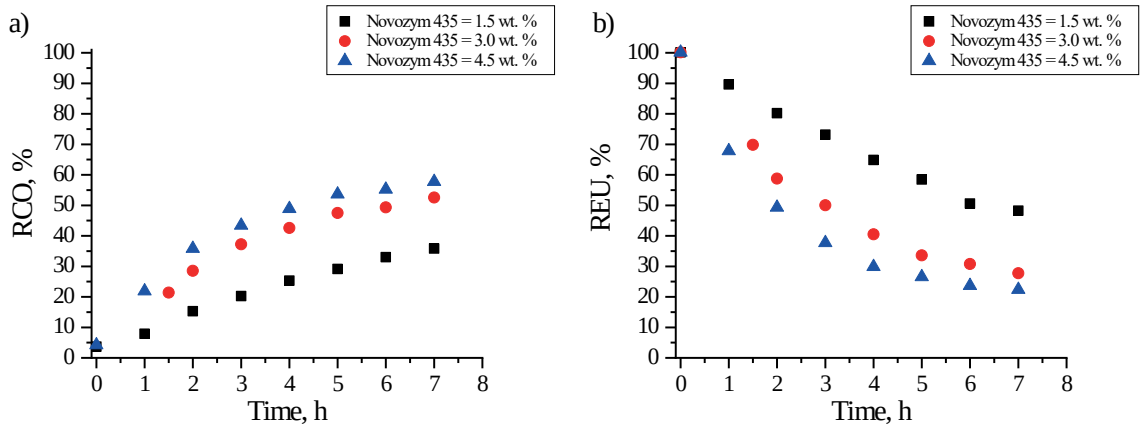

Fig 3.31. a) ROC b) REU at different Novozym® 435 catalyst content (T_{synth} =40 °C; H_2O_2 = 20 %; C=C/H_2O_2 = 1.0/1.1).

Table 3.8

Summary of the Highest Achieved Relative Conversion to Oxirane and Respective Relative Conversion of Double Bonds at Respective Synthesis Time

	Synthesis time, h	OO_{ex}, %	RCO, %	Iodine value, g_{I2} per 100 g	UBC, %	S, %
C=C/H_2O_2 molar ratio	TOFA epoxidation Novozym®435 = 3.0 wt. %; H_2O_2 = 20 wt. %					
1.0/1.0	7	4.65	52.2	50.6	67.4	77.5
1.0/1.1	7	4.49	50.5	43.0	72.3	69.9
1.0/1.2	7	4.02	45.1	52.1	66.4	68.0
Novozym®435 wt. %	TOFA epoxidation C=C/H_2O_2 = 1.0/1.1; H_2O_2 = 20 wt. %					
1.5 %	7	3.19	35.9	74.8	51.8	69.3
3.0 %	7	4.49	50.5	43.0	72.3	69.9
4.5 %	7	5.14	57.8	34.7	77.6	74.4
H_2O_2 wt. %	TOFA epoxidation C=C/H_2O_2 = 1.0/1.1; Novozym®435 = 3.0 wt. %					
15 %	7	3.76	42.2	63.8	58.8	58.8
20 %	7	4.49	50.5	43.0	72.3	69.9
25 %	7	5.54	62.2	45.0	71.0	87.7
30 %	7	6.00	67.4	37.0	76.1	76.1
35 %	6	5.07	57.0	30.4	80.4	70.9

CONCLUSIONS

- Bio-based, as well as APP based polyols, were suitable raw material for the development of high-density rigid PU foams. Rigid PU foams from APP polyols delivered higher mechanical properties than rigid PU foams obtained from bio-based polyols.
- Rigid PU foam impact absorption material applicable in automotive industry was developed using APP polyol – NEO_380.
- Mathematical model of apparent density and deformation strain rate influence on the stress-strain response of developed rigid PU foam was calibrated to predict compression behaviour of foams in a broad range of densities (~100–500 kg/m^3) and strain rates (0.00167–180 s^{-1}).
- Mechanical properties of developed rigid PU foams were increased by introducing nanoclay filler into foam structure. When nanoclays were dispersed into NEO_380 polyol, their inter-lattice structure was intercalated, whereas nanoclay lattice plane exfoliation was achieved by their dispersion into polyisocyanate component of rigid PU foams.
- Compression strength increase of ~15–20 % was achieved by dispersing 1.29–2.68 wt. % of nanoclay into rigid PU foams. Exfoliation of Cloisite 30 B nanoclay allowed to achieve the same compression strength increase at lower nanoclay content of 0.25–0.76 wt. %;
- TO_DEOA polyol, which was obtained from distilled tall oil, was suitable to develop rigid PU/PIR foam thermal insulation material with low thermal conductivity value of 22.80 mW/(m·K). In developed rigid PU foam formulation harmful halogenated flame retardant TCPP was replaced with graphite based intumescent flame retardant.
- The one-step bio-polyol synthesis process was combined with RO epoxidation and epoxy ring opening to obtain high functionality polyols with f_n = 3.6–5.8. Developed high functionality polyols were used to obtain rigid PU foam thermal insulation with closed cell content above 95 %, the apparent density of ~40 kg/m^3 and thermal conductivity of 21.5–23.3 mW/(m·K) and excellent mechanical properties; compression strength above 0.20 MPa and compression modulus above 5 MPa in parallel to the foaming direction.
- A novel method of neat TOFA epoxidation that agrees with the principles of green chemistry was developed. Ion exchange Amberlite IR 120H resin catalyst delivered superior RCO than conventional H_2SO_4 catalyst (RCO of 45.5 % and 19.7 %, respectively).
- Eley-Rideal surface reaction mechanism model was successfully applied to the TOFA epoxidation process. The developed model showed that unfortunately, Amberlite IR 120H ion exchange resin promotes the undesired oxirane ring cleavage reactions almost to the same level as the epoxidation of the double bonds.
- Novel Lipase based heterogeneous phase catalyst was applied for TOFA epoxidation and the highest RCO = 67.4 % was achieved at relatively low catalyst content of 3.0 wt. %. Novozym®435 Lipase based catalyst was selected as the most promising catalyst as it allowed to develop simple, solvent-free, without use of intermediate products, high efficiency (RCO > 67 %), low energy requirement (T_{stynt} = 40 °C), sustainable TOFA epoxidation process.

REFERENCES

[1] M. Szycher, Szycher's Handbook of Polyurethanes, First Edit, CRC Press, 1999.

[2] M. Ionescu, Chemistry and technology of polyols for polyurethanes., 2007. doi:10.1002/pi.2159.

[3] Grand View Research Inc. Report ID: 5741307, Polyols Market Size, Share & Trends Analysis Report By Product, By Application And Segment Forecasts, 2018–2025, 2018.

[4] S. Fu, Y. Qin, L. Qiao, X. Wang, F. Wang, Propylene oxide end-capping route to primary hydroxyl group dominated CO2-polyol, Polymer (Guildf). 153 (2018) 167–172. doi:10.1016/j.polymer.2018.08.014.

[5] S. Liu, X. Wang, Polymers from carbon dioxide: Polycarbonates, polyurethanes, Curr. Opin. Green Sustain. Chem. 3 (2017) 61–66. doi:10.1016/j.cogsc.2016.08.003.

[6] R.A. Sheldon, Green and sustainable manufacture of chemicals from biomass: state of the art, Green Chem. 16 (2014) 950–963. doi:10.1039/C3GC41935E.

[7] J. Philp, The bioeconomy, the challenge of the century for policy makers, N. Biotechnol. 40 (2018) 11–19. doi:10.1016/j.nbt.2017.04.004.

[8] C. Zhang, T. F. Garrison, S. A. Madbouly, M. R. Kessler, Recent advances in vegetable oil-based polymers and their composites, Prog. Polym. Sci. 71 (2017) 91–143. doi:10.1016/j.progpolymsci.2016.12.009.

[9] L. Montero De Espinosa, M.A.R.R. Meier, Plant oils: The perfect renewable resource for polymer science?!, Eur. Polym. J. 47 (2011) 837–852. doi:10.1016/j.eurpolymj.2010.11.020.

[10] U. Biermann, U. Bornscheuer, M.A.R. Meier, J.O. Metzger, H.J. Schäfer, Oils and Fats as Renewable Raw Materials in Chemistry, Angew. Chemie Int. Ed. 50 (2011) 3854–3871. doi:10.1002/anie.201002767.

[11] Z. S. Petrovic, Polyurethanes from Vegetable Oils, Polym. Rev. 48 (2008) 109–155. doi:10.1080/15583720701834224.

[12] J. G. Drobny, Handbook of Thermoplastic Elastomers, 2014. doi:10.1016/B978-0-323-22136-8.00006-5.

[13] G. Lligadas, J. C. Ronda, M. Galià, V. Cádiz, Oleic and Undecylenic Acids as Renewable Feedstocks in the Synthesis of Polyols and Polyurethanes, Polymers (Basel). 2 (2010) 440–453. doi:10.3390/polym2040440.

[14] U. Stirna, A. Fridrihsone, M. Misane, D. Vilsone, L. State, W. Chemistry, Rapeseed Oil as Renewable Resource for Polyol Synthesis, Environ. Clim. Technol. 6 (2011) 85–90. doi:10.2478/v10145-011-0012-4.

[15] M. Kirpluks, U. Cābulis, M. Kurańska, A. Prociak, Three Different Approaches for Polyol Synthesis from Rapeseed Oil, Key Eng. Mater. 559 (2013) 69–74. doi:10.4028/www.scientific.net/KEM.559.69.

[16] M. Desroches, M. Escouvois, R. Auvergne, S. Caillol, B. Boutevin, From Vegetable Oils to Polyurethanes: Synthetic Routes to Polyols and Main Industrial Products, Polym. Rev. 52 (2012) 38–79. doi:10.1080/15583724.2011.640443.

[17] S. G. Tan, W. S. Chow, Biobased epoxidized vegetable oils and its greener epoxy blends: A review, Polym. – Plast. Technol. Eng. 49 (2010) 1581–1590. doi:10.1080/03602559.2010.512338.

[18] T. Saurabh, M. Patnaik, S. L. Bhagt, V. C. Renge, Epoxidation of vegetable oils:, A Rev. Int. J. Adv. Eng. Technol. 2 (2011) 491–501.

[19] M. M. Patel, B. P. Patel, N. K. Patel, Utilization of soya-based polyol for High solid PU-coating application, Int. J. Plast. Technol. 16 (2012) 67–79. doi:10.1007/s12588-012-9030-8.

[20] R. Mungroo, N. C. Pradhan, V. V. Goud, A.K. Dalai, Epoxidation of canola oil with hydrogen peroxide catalyzed by acidic ion exchange resin, J. Am. Oil Chem. Soc. 85 (2008) 887–896. doi:10.1007/s11746-008-1277-z.

[21] T. S. Omonov, E. Kharraz, J. M. Curtis, The epoxidation of canola oil and its derivatives, RSC Adv. 6 (2016) 92874–92886. doi:10.1039/c6ra17732h.

[22] M. Kirpluks, D. Kalnbunde, Z. Walterova, U. Cabulis, Rapeseed Oil as Feedstock for High Functionality Polyol Synthesis, J. Renew. Mater. 5 (2017) 1–23. doi:10.7569/JRM.2017.634116.

[23] S. Sinadinovic-Fiser, M. Jankovi, O. Borota, Epoxidation of castor oil with peracetic acid formed in situ in the presence of an ion exchange resin, Chem. Eng. Process. Process Intensif. 62 (2012) 106–113. doi:10.1016/j.cep.2012.08.005.

[24] A. S. A. Hazmi, M. M. Aung, L. C. Abdullah, M. Z. Salleh, M. H. Mahmood, Producing Jatropha oil-based polyol via epoxidation and ring opening, Ind. Crops Prod. 50 (2013) 563–567. doi:10.1016/j.indcrop.2013.08.003.

[25] V. V. Goud, A. V. Patwardhan, S. Dinda, N.C. Pradhan, Kinetics of epoxidation of jatropha oil with peroxyacetic and peroxyformic acid catalysed by acidic ion exchange resin, Chem. Eng. Sci. 62 (2007) 4065–4076. doi:http://dx.doi.org/10.1016/j.ces.2007.04.038.

[26] P. D. Meshram, R. G. Puri, H. V Patil, Epoxidation of Wild Safflower (Carthamus oxyacantha) Oil with Peroxy acid in presence of strongly Acidic Cation Exchange Resin IR- 122 as Catalyst, Int. J. ChemTech Res. 3 (2011) 1152–1163.

[27] V. V. Goud, A. V. Patwardhan, N. C. Pradhan, Studies on the epoxidation of mahua oil (Madhumica indica) by hydrogen peroxide, Bioresour. Technol. 97 (2006) 1365–1371. doi:10.1016/j.biortech.2005.07.004.

[28] S. Dinda, A. V. Patwardhan, V. V. Goud, N.C. Pradhan, Epoxidation of cottonseed oil by aqueous hydrogen peroxide catalysed by liquid inorganic acids, Bioresour. Technol. 99 (2008) 3737–3744. doi:10.1016/j.biortech.2007.07.015.

[29] V. V. Goud, A. V. Patwardhan, S. Dinda, N. C. Pradhan, Epoxidation of karanja (Pongamia glabra) oil catalysed by acidic ion exchange resin, Eur. J. Lipid Sci. Technol. 109 (2007) 575–584. doi:10.1002/ejlt.200600298.

[30] J. C. de Haro, I. Izarra, J. F. Rodríguez, Á. Pérez, M. Carmona, Modelling the epoxidation reaction of grape seed oil by peracetic acid, J. Clean. Prod. 138 (2016) 70–76. doi:https://doi.org/10.1016/j.jclepro.2016.05.015.

[31] A. E. V Hagström, U. Törnvall, M. Nordblad, R. Hatti-Kaul, J. M. Woodley, Chemo-enzymatic epoxidation-process options for improving biocatalytic productivity, Biotechnol. Prog. 27 (2011) 67–76. doi:10.1002/btpr.504.

[32] H. Rakotondramaro, J. Wärnå, L. Estel, T. Salmi, S. Leveneur, Cooling and stirring failure for semi-batch reactor: Application to exothermic reactions in multiphase reactor, J. Loss Prev. Process Ind. 43 (2016) 147–157. doi:10.1016/j.jlp.2016.05.011.

[33] J. V. de Quadros, R. Giudici, Epoxidation of soybean oil at maximum heat removal and single addition of all reactants, Chem. Eng. Process. Process Intensif. 100 (2016) 87–93. doi:10.1016/j.cep.2015.11.007.

[34] V. Casson Moreno, V. Russo, R. Tesser, M. Di Serio, E. Salzano, Thermal risk in semi-batch reactors: The epoxidation of soybean oil, Process Saf. Environ. Prot. 109 (2017) 529–537. doi:10.1016/j.psep.2017.05.001.

[35] N. E. Marcovich, M. Kurańska, A. Prociak, E. Malewska, K. Kulpa, Open cell semi-rigid polyurethane foams synthesized using palm oil-based bio-polyol, Ind. Crops Prod. 102 (2017) 88–96. doi:10.1016/j.indcrop.2017.03.025.

[36] P. Rojek, A. Prociak, Effect of different rapeseed-oil-based polyols on mechanical properties of flexible polyurethane foams, J. Appl. Polym. Sci. 125 (2012) 2936–2945. doi:10.1002/app.36500.

[37] M. Kurańska, A. Prociak, The influence of rapeseed oil-based polyols on the foaming process of rigid polyurethane foams, Ind. Crops Prod. 89 (2016) 182–187. doi:10.1016/j.indcrop. 2016.05.016.

[38] M. Zieleniewska, M. K. Leszczyński, M. Kurańska, A. Prociak, L. Szczepkowski, M. Krzyzowska, J. Ryszkowska, Preparation and characterisation of rigid polyurethane foams using a rapeseed oil-based polyol, Ind. Crops Prod. 74 (2015) 887–897. doi:10.1016/j.indcrop.2015.05.081.

[39] U. Stirna, A. Fridrihsone-Girone, V. Yakushin, D. Vilsone, Processing and properties of spray-applied, 100% solids polyurethane coatings from rapeseed oil polyols, J. Coatings Technol. Res. 11 (2014) 409–420. doi:10.1007/s11998-013-9545-8.

[40] C. Tu, Yuan, P. Kiatsimkul, G. Suppes, F.-H. Hsieh, Physical properties of water-blown rigid polyurethane foams from vegetable oil-based polyols, J. Appl. Polym. Sci. 105 (2007) 453–459. doi:10.1002/app.26060.

[41] M. Acar, S. Çoban, B. Hazer, Novel Water Soluble Soya Oil Polymer from Oxidized Soya Oil Polymer and Diethanol Amine, J. Macromol. Sci. Part A. 50 (2013) 287–296. doi:10.1080/10601325.2013.755443.

[42] K. Pietrzak, M. Kirpluks, U. Cabulis, J. Ryszkowska, Effect of the addition of tall oil-based polyols on the thermal and mechanical properties of ureaurethane elastomers, Polym. Degrad. Stab. 108 (2014) 201–211. doi:10.1016/j.polymdegradstab.2014.03.038.

[43] U. Cabulis, M. Kirpluks, U. Stirna, M. J. J. Lopez, M.C.D.C.D.C. Vargas-Garcia, F. Suarez-Estrella, J. Moreno, M. Del Carmen Vargas-Garcia, Rigid polyurethane foams obtained from tall oil and filled with natural fibers: Application as a support for immobilization of lignin-degrading microorganisms, J. Cell. Plast. 48 (2012) 500–515. doi:10.1177/0021955X12443142.

[44] M. Kirpluks, U. Cabulis, A. Ivdre, M. Kuranska, M. Zieleniewska, M. Auguscik, Mechanical and Thermal Properties of High-Density Rigid Polyurethane Foams from Renewable Resources, J. Renew. Mater. 4 (2016) 86–100. doi:10.7569/JRM.2015.634132.

[45] S. Tan, T. Abraham, D. Ference, C. W. Macosko, Rigid polyurethane foams from a soybean oil-based Polyol, Polymer (Guildf). 52 (2011) 2840–2846. doi:10.1016/j.polymer.2011.04.040.

[46] Y. Li, X. Luo, S. Hu, Bio-based Polyols and Polyurethanes, Springer, 2015.

[47] H. Dai, L. Yang, B. Lin, C. Wang, G. Shi, Synthesis and Characterization of the Different Soy-Based Polyols by Ring Opening of Epoxidized Soybean Oil with Methanol, 1,2-Ethanediol and 1,2-Propanediol, J. Am. Oil Chem. Soc. 86 (2009) 261–267. doi:10.1007/s11746-008-1342-7.

[48] C.-S.S.C.S. Wang, L.-T.T.L.T. Yang, B.-L.L. Ni, G. Shi, H. Dai, B. Lin, S. Guang, Polyurethane networks from different soy-based polyols by the ring opening of epoxidized soybean oil with methanol, glycol, and 1,2-propanediol, J. Appl. Polym. Sci. 114 (2009) 125–131. doi:10.1002/app.30493.

[49] R. Rao, L. Mondy, D. Noble, V. Brunini, K. Long, C. Roberts, N. Wyatt, M. Celina, K. Thompson, J. Tinsley, Density predictions using a finite element/level set model of polyurethane foam expansion and polymerization, Comput. Fluids. 175 (2018) 20–35. doi:10.1016/j.compfluid.2018.08.010.

[50] M. Kirpluks, L. Stiebra, A. Trubaca-Boginska, U. Cabulis, J. Andersons, Rigid closed-cell PUR foams containing polyols derived from renewable resources: The effect of polymer composition, foam density, and organoclay filler on their mechanical properties, in: K. Thakur, Vijay, M.K. Thakur, M.R. Kessler (Eds.), Handb. Compos. from Renew. Mater., Scrivener Publishing LLC, 2017: pp. 313–339. doi:10.1002/9781119441632.ch31.

[51] K. P. Menard, Dynamic Mechanical Analysis A Practical Introduction, 1999. doi:10.1201/9781420049183.ch2.

[52] F. V. Billotto, M. M. Mirdamadi, B. A. Pearson, Design, Application Development, and Launch of Polyurethane Foam Systems in Vehicle Structures, SAE Tech. Pap. (2003). doi:10.4271/2003-01-0333.

[53] M. Kirpluks, U. Cabulis, J. Andersons, G. Japins, K. Kalnins, Modeling the Effect of Foam Density and Strain Rate on the Compressive Response of Polyurethane Foams, SAE Int. J. Mater. Manuf. 11 (2018). doi:10.4271/05-11-02-0014.

[54] M. C. Hawkins, B. O'Toole, D. Jackovich, Cell Morphology and Mechanical Properties of Rigid Polyurethane Foam, J. Cell. Plast. 41 (2005) 267–285. doi:10.1177/0021955X05053525.

[55] S. H. Goods, C. L. Neuschwanger, C. C. Henderson, D. M. Skala, Mechanical properties of CRETE, a polyurethane foam, J. Appl. Polym. Sci. 68 (1998) 1045–1055. doi:10.1002/(SICI)1097-4628(19980516)68:7<1045::AID-APP2>3.0.CO;2-F.

[56] L. Marsavina, D. M. Constantinescu, E. Linul, D. A. Apostol, T. Voiconi, T. Sadowski, Refinements on fracture toughness of PUR foams, Eng. Fract. Mech. 129 (2014) 54–66. doi:10.1016/j.engfracmech.2013.12.006.

[57] M. E. Kabir, M. C. Saha, S. Jeelani, Tensile and fracture behavior of polymer foams, Mater. Sci. Eng. A. 429 (2006) 225–235. doi:10.1016/j.msea.2006.05.133.

[58] M. Avalle, G. Belingardi, A. Ibba, Mechanical models of cellular solids: Parameters identification from experimental tests, Int. J. Impact Eng. 34 (2007) 3–27. doi:10.1016/j.ijimpeng.2006.06.012.

[59] Q. Liu, G. Subhash, X.-L. Gao, A Parametric Study on Crushability of Open-Cell Structural Polymeric, J. Porous Mater. 12 (2005) 233–248. doi:10.1007/s10934-005-1652-1.

[60] A. Nagy, W. L. Ko, U. S. Lindholm, Mechanical Behavior of Foamed Materials Under Dynamic Compression, J. Cell. Plast. 10 (1974) 127–134. doi:10.1177/0021955X7401000306.

[61] D. A. Apostol, D. M. Constantinescu, Temperature and speed of testing influence on the densification and recovery of polyurethane foams, Mech. Time-Dependent Mater. 17 (2013) 111–136. doi:10.1007/s11043-012-9179-8.

[62] L. Mkrtchyan, M. Maier, U. Huber, Structural polyurethane foam: Testing and modelling for automotive applications, Int. J. Crashworthiness. 13 (2008) 523–532. doi:10.1080/13588260802221310.

[63] M. Schulz, D. Kourkoulas, Regulation (EU) No 333/2014, Off. J. Eur. Union. (2014) 15–21. http://eur-lex.europa.eu/legal-content/EN/TXT/PDF/?uri=CELEX:32014R0333&from=EN.

[64] R. K. Helling, D. A. Russell, Use of life cycle assessment to characterize the environmental impacts of polyol production options, Green Chem. 11 (2009) 380. doi:10.1039/b815833a.

[65] R. K. Helling, D. A. Russell, Investigation of the Trade-off Between Lightweight and Battery Cost for an Aluminium-intensive, Green Chem. 11 (2009) 380. doi:10.1039/b815833a.

[66] E. Cischino, F. Di Paolo, E. Mangino, D. Pullini, C. Elizetxea, C.C.C.C. Maestro, E. Alcalde, J. D. Christiansen, An Advanced Technological Lightweighted Solution for a Body in White, Transp. Res. Procedia. 14 (2016) 1021–1030. doi:10.1016/j.trpro.2016.05.082.

[67] E. Cischino, Z. Vuluga, C. E. Ezeiza, I. L. Benito, E. Mangino, J. De Claville Christiansen, C.-G. Sanporean, F. Di Paolo, M. Kirpluks, P. Cabulis, A Concrete and Viable Example of Multimaterial Body: The Evolution Project Main Outcomes, in: Procedia CIRP, 2017: pp. 300–305. doi:10.1016/j.procir.2017.03.292.

[68] S. Pardo-Alonso, E. Solórzano, L. Brabant, P. Vanderniepen, M. Dierick, L. Van Hoorebeke, M.A. Rodríguez-Pérez, 3D Analysis of the progressive modification of the cellular architecture in polyurethane nanocomposite foams via X-ray microtomography, Eur. Polym. J. 49 (2013) 999–1006. doi:10.1016/j.eurpolymj.2013.01.005.

[69] P. Mondal, D. V. Khakhar, Rigid Polyurethane–Clay Nanocomposite Foams: Preparation and Properties, J. Appl. Polym. Sci. 103 (2007) 2802–2809. doi:10.1002/app.

[70] T. Widya, C. Macosko, Nanoclay-Modified Rigid Polyurethane Foam, J. Macromol. Sci. Part B Phys. 44 (2005) 897–908. doi:10.1080/00222340500364809.

[71] S. Estravís, J. Tirado-Mediavilla, M. Santiago-Calvo, J. L. Ruiz-Herrero, F. Villafañe, M. Á. Rodríguez-Pérez, Rigid polyurethane foams with infused nanoclays: Relationship between cellular structure and thermal conductivity, Eur. Polym. J. 80 (2016) 1–15. doi:10.1016/j.eurpolymj.2016.04.026.

[72] J. M. Herrera-Alonso, E. Marand, J. C. Little, S. S. Cox, Transport properties in polyurethane/clay nanocomposites as barrier materials: Effect of processing conditions, J. Memb. Sci. 337 (2009) 208–214. doi:10.1016/j.memsci.2009.03.045.

[73] S. Pardo-Alonso, E. Solórzano, S. Estravís, M. A. Rodríguez-Perez, J. A. de Saja, In situ evidence of the nanoparticle nucleating effect in polyurethane–nanoclay foamed systems, Soft Matter. 8 (2012) 11262. doi:10.1039/c2sm25983d.

[74] J. H. Park, S. C. Jana, Mechanism of Exfoliation of Nanoclay Particles in Epoxy-Clay Nanocomposites, Macromolecules. 36 (2003) 2758–2768. doi:10.1021/ma021509c.

[75] M. Joshi, B. Adak, B. S. Butola, Polyurethane nanocomposite based gas barrier films, membranes and coatings: A review on synthesis, characterization and potential applications, Prog. Mater. Sci. 97 (2018) 230–282. doi:10.1016/j.pmatsci.2018.05.001.

[76] M. Thirumal, D. Khastgir, N. K. Singha, B. S. Manjunath, Y. P. Naik, Effect of a nanoclay on the mechanical, thermal and flame retardant properties of rigid polyurethane foam, J. Macromol. Sci. Part A Pure Appl. Chem. 46 (2009) 704–712. doi:10.1080/10601320902939101.

[77] P. Mondal, D. V. Khakhar, Regulation of Cell Structure in Water Blown Rigid Polyurethane Foam, Macromol. Symp. 216 (2004) 241–254. doi:10.1002/masy.200451223.

[78] S. Sinha Ray, M. Okamoto, Polymer/layered silicate nanocomposites: A review from preparation to processing, Prog. Polym. Sci. 28 (2003) 1539–1641. doi:10.1016/j.progpolymsci.2003.08.002.

[79] L. Wu, J. Van Gemert, R. E. Camargo, Rheology Study in Polyurethane Rigid Foams, Huntsman Corp. Tech. Pap. (2009) 12.

[80] A. Prociak, G. Rokicki, J. Ryszkowska, Materialy poliuretanowe, 1st ed., Wydawnictwo Naukowe PWN, Warsaw, 2014.

[81] L. Gao, G. Zheng, Y. Zhou, L. Hu, G. Feng, M. Zhang, Synergistic effect of expandable graphite, diethyl ethylphosphonate and organically-modified layered double hydroxide on flame retardancy and fire behavior of polyisocyanurate-polyurethane foam nanocomposite, Polym. Degrad. Stab. 101 (2014) 92–101. doi:10.1016/j.polymdegradstab.2013.12.025.

[82] C. N. Hoang, C. T. Pham, T. M. Dang, D. Hoang, P. Lee, S. Kang, J. Kim, Novel Oligo-Ester-Ether-Diol Prepared by Waste Poly (ethylene terephthalate) Glycolysis and Its Use in Preparing Thermally Stable and Flame Retardant Polyurethane Foam, Polymers (Basel). 11 (2019) 1–17. doi:10.3390/polym11020236.

[83] J. G. Quintiere, Fundamentals of Fire Phenomena, John Wiley & Sons Ltd, The Atrium, Southern Gate, Chichester, 2006.

[84] A. S. Hansen, Prediction of heat release in the single burning item test, Fire Mater. 26 (2002) 87–97. doi:10.1002/fam.789.
[85] L. Stefan, European fire classification of construction products, new test method “SBI”, and introduction of the European classification system into German building regulations, Otto-Graf-Journal Vol. 16 (2005) 151–166.
[86] M. Kirpluks, Dabas izcelsmes pildvielu ietekme uz talleļļas poliolu putupoliuretānu īpašībām, Riga Technical University, 2012.
[87] A. Prociak, M. Kurańska, U. Cabulis, M. Kirpluks, Rapeseed oil as main component in synthesis of bio-polyurethane-polyisocyanurate porous materials modified with carbon fibers, Polym. Test. 59 (2017) 478–486. doi:10.1016/j.polymertesting.2017.03.006.
[88] A. Fridrihsone-Girone, U. Stirna, M. Misane, B. Lazdiņa, L. Deme, Spray-applied 100% volatile organic compounds free two component polyurethane coatings based on rapeseed oil polyols, Prog. Org. Coatings. 94 (2016) 90–97. doi:10.1016/j.porgcoat.2015.11.022.
[89] E. Žagar, J. Grdadolnik, An infrared spectroscopic study of H-bond network in hyperbranched polyester polyol, J. Mol. Struct. 658 (2003) 143–152. doi:10.1016/S0022-2860(03)00286-2.
[90] T. Aro, P. Fatehi, Tall oil production from black liquor: Challenges and opportunities, Sep. Purif. Technol. 175 (2017) 469–480. doi:10.1016/j.seppur.2016.10.027.
[91] F. Balo, Feasibility Study of “Green” Insulation Materials Including Tall Oil: Environmental, Economical and Thermal Properties, Energy Build. 86 (2014) 161–175. doi:10.1016/j.enbuild.2014.09.027.
[92] J. G. Speight, Gasification for Synthetic Fuel Production, 2014. doi:10.1016/B978-0-85709-802-3.00010-2.
[93] A. Keskin, A. Yaşar, M. Gürü, D. Altiparmak, Usage of methyl ester of tall oil fatty acids and resinic acids as alternative diesel fuel, Energy Convers. Manag. 51 (2010) 2863–2868. doi:10.1016/j.enconman.2010.06.025.
[94] K. White, N. Lorenz, T. Potts, W. Roy Penney, R. Babcock, A. Hardison, E. A. Canuel, J. A. Hestekin, Production of biodiesel fuel from tall oil fatty acids via high temperature methanol reaction, Fuel. 90 (2011) 3193–3199. doi:10.1016/j.fuel.2011.06.017.
[95] S. P. Pyl, T. Dijkmans, J. M. Antonykutty, M.-F. Reyniers, A. Harlin, K. M. Van Geem, G.B. Marin, Wood-derived olefins by steam cracking of hydrodeoxygenated tall oils, Bioresour. Technol. 126 (2012) 48–55. doi:10.1016/j.biortech.2012.09.037.
[96] B. Hedman, P. Piispanen, E. Alami, T. Norin, Synthesis and Characterization of Surfactants via Epoxidation of Tall Oil Fatty Acid, J. Surfactants Deterg. 6 (2003) 47–53.
[97] J. V. Satur, B.P. Calabia, M. Hoshino, S. Morita, Y. Seo, Y. Kon, T. Takagi, Y. Watanabe, L. Mutele, S. Foya, Flotation of rare earth minerals from silicate-hematite ore using tall oil fatty acid collector, Miner. Eng. 89 (2016) 52–62. doi:10.1016/j.mineng.2016.01.004.
[98] U. Törnvall, P. Börjesson, L. M. Tufvesson, R. Hatti-Kaul, ORIGINAL RESEARCH: Biocatalytic production of fatty epoxides from rapeseed & tall oil derivatives: Process & environmental evaluation, Ind. Biotechnol. 5 (2009) 184–192. doi:10.1089/ind.2009.3.184.
[99] K. Mizera, M. Kirpluks, U. Cabulis, M. Leszczyńska, M. Półka, J. Ryszkowska, Characterisation of ureaurethane elastomers containing tall oil based polyols, Ind. Crops Prod. 113 (2018) 98–110. doi:10.1016/j.indcrop.2018.01.019.
[100] P. K. Gamage, M. O'Brien, L. Karunanayake, Epoxidation of some vegetable oils and their hydrolysed products with peroxyformic acid - Optimised to industrial scale, J. Natl. Sci. Found. Sri Lanka. 37 (2009) 229–240. doi:10.4038/jnsfsr.v37i4.1469.

[101] N. C. Goud, V. V., Patwardhan, A. V. and Pradha, Kinetics of in-situ epoxidation of natural triglycerides catalyzed by acidic ion exchange resin, Ind. Eng. Chem. Res. 46 (2007) 3078–3085.
[102] N. Sad, K. Polymer, Kinetics of in situ Epoxidation of Soybean Oil in Bulk Catalyzed by Ion Exchange Resin, 78 (2001).
[103] Z. S. Petrović, A. Zlatanić, C. C. Lava, S. Sinadinović-Fišer, Epoxidation of soybean oil in toluene with peroxoacetic and peroxoformic acids - Kinetics and side reactions, Eur. J. Lipid Sci. Technol. 104 (2002) 293–299. doi:10.1002/1438-9312(200205)104:5<293::AID-EJLT293>3.0.CO;2-W.
[104] R. Liang, A. Hu, M. Hatat-Fraile, Z. N., Fundamentals on Adsorption, Membrane Filtration, and Advanced Oxidation Processes for Water Treatment. In: Hu A., Apblett A. (eds) Nanotechnology for Water Treatment and Purification., Springer, Cham, 2014. doi:10.1007/978-3-319-06578-6.
[105] T. Cooney, F. Cardona, T. Tran-Cong, Kinetics of in situ epoxidation of hemp oil under heterogeneous reaction conditions: an overview with preliminary results, Proc. 1st Int. Postgrad. Conf. Eng. Des. Dev. Built Environ. Sustain. Wellbeing. (2011) 106–111. http://eprints.usq.edu.au/19247.
[106] S. Sinadinović-Fišer, M. Janković, Z. S. Petrović, Kinetics of in situ epoxidation of soybean oil in bulk catalyzed by ion exchange resin, J. Am. Oil Chem. Soc. 78 (2001) 725–731. doi:10.1007/s11746-001-0333-9.
[107] X. Wang, Q. Tang, G. M. Popowicz, B. Yang, Y. Wang, A mechanistic study into the epoxidation of carboxylic acid and alkene in a mono, di-acylglycerol lipase, Biochem. Biophys. Res. Commun. 460 (2015) 392–396. doi:10.1016/j.bbrc.2015.03.044.
[108] F. Björkling, H. Frykman, S. E. Godtfredsen, O. Kirk, Lipase catalyzed synthesis of peroxycarboxylic acids and lipase mediated oxidations., Tetrahedron. 48 (1992) 4587–4592. doi:10.1016/S0040-4020(01)81232-1.
[109] M. Rüsch Gen. Klaas, S. Warwel, Complete and partial epoxidation of plant oils by lipase-catalyzed perhydrolysis, Ind. Crops Prod. 9 (1999) 125–132. doi:10.1016/S0926-6690(98)00023-5.
[110] R. de C. S. Schneider, L. R. S. Lara, T. B. Bitencourt, M. da G. Nascimento, M. R. dos S. Nunes, Chemo-enzymatic epoxidation of sunflower oil methyl esters, J. Braz. Chem. Soc. 20 (2009) 1473–1477. doi:10.1590/S0103-50532009000800013.
[111] S. Sun, X. Ke, L. Cui, G. Yang, Y. Bi, F. Song, X. Xu, Enzymatic epoxidation of Sapindus mukorossi seed oil by perstearic acid optimized using response surface methodology, Ind. Crops Prod. 33 (2011) 676–682. doi:10.1016/j.indcrop.2011.01.002.
[112] S. Sun, G. Yang, Y. Bi, H. Liang, Enzymatic epoxidation of corn oil by perstearic acid, J. Am. Oil Chem. Soc. 88 (2011) 1567–1571. doi:10.1007/s11746-011-1820-1.
[113] T. Vlček, Z. S. Petrović, Optimization of the chemoenzymatic epoxidation of soybean oil, J. Am. Oil Chem. Soc. 83 (2006) 247–252. doi:10.1007/s11746-006-1200-4.
[114] C. Orellana-Coca, U. Törnvall, D. Adlercreutz, B. Mattiasson, R. Hatti-Kaul, Chemo-enzymatic epoxidation of oleic acid and methyl oleate in solvent-free medium, Biocatal. Biotransformation. 23 (2005) 431–437. doi:10.1080/10242420500389488.
[115] G. D. Yadav, K. Manjula Devi, A kinetic model for the enzyme-catalyzed self-epoxidation of oleic acid, J. Am. Oil Chem. Soc. 78 (2001) 347–351. doi:10.1007/s11746-001-0267-2.
[116] C. Orellana-Coca, S. Camocho, D. Adlercreutz, B. Mattiasson, R. Hatti-Kaul, Chemo-enzymatic epoxidation of linoleic acid: Parameters influencing the reaction, Eur. J. Lipid Sci. Technol. 107 (2005) 864–870. doi:10.1002/ejlt.200500253.